Par **Abbas CHOKOR**

# Design of several centralized and decentralized multilayer robust control architectures for global chassis control

Thèse présentée
pour l'obtention du grade
de Docteur de l'UTC

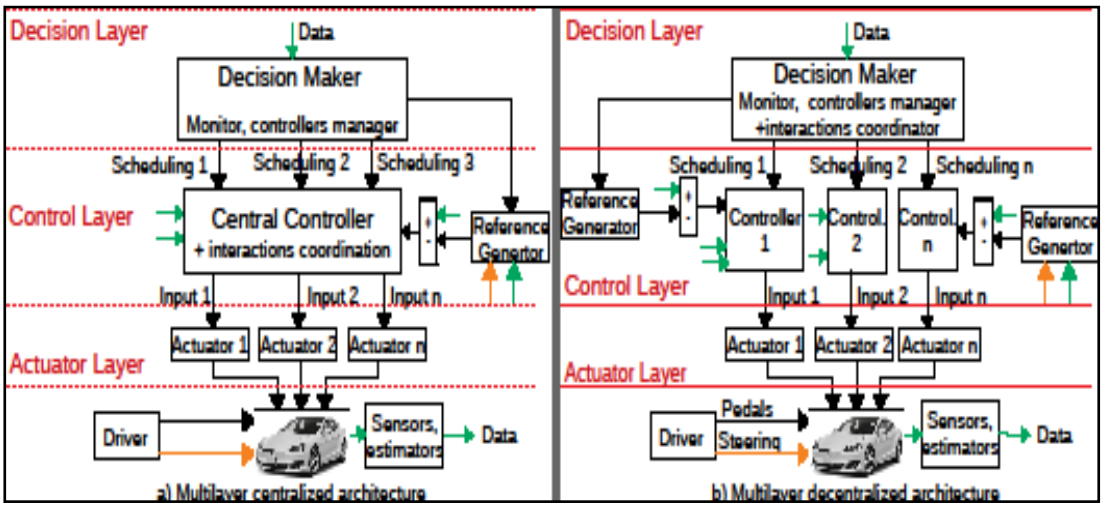


Soutenue le 8 novembre 2019
**Spécialité :** Sciences et Technologies de l'Information et des Systèmes et Automatique : Unité de recherche Heudyasic (UMR-7253)

D2514

# Design of Several Centralized and Decentralized Multilayer Robust Control Architectures for Global Chassis Control

CHOKOR Abbas

Spécialité : Sciences et Technologies de l'Information et des Systèmes et Automatique

---

Thesis defended on November 08, 2019 in front of the jury composed of:

**Reporters:**

| | |
|---|---|
| *MOREAU Xavier* | *SENAME Olivier* |
| Full Professor | Full Professor |
| Univ. de Bordeaux | Univ. Grenoble Alpes |

**Examiners:**

| | | |
|---|---|---|
| *D'ANDREA NOVEL Brigitte* | *EL HAJJAJI Ahmed* | DE MIRAS Jérôme |
| Full Professor | Full Professor | Associate-professor |
| Sorbonne Université | Univ. de Picardie Jules Verne | Univ. de Technologie de Compiègne |

**Thesis co-directors/co-supervisors:**

| | |
|---|---|
| *TALJ Reine* | *CHARARA Ali* |
| CNRS researcher | Full professor |
| Univ. de Technologie de Compiègne | Univ. de Technologie de Compiègne |

**Thesis co-supervisor:**

*DOUMIATI Moustapha*
Associate-professor
ESEO-IREENA Angers

---

Université de technologie de Compiègne

Heudiasyc Laboratory UMR CNRS 7253

11 - 08 - 2019

**Thesis funding**

Hauts-de-France Region and the European Regional Development Fund (ERDF)

UNION EUROPEENNE

Le projet « SYSCOVI » est cofinancé dans le cadre du Fonds européen de développement économique et régional (FEDER) 2014/2020.

dedicated to

# *Acknowledgments*

# *Contents*

# *List of Figures*

# *List of Tables*

# *Notations*

Table 1 – Notations

| Symbol | Description | Unit |
|---|---|---|
| $i$ | $i = \{f : front, r : rear\}$ | $[-]$ |
| $j$ | $j = \{r : right, l : left\}$ | $[-]$ |
| $z_{s,ij}$ | Sprung mass bounce at the corner $ij$ | $[m]$ |
| $z_{us,ij}$ | Unsprung mass bounce at the corner $ij$ | $[m]$ |
| $z_{r,ij}$ | Road vertical profile at the corner $ij$ | $[m]$ |
| $z_s$ | CG vertical displacement (bounce/heave) | $[m]$ |
| $z_{s,ij}$ | Sprung mass bounce at the corner $ij$ | $[m]$ |
| $z_{us,ij}$ | Unsprung mass bounce at the corner $ij$ | $[m]$ |
| $F_{ij}$ | Passive suspension vertical force (corner $ij$) | $[N]$ |
| $F_{s,ij}$ | Suspension total force (corner $ij$) | $[N]$ |
| $U_{ij}$ | Active suspension force (corner $ij$) | $[N]$ |
| $F_{z,ij}$ | Tire $ij$ vertical force | $[N]$ |
| $F_{x,ij}$ | Tire $ij$ longitudinal force | $[N]$ |
| $F_{y,ij}$ | Tire $ij$ lateral force | $[N]$ |
| $F_{zj}$ | Vertical load on the vehicle side j | $[N]$ |
| $F_{yi}$ | Lateral forces at the $i$ axle (bicycle model) | $[N]$ |
| $a_x$ | Longitudinal acceleration at the CG | $[m/s^2]$ |
| $a_y$ | Lateral acceleration at the CG | $[m/s^2]$ |
| $x$ | Vehicle longitudinal displacement (body frame) | $[m]$ |
| $y$ | Vehicle lateral displacement (body frame) | $[m]$ |
| $\theta$ | Sprung mass roll angle | $[rad]$ |
| $\phi$ | Sprung mass pitch angle | $[rad]$ |
| $\psi$ | Vehicle yaw angle | $[rad]$ |
| $\theta_{des}$ | Desired roll angle (Set point) | $[rad]$ |

| Symbol | Description | Unit |
|---|---|---|
| $\delta_{fj}$ | Front j (left or right) steering angle | $[rad]$ |
| $\delta_d$ | Driver steering angle on front tires | $[rad]$ |
| $\delta_c$ | Control steering angle | $[rad]$ |
| $\delta_t$ | Total steering angle | $[rad]$ |
| $\delta_f$ | front steering angle (bicycle model) | $[rad]$ |
| $V$ | Vehicle speed | $[m/s]$ |
| $\omega_{ij}$ | Wheel $ij$ angular velocity | $[rad/s]$ |
| $\beta$ | Vehicle side-slip angle at CG | $[rad]$ |
| $\alpha_{ij}$ | Side-slip angle of the tire $ij$ | $[rad]$ |
| $C_{m,ij},\ C_{f,ij}$ | Motor, braking torques at the wheel $ij$ | $[N.m]$ |
| $\alpha_f,\ \alpha_r$ | Front, rear tire side-slip angle (bicycle model) | $[rad]$ |
| $\sigma_{x,ij}$ | Longitudinal tire slipping | $[-]$ |

Table 2 – Vehicle parameters

| Symbol | Description | Value |
|---|---|---|
| $m_{s,ij}$ | Sprung mass mass at the corner $ij$ | 281.6 $[kg]$ |
| $m_{us,ij}$ | Unsprung mass mass at the corner $ij$ | 40 $[kg]$ |
| $K_{s,fr},\ K_{s,fl}$ | Suspension stiffness coefficient (front tires) | 20000 $[N/m]$ |
| $K_{s,rr},\ K_{s,rl}$ | Suspension stiffness coefficient (rear tires) | 13000 $[N/m]$ |
| $C_{s,fr},\ C_{s,fl}$ | Suspension damping coefficient (front tires) | 9830 $[N.s/m]$ |
| $C_{s,rr},\ C_{s,rl}$ | Suspension damping coefficient (rear tires) | 3000 $[N.s/m]$ |
| $K_t$ | Tire stiffness coefficient | 467000 $[N/m]$ |
| $C_t$ | Tire damping coefficient | 500 $[N.s/m]$ |
| $t_f$ | Half front track | 0.773 $[m]$ |
| $t_r$ | Half rear track | 0.773 $[m]$ |
| $l_f$ | Wheelbase to the front | 1.0385 $[m]$ |
| $l_r$ | Wheelbase to the rear | 1.6015 $[m]$ |
| $h$ | Height of the vehicle CG | 0.58 $[m]$ |
| $h_r$ | Height of the unsprung mass CG | 0.31 $[m]$ |
| $h_\theta$ | Sprung mass roll arm | 0.27 $[m]$ |
| $h_\phi$ | Sprung mass pitch arm | 0.27 $[m]$ |
| $M$ | Total vehicle mass | 1286.4 $[kg]$ |
| $M_s$ | Sprung mass | 1126.4 $[kg]$ |
| $I_x$ | Roll moment of inertia of sprung mass | 534 $[kg.m^2]$ |
| $I_y$ | Pitch moment of inertia of sprung mass | 1860 $[kg.m^2]$ |
| $I_z$ | Vehicle yaw moment of inertia | 1970 $[kg.m^2]$ |
| $I_{xz}$ | Vehicle yaw-roll product of inertia | 743 $[kg.m^2]$ |
| $g$ | Gravity constant | 9.81 $[m/s^2]$ |
| $C_{\sigma,ij}$ | Longitudinal tire stiffness | 18700 $[N/m]$ |
| $C_{\alpha,ij}$ | Lateral (cornering) tire stiffness | 38388 $[N/rad]$ |
| $\mu$ | Road adherence coefficient | dry surface= 1 $[-]$ |
| $r_{ij}$ | Effective wheel radius | 0.3 $[m]$ |
| $I_r$ | Tire moment of inertia around rotational axis | 0.85 $[kg.m^2]$ |
| $C_f,\ C_r$ | Front, rear tire cornering stiffness (bicycle model) | 76776 $[N/rad]$ |
| $K_\theta$ | Roll suspension angular stiffness | 30000 $[N.m/s]$ |
| $C_\theta$ | Roll suspension angular damper | 10000 $[N.m/s]$ |

# *Acronyms*

| | |
|---|---|
| $ABCA$ | Active Braking for Collision Avoidance |
| $ABS$ | Anti-lock Braking System |
| $ADAS$ | Advanced Driving Assistance Systems |
| $ADB$ | Active Differential Braking |
| $AFS$ | Active Front Steering |
| $ARB$ | Active anti-Roll Bar |
| $ASus$ | Active Suspensions |
| $BRL$ | Bounded Real Lemma |
| $CG$ | Center of Gravity |
| $DLC$ | Double Lane Change |
| $DYC$ | Direct Yaw Control |
| $EMB$ | Electro-Mechanical Brakes |
| $EPS$ | Electronic Power Steering |
| $ESP$ | Electronic Stability Program |
| $FLC$ | Fuzzy Logic Controller |
| $GCC$ | Global Chassis Control |
| $\mathcal{H}_\infty$ | H infinity |
| $LMI$ | Linear Matrix Inequality |
| $LPV$ | Linear Parameter Varying |
| $LQR$ | Linear Quadratic Regulator |
| $LTI$ | Linear Time Invariant |
| $LTR$ | Load Transfer Ratio |
| $MIMO$ | Multi-Input-Multi-Output |
| $NHTSA$ | National Highway Traffic Safety Administration |
| $RMS$ | Root Mean Square |
| $SDP$ | Semi-Definite Program |
| $SI$ | Stability Index |
| $SISO$ | Single-Input-Single-Output |
| $STSM$ | Super-Twisting Sliding Mode |
| $VSC$ | Vehicle Stability Control |

# *Publications*

The contributions presented in this thesis were the subject of some published papers and other submitted ones.

**Journal articles (submitted)**

- A.Chokor, R. Talj, M. Doumiati, A. Hamdan, and A. Charara. "A comparison between a centralized multilayer $LPV/\mathcal{H}_\infty$ and a decentralized multilayer sliding mode control architectures for vehicle's global chassis control". Submitted to International Journal of Control (IJC).
- A.Chokor, M. Doumiati, R. Talj, and A. Charara. "Effects of roll motion control on vehicle dynamics behavior in the context of global chassis control". Submitted to European Journal of Control (EJC).

**Conference articles (accepted/published)**

- A.Chokor, M. Doumiati, R. Talj, and A. Charara. "Design of a new gain-scheduled $LPV/\mathcal{H}_\infty$ controller for vehicle's global chassis control". Accepted in IEEE 58th Conference on Decision and Control (CDC 2019), Nice, France, 2019.
- A.Chokor, R. Talj, M. Doumiati, and A. Charara. "A global chassis control system involving active suspensions, direct yaw control and active front steering". Accepted in 9th IFAC International Symposium on Advances in Automotive Control (AAC 2019), Orléans, France, 2019.
- A.Chokor, R. Talj, M. Doumiati, A. Charara, and A. Rabhi. "Rollover prevention using active suspension system". In IEEE 20th International Conference on Intelligent Transportation Systems (ITSC 2017), Yokohama, Japan, pp. 1706–1711, 2017.
- A. Chokor, R. Talj, A. Charara, H. Shraim, and C. Francis. "Active suspension control to improve passengers comfort and vehicle's stability". In IEEE 19th International Conference on Intelligent Transportation Systems (ITSC 2016), Rio de Janeiro, Brasil, pp. 296–301, 2016.

**Conference articles (submitted)**

- A.Chokor, R. Talj, M. Doumiati, and A. Charara. "Vehicle roll control for lateral stability enhancement and rollover avoidance". Submitted to IEEE 2020 American Control Conference (ACC 2020).

# *Résumé*

Le Contrôle Global du Châssis ($CGC$) est une tâche cruciale dans les véhicules intelligents. Il consiste à assister le conducteur par l'intermédiaire de plusieurs fonctionnalités automatisées, notamment à des fins de sécurité active et de confort. Etant donné que les dynamiques de ces fonctionnalités sont interconnectées, les performances attendues sont parfois contradictoires. Par conséquent, le $CGC$ consiste à coordonner les différents systèmes $ADAS$ "Advanced Driving Assistance Systems" afin de créer des synergies entre les dynamiques interconnectées pour améliorer les performances globales du véhicule. Plusieurs stratégies de coordination puissantes ont déjà été développées, soit dans le monde académique, soit dans le monde industriel pour gérer ces interconnexions. Du fait que les besoins en matière de sécurité active augmentent d'un côté et que la technologie pouvant être intégrée dans les véhicules évolue, une intense activité de recherche et développement est toujours en cours dans le domaine du contrôle global du châssis.
Cette thèse analyse différentes interconnexions dynamiques et développe des nouvelles stratégies $CGC$ dans lesquelles le braquage actif avant, le freinage différentiel actif et les suspensions actives sont coordonnés - tous ensemble ou partiellement - afin d'améliorer les performances globales du véhicule, à savoir l'évitement du renversement, la stabilité latérale, le confort de conduite (manoeuvrabilité) et confort des passagers. Plusieurs architectures multicouches formées par trois couches hiérarchiques sont proposées. La couche inférieure représente les actionneurs implémentés dans le véhicule qui génèrent leurs entrées de commande en fonction des ordres envoyés depuis la couche intermédiaire. La couche intermédiaire est la couche de contrôle qui est chargée de générer les entrées de contrôle qui minimisent les erreurs entre les variables d'état souhaitées et réelles du véhicule, à savoir les mouvements de lacet, de dérapage, de roulis, de tangage et de soulèvement, quelle que soit la situation de conduite. La couche supérieure est la couche de prise de décision. Elle surveille instantanément la dynamique du véhicule selon différents critères, puis génère des paramètres de pondération pour adapter les performances des contrôleurs en fonction des conditions de conduite, c'est-à-dire pour améliorer la manoeuvrabilité, la stabilité latérale, l'évitement du renversement et le confort de conduite du véhicule.
Les architectures proposées se diffèrent dans les couches de contrôle et de décision en fonction des actionneurs intégrés proposés. Par exemple, les couches de décisions se diffèrent par les critères qui surveillent la dynamique du véhicule et la manière dont la décision est prise (logique floue ou relations explicites). Les couches de contrôle se diffèrent par leurs structures, où des contrôleurs centralisés et décentralisés sont développés. Dans l'architecture centralisée, un seul contrôleur optimal MEMS

Multi-Entrées-Multi-Sorties génère les entrées de commande optimales basées sur la technique de commande $LPV/\mathcal{H}_\infty$. Dans l'architecture décentralisée, les contrôleurs sont découplés. La technique $STSM$ (Super-Twisting Sliding Mode) est appliquée pour déduire chaque entrée de commande. Les architectures proposées sont testées et validées sur le simulateur professionnel "SCANeR Studio" et sur un modèle complexe non linéaire du véhicule. La simulation montre que toutes les architectures sont pertinentes pour le contrôle global du châssis. Celle centralisée est optimale, complexe et garantit la stabilité globale, tandis que celle décentralisée ne garantit pas la stabilité globale, mais elle est intuitive, simple et robuste.

**Mots Clés :** *Contrôle Global du Châssis, Contrôle hiérarchique, Contrôle centralisé, Contrôle décentralisé, Mode glissant "Super-twisting", $LPV/\mathcal{H}_\infty$.*

# *Abstract*

Global Chassis Control ($GCC$) is crucial task in intelligent vehicles. It consists of assisting the driver by several automated functionalities especially for active safety and comfort purposes. Due to the fact that the dynamics of these functionalities are interconnected, thus the awaited performances are sometimes contradictory. Hence, the main task in $GCC$ field is to coordinate the different Advanced Driving Assistance Systems ($ADAS$) to create synergies between the interconnected dynamics in order to improve the overall vehicle performance. Several powerful coordination strategies have already been developed either in the academic world or in the industrial one to manage these interconnections. Because the active safety needs are increasing from one side, and the technology that can be embedded into vehicles is evolving, an intense research and development is still involved in the field of global chassis control.

This thesis analyzes different dynamics interconnections and develops new several $GCC$ strategies where the Active Front Steering, Active Differential Braking, and the Active Suspensions are coordinated - all together or partially - to improve the vehicle overall performance i.e. the rollover avoidance, the lateral stability, the driving comfort (maneuverability), and the ride comfort. Several multilayer architectures formed by three hierarchical layers are proposed. The lower layer represents the actuators implemented into the vehicle which generate their control inputs based on the orders sent from the middle layer. The middle layer is the control layer which is responsible to generate the control inputs that minimize the errors between the desired and actual vehicle state variables i.e. the yaw, side-slip, roll, pitch, and heave motions, regardless of the driving situation. The higher layer is the decision making layer. It instantly monitors the vehicle dynamics by different criteria, then, it generates weighting parameters to adapt the controllers performances according to the driving conditions i.e. to improve the vehicle's maneuverability, lateral stability, rollover avoidance, and ride comfort.

The proposed architectures differ in the control and decision layers depending on the proposed embedded actuators. For instance, the decision layers differ in the monitored criteria and the way the decision is taken (fuzzy logic or explicit relations). The control layers differ in structure, where centralized and decentralized controllers are developed. In the centralized architecture, one single Multi-Input-Multi-Output optimal controller generates the optimal control inputs based on the Linear Parameter Varying ($LPV$)/$\mathcal{H}_\infty$ control technique. In the decentralized architecture, the controllers are decoupled, where the Super-Twisting Sliding Mode ($STSM$) technique is applied to derive each control input apart.

The proposed architectures are tested and validated on the professional simulator

"SCANeR Studio" and on a Full vehicle nonlinear complex model. Simulation shows that all architectures are relevant to the global chassis control. The centralized one is optimal, complex and overall stability is guaranteed, while the decentralized one does not guarantee the overall stability, but it is intuitive, simple, and robust.

**Key Words:** *Global Chassis Control, Hierarchical control, Centralized control, Decentralized control, Super-twisting sliding mode, LPV/$\mathcal{H}_\infty$.*

# *Introduction*

Ground vehicles comprise several mechanical, hydraulic, electronic and electrical components and systems that have different objectives/goals. Each of these systems is involved and effects the vehicle dynamics and performance. Indeed, the suspension system, the steering system, the braking system, the power transmission system and even the tires have been evolved for several decades in order to improve the vehicle performance. In this thesis, we treat one of several manners to improve the behavior of these systems which is the development of automatically controlled systems where the electronic devices and algorithms enhance the performance of the mechanical components. These enhancements in systems behaviors are reflected to the entire vehicle performance. Due to the fact that these systems are inter-connected by acting on the vehicle/chassis dynamics, creating synergies between them removes the conflicts among the control objectives and retains the maximum benefice of each of these systems. These synergies consist of making some or all the sub-systems cooperate together to achieve new global goals like comfort enhancement, stability enhancement, energy consumption reduction, etc...

## 0.1 Motivation

Driving safety is a major challenge for our society. According to the US Department of Transportation "National Highway Traffic Safety Administration ($NHTSA$)" statistics, human errors commit almost 90% of road accidents as explained in [Rajamani, 2012]. The integration of an Advanced Driving Assistance System ($ADAS$) or active safety system in the vehicle permits to act in an appropriate way to avoid accidents, skidding, and rollover. Moreover, nowadays $ADAS$ systems cross over vehicle active safety to include ride and driving comfort [Chen et al., 2016], [Sename et al., 2013], [Chokor et al., 2016]. $ADAS$ systems are formed by several single-actuator approaches that have been proposed and marketed, such as: Vehicle Stability Control ($VSC$) or Electronic Stability Program ($ESP$) including Direct yaw Control ($DYC$), Anti-lock Braking System ($ABS$), Active Differential Braking ($ADB$) and others, to enhance the vehicle handling and stability; Active Front Steering ($AFS$), 4 Wheel Steering ($4WS$), and Electronic Power Steering ($EPS$) to improve the vehicle maneuverability or lane keeping; and Active Suspensions ($ASus$), Semi-Active Suspensions (Semi-$ASus$), and Active anti-Roll Bar ($ARB$) to improve comfort and road holding. There are also several other active controllers concerned with the vehicle dynamics like Active Braking for Collision Avoidance ($ABCA$), (adaptive-)cruise controller for speed control, etc...However, these systems

are not involved in this thesis.
*ADAS* systems, when equipped into vehicles, often operate independently, while inevitably, it occurs interactions among their local control objectives. Indeed, the vehicle motions in the vertical, lateral, and longitudinal directions are coupled together. Consequently, creating synergies among these different systems can exploit the existence of the interactions between the dynamics to achieve new objectives using the available *ADAS*.
Current and future intelligent vehicles are incorporating more sophisticated chassis control systems, known by Global Chassis Control (*GCC*) systems. *GCC* is an integrated vehicle chassis control system that coordinates several *ADAS* systems to improve the overall vehicle performance, including handling stability (lateral and longitudinal stability), vertical stability (rollover avoidance), and ride and driving comfort.
The noticed enhancements in the *GCC* approach have motivated us to study the ways these synergies can be created, either by using different actuators technology or by creating different control architectures.
This thesis is a part of the SYSCOVI (*approche SYstèmes de Systèmes pour la COmmande de la dynamique de Véhicules Intelligents*) project, co-funded by the Hauts-de-France region and the European Regional Development Fund (ERDF) 2014/2020.

## 0.2 State of the Art

### 0.2.1 Global Chassis Control

In the *GCC* field, there is a distinguish between two types of controllers coordination, one type is concerned with the nature of the equipped technology and the controlled objectives, and the other type concerns the form of the designed *GCC* architecture. In this context, several coordination strategies can be developed, either by coordinating two or more actuators to achieve one, two or more objective(s), or by designing different coordination architectures such as centralized, decentralized, hierarchical, and multilayer architectures, etc...
In this section, we will briefly introduce the actuators, control objectives, and the different control architectures that are involved in the *GCC*.
Different actuator's technologies can be embedded into vehicles to achieve the *GCC* objectives. We cite some of the active actuators that can be added and controlled: *AFS* using a controlled electric motor, *ADB* using electro-hydraulic independent braking, *ASus* using electro-hydraulic cylinder, semi-*ASus* using controlled damper, *ARB*, 4-Wheel Motorized and (4*WS*) systems.
In this thesis, we focus on the coordination of the *AFS*, *DYC* through *ADB*, and the *ASus*. More discussions on the actuators are developed later throughout this manuscript.
The control objectives -in interest of this thesis- are the lateral stability, rollover avoidance, driving comfort (maneuverability) and ride comfort. These objectives are to be achieved by the active actuators, knowing that each of the actuator acts

either by enhancing or deteriorating one or more objective(s).
The lateral stability is the feature of handling the road without lateral skidding. This latter can happen due to several vehicle's excitations such as: sudden steering (high steering frequency/rate) at high speed when avoiding accident, high steering amplitude at high or low speed when cornering or drifting, change of the road adherence or $\mu$-split...
The rollover is the phenomenon when the vehicle turns around the virtual axis joining the vehicle wheels of the same side (left of right). Rollover happens either by external effect (accident, wind, bump...), or at high speed when cornering.
Rollover and lateral skidding commit the major fatal injuries [DOT, 2010], [Deutermann, 2002]. For that reason, rollover avoidance and lateral stability are essential objectives in lot of research concerned by $GCC$. These objectives were usually achieved by coordinating the $AFS$ and the $DYC$, while the $ASus$ are lately introduced for road holding and passengers comfort.
The driving comfort, the maneuverability or the steer-ability aims at enhancing the response of the vehicle when the driver steers, in the normal driving range. The steer-ability is the feature of making the vehicle yaw rate linear to the driver steering angle. This linear relation makes the driver feels comfortable since the vehicle orientation becomes more predictable by the driver when steering.
The ride comfort includes the roll, pitch and heave motions of the vehicle (sprung mass). These solicitations should be controlled to enhance the passenger's comfort because the natural/induced motions due to the vehicle dynamics (lateral acceleration, longitudinal acceleration...) or external effects (bump, road irregularities...) are not awaited despite the fact that passengers are used to be subjected to these solicitations. These solicitations have to be attenuated or controlled to predefined reference trajectories.

The coordination between the $AFS$ and the $DYC$ to simultaneously improve the vehicle maneuverability and lateral stability depending on the driving situation is one of the main tasks in $GCC$ field. Indeed, an intense research is involved by the coordination of the $AFS$ with the $DYC$, where several advanced control methods have been developed for this issue. In a decentralized approach, authors in [He et al., 2006] and [Bardawil et al., 2014] have developed a $DYC$ controller for lateral stability purpose and an $AFS$ controller for maneuverability purpose, based on sliding mode technique, and then a monitor switches between both stand-alone controllers according to the driving situations. Similarly, based on the fuzzy-logic technique, a coordination approach between $AFS$ and $DYC$ has been developed in [Karbalaei et al., 2007]. However, the decentralized strategy does not guarantee the overall stability of the system when switching between controllers or when both controllers are actuated simultaneously. [Poussot-Vassal et al., 2009], [Doumiati et al., 2013], [Fergani et al., 2017], [Fergani et al., 2013], [Fergani et al., 2016a] and [Doumiati et al., 2014] have developed several robust and optimal Multi-Input-Multi-Output ($MIMO$) centralized controllers based on Linear Parameter Varying ($LPV$)/$\mathcal{H}_\infty$ control technique, where the $LPV/\mathcal{H}_\infty$ controller penalizes or relaxes the steering and braking to enhance maneuverability and lateral stability. The overall stability of the system is thus guaranteed, since the controllers' actuation is automated based on the polytopic approach. However, these controllers does not directly involve

the vehicle roll motion and rollover problem in the controller synthesis. Some of them state the advantage on the rollover problem as a consequence of the controller without guaranteeing the rollover avoidance.
The vehicle rollover is treated, by some authors, as a different *ADAS* system either by braking (differential or normal) or by steering [Ackermann and Odenthal, 1998],[Odenthal et al., 1999],[Solmaz et al., 2007], [Gáspár et al., 2005]. These approaches had to be included in the *GCC* architecture, thus, the focus has started on creating a unified chassis controller, centralized or hierarchical, which merges all the control systems in a one single controller [Yoon et al., 2010],[Akhmetov et al., 2010], [Alberding et al., 2009], [Chou and D'Andréa-Novel, 2005]. In [Yoon et al., 2010], the authors propose a DYC controller that has the desired yaw rate to switch between two expressions, one is to enhance the lateral stability and the other one is to avoid rollover. At low level control the desired yaw rate is achieved through simple braking, which has the disadvantage of decelerating the vehicle. Authors in [Akhmetov et al., 2010] have shown a better performance by achieving the same *DYC* objective through *ADB*.
Some other relevant research such as [Ackermann and Odenthal, 1998],[Odenthal et al., 1999], and [Solmaz et al., 2007] propose to control the roll motion by the steering and/or braking to avoid the rollover, regardless of the maneuverability and the vehicle trajectory.
When the (semi)-*ASus* started to appear, the intention was to improve the ride comfort and road holding [Chamseddine et al., 2006],[Savaresi et al., 2010], which indirectly improves the stability handling. *ASus* is thus the main tool to achieve passengers comfort, where the goal of this type of controllers is to isolate the chassis from any road perturbation by ensuring less roll, pitch and vertical displacement of the sprung mass [Chokor et al., 2016]. *ASus* also aim to improve road-holding by minimizing tires' strokes and suspensions' deflections. One type of the *ASus* is the CRONE suspension, where the traditional suspension components i.e. the spring and the damper are replaced by a mechanical and hydro-pneumatic system defined by a fractional (so-called non-integer) order force-displacement transfer function [Oustaloup et al., 1997]. The Crone Suspension is a powerful tool to isolate the chassis since the analysis and the design of the controller are done in the frequency-domain, where robust performance and internal stability are guaranteed [Moreau et al., 2003].
Later on, authors in [Alberding et al., 2009] have solved the yaw stabilizing optimal control problem after introducing the rollover as a constraint on the control allocation process. Authors in [Chou and D'Andréa-Novel, 2005] have completely decoupled the problem of *GCC* stabilization, such that the yaw rate is controlled through the braking while the roll and pitch rates are controlled through the suspensions. From the other side, many recent research (centralized and decentralized) such as [Vu et al., 2017], [Yao et al., 2017], and [Mirzaei and Mirzaeinejad, 2017] propose to control the vertical load transfer, as a function of the roll angle and its angular velocity, through the integration of the (semi-)*ASus* or *ARB* into the chassis to avoid rollover. They also conclude the enhancements on lateral stability as a consequence. [Sename et al., 2013], [Chen et al., 2016] and [Fergani et al., 2013] have developed several powerful centralized $LPV/\mathcal{H}_\infty$ controllers, where the

decoupled lateral and vertical vehicle dynamics are respectively controlled by the $AFS$+$DYC$ and by the (semi-)$ASus$.

## 0.2.2 Performance Criteria - Stability and Comfort

Several criteria are defined in literature to quantify the vehicle performance, especially the rollover risk, the lateral stability, the maneuverability, and the driving comfort, while a few criteria are involved in the quantification of the riding comfort, since the ride comfort is a subjective feeling. These criteria are used either to posteriorly evaluate the performance objective or to schedule the different controllers to adapt their performance to the driving situation. This section introduces different criteria developed in literature for each of the cited objectives.

### 0.2.2.1 Rollover Criteria

Despite the fact that the rollover is a rare phenomenon, but its consequence are very dangerous. This is why there is a serious work either in industry or academic institutions to avoid the rollover. The vehicle rollover could happen due to external perturbation (lateral wind, bump...), in this case it is called tripped rollover, or to an internal dynamical effect such as an excess of the lateral acceleration, high frequency steering, high amplitude and rate of the roll motion, in this case it is called un-tripped rollover. In this thesis, we are interested in the un-tripped rollover whose study is given in Chapter 1. In [Dahlberg, 2000], the rollover criterion is calculated based on the maximal lateral acceleration that the vehicle could handle before starting rollover in the steady state regime. Thus, the rollover criterion is called $SRT$ for Steady-state Rollover Threshold. In the same paper, another criterion to detect the rollover risk in the different dynamical regimes is provided. It is called $DRT$ as Dynamic Rollover Threshold.
In [Dahlberg, 1999], an energetic criterion is addressed to detect the rollover. Mainly, the kinetic and potential energies of the roll motion expressed as functions of the roll rate, the roll stiffness, and the heave rate are used to calculate the Dynamic Rollover Energy Margin $DREM$ criterion.
In [Chen and Peng, 1999], a criterion called Time To Rollover $TTR$ predicts in the horizon of 3 seconds the roll angle of the vehicle that corresponds to the steering angle at the current time, thus, 3 seconds before rollover the driver is alerted.
The most commonly used criterion in literature is based on the load transfer between the right and left tires' vertical forces. It is called the Load Transfer Ratio ($LTR$) which normalizes the load transfer by the total vertical forces on the tires. Because tires' vertical forces are hard to be measured, the $LTR$ criterion is used only for performance evaluation by simulation, while to schedule the controllers' performances in real-time application, several estimations of $LTR$ are developed in literature. The estimated criterion is based on a liner relation between the vehicle roll angle, roll rate, and lateral accelerations, where weighting coefficients have to be identified for each vehicle. The estimated criterion is still called $LTR$ [Doumiati et al., 2012] or Rollover Index $RI$ as in [Yoon et al., 2007] or Rollover Warning

$RW$ as in [Peng and Eisele, 2000]. The $LTR$ criterion is adopted in this thesis, its detailed formulation is provided in Chapter 1.

#### 0.2.2.2 Lateral Stability Criteria

Vehicle lateral stability is a crucial objective in chassis control. When performing a lateral motion, the road/tires lateral forces might be saturated and thus the vehicle laterally skids causing dangerous consequences. Therefrom, researchers have done an intensive work to estimate the tires lateral forces, we cite [Hsu, 2009], [Doumiati et al., 2010a], [Anderson and Bevly, 2005], and [Wang and Wang, 2013]. The saturation of the tires lateral forces could be caused due to an excess of the lateral acceleration beyond the maximal value that could be handled by the vehicle to maintain adherent to the road. In this context, authors of [Rajamani, 2012] propose to saturate the vehicle yaw rate at a dynamic threshold dependent on the road adherence coefficient and the vehicle speed, where the lateral acceleration of the vehicle remains 15% lower than the maximal one calculated based on the adherence and the gravitational acceleration constant. In [Yu and Huang, 2008], authors propose to control the kinetic energy of the vehicle yaw rate based on the yaw-rate/side-slip phase plan and limit cycle analysis. However, the most famous criterion to evaluate the lateral stability is called "Stability Index" ($SI$). $SI$ is designed in several works based on the side-slip-angle/side-slip-velocity ($\beta - \dot{\beta}$) phase plane [Inagaki et al., 1994], [Rajamani, 2012]. The use of $SI$ as a monitoring criterion needs the real-time estimation of the side-slip angle and velocity at the vehicle center of gravity. For this, several observers are developed in literature such as: [Baffet et al., 2009], [Chung and Yi, 2006], [Doumiati et al., 2010b] and [Baffet et al., 2008]. The $SI$ is the criterion chosen in this thesis to evaluate and monitor the lateral stability of the vehicle, a detailed formulation of $SI$ is provided in Chapter 1.

#### 0.2.2.3 Driving Comfort/Maneuverability Criteria

The driving comfort, the maneuverability or the steer-ability is the feature of making the vehicle yaw rate linear to the driver steering angle. This linear relation makes the driver feels comfortable since the vehicle orientation becomes more predictable by the driver when steering, especially in the stable driving situations. Static and dynamic relations are derived in literature to enhance the maneuverability. In [Aripin et al., 2014], and [Xiao et al., 2009] a static linear relation between the ideal yaw rate and the driver steering angle is given, for the steady state regime, depending on the vehicle parameters, speed, and stability factors. While the dynamic relation known as the bicycle model, provides the ideal yaw acceleration and side slip angle for a given steering angle at a given speed, then the desired yaw rate is integrated from the ideal yaw acceleration [Sierra et al., 2006],[Smith and Starkey, 1995], [Yoon et al., 2010], and [Oh et al., 2003]. Another definition of the driving comfort is the requirement of making the active safety actuators operate in the ranges where the driver does not feel their existence. This requirement can be fulfilled through filtering the actuation signals as done in [Ackermann and Bünte, 1997], [Poussot-Vassal et al., 2009], and [Doumiati et al., 2013].

#### 0.2.2.4 Ride Comfort Criteria

Ride comfort is a subjective passengers feeling. It is known as attenuating any chassis body motion i.e the sprung mass roll, pitch and heave motions at some or all frequencies -if possible- [Gillespie, 1992]. To do this, many developments have been done to isolate the vehicle body from external disturbances (like bumps) and internal disturbances caused by the vehicle dynamics interactions (like acceleration, braking, cornering...). These developments are not limited to the design of the passive suspension parameters, but also to the control of the (semi-)*ASus* or the *ARB*. Mainly, two methods are widely developed in literature for both *ASus* and semi-*ASus*: the first one is to directly control the roll, pitch and heave motions -with their velocities- at the body center of gravity, through virtual inputs, then an allocation procedure is applied to find the actuator forces at each vehicle quarter suspension as done in [Chou and D'Andréa-Novel, 2005], [Yoon et al., 2010], and [Vu et al., 2017]; the second one is to control each quarter vehicle suspension alone, where the objective is to minimize the quarter sprung mass vibrations as done in [Moreau et al., 2009], [Savaresi et al., 2010] and [Chamseddine et al., 2006]. To evaluate the comfort, research focus on the peak values and root mean square reductions by doing time-domain tests, or in the frequency-domain by the power-spectral density measure [Chen et al., 2016], [Rajamani, 2012], and [Savaresi et al., 2010].
Ride comfort is a conflict objective with the road holding, this is why some research are interested in orienting the suspension control depending the suspension frequency and vehicle stability, we cite [Moreau et al., 2009], and [Savaresi et al., 2010].

## 0.3 Thesis Contribution

The main contributions of this thesis are:

- a new *ASus* controller which attenuates the roll, pitch, and heave motions based on virtual inputs allocation;
- a frequency and time domain analysis of the effect (enhancement) of the roll control on the lateral stability and rollover avoidance. Then, a development of a Linear Quadratic Regulator (*LQR*), a Lyapunov-based, and a robust Super-Twisting Sliding Mode *STSM* controllers to control the roll motion. A comparison between the roll angle control towards zero, which can be achieved using either *ASus*, or semi-*ASus* or *ARB*, and its control to the new designed roll angle which can be only achieved using the *ASus* is also done;
- a new multilayer *GCC* controller which coordinates the *AFS*, *DYC* and *ASus* to enhance the maneuverability, lateral stability, rollover avoidance, and ride comfort (roll, pitch, and heave motions) at once. The sub-controllers are designed based on the *STSM*. The decision layer monitors the dynamics of the vehicle (driving situation), based on fuzzy logic rules and a stability criterion, to promote/attenuate the control objectives;
- a new multilayer decentralized control architecture which facilitates the *GCC*, by decoupling the control problem into two sub-control problems, and adopting

the $STSM$ control technique, where $AFS$ is responsible on the control of the yaw rate, and the roll angle, and $DYC$ is responsible on the control of the side-slip angle, while maintaining a high maneuverability, lateral stability and rollover avoidance performances;

- a new multilayer centralized control architecture which coordinates the $AFS$ and $DYC$, and combines the yaw rate control, the side-slip angle control, and the roll control, in one single $MIMO\ LPV/\mathcal{H}_\infty$ centralized controller, ensuring internal stability when switching between maneuverability, lateral stability and rollover avoidance objectives.

## 0.4 Thesis Outline

The thesis is organized in 5 chapters:

- **Chapter 1**: presents a full-vehicle nonlinear model validated on the professional simulator "SCANeR Studio", which can serve as a validation model, and different simplified vehicle models used for control purposes. Then, rollover and lateral stability performance criteria are evoked in the same chapter.

- **Chapter 2**: provides a brief introduction to the control techniques that are used in this thesis i.e. the immersion and invariance as a robust Lyapunov-based technique, the $STSM$ (robust) technique, and the $MIMO\ LPV/\mathcal{H}_\infty$ (robust and optimal) technique.

- **Chapter 3**: exposes the effect of roll control through the $ASus$ on the ride comfort, rollover avoidance, and the lateral stability based on time and frequency domains analysis. Roll reference generator is then proposed. Finally, several control laws are developed and compared together to control the roll motion through the $ASus$.

- **Chapter 4**: develops a decentralized multilayer $GCC$ controller involving $AFS$, $DYC$, and $ASus$. The $STSM$ technique is applied to develop the control layer, while some logic and fuzzy-logic rules are developed in the decision layer to coordinate the different controllers.

- **Chapter 5**: develops and compares a centralized and a decentralized multilayer architectures for $GCC$, involving only $AFS$ and $DYC$. The novelty w.r.t literature is the introduction of the roll control into the $GCC$ strategy without the need to include the suspensions. The $MIMO\ LPV/\mathcal{H}_\infty$ (respectively $STSM$) robust control technique is applied to develop the control layer of the centralized (respectively decentralized) architecture, while endogenous weighting parameters are developed in the decision layer for both architectures to coordinate the different controllers and objectives.

Finally, the thesis concludes with a summary about the obtained results and an outlook about potential improvements of our work.

## 0.5 Conclusion

In this chapter, the motivation of this work and a state of the art on *GCC* are exposed. Then, the vehicle dynamics performance criteria, including rollover avoidance, lateral stability, driving comfort, and ride comfort, are presented. Next chapter reviews the vehicle dynamics.

# Vehicle Dynamics

This chapter presents and analyzes several vehicle models aiming at understanding the vehicle dynamics. A complex nonlinear model called "full vehicle model" which is composed of several connected sub-models i.e. the vertical model, the lateral model, the longitudinal model, the road/tire contact model and the wheels dynamics model, is developed and validated on the professional simulator "SCANeR Studio". The full vehicle model serves to validate the active controllers when real experimentation and access to a professional simulator are not available. Another vehicle model which is called "bicycle model" is also presented in this chapter. The bicycle model is a simple linear model which describes the lateral vehicle motion when the vehicle operates in a stable region (no lateral skidding). This model can be used as a nominal (synthesis) model for controllers development. An "extended bicycle model" is also presented in this chapter. It a simple linear model which describes the coupled roll-lateral motion, showing the interaction between both dynamics.
Beside the vehicle models, the lateral stability (Stability Index $SI$) and the rollover avoidance (Load Transfer Ratio $LTR$) performance criteria defined in the Introduction Chapter are exposed.
Finally, the active actuators that will be controlled throughout this thesis i.e., the $AFS$, $ADB$, and $ASus$ are briefly introduced.

## 1.1 Full Vehicle Model

The literature is rich in vehicle models, more or less complex, depending on the use objective. Authors interested in vehicle stability have developed vehicle dynamics models in the horizontal plane called longitudinal and lateral models [Villagra et al., 2007], [Rajamani, 2012], [Guldner et al., 1996], [Doumiati et al., 2012], and [Ray, 1997]. Others motivated by the passengers' comfort and road holding, have developed quarter, semi and/or full vertical models to describe sprung mass roll, pitch and vibrations [Milliken et al., 1995], [Kiencke and Nielsen, 2000], [Rajamani, 2012], and [Chou and D'Andréa-Novel, 2005]. Based on these models, several full vehicle model have been developed in literature which consider the interaction effect between the different dynamics. In this section, a full vehicle model is presented, including a description of the sub-systems (components) that influence the most the vehicle dynamics i.e the tires, the suspension system, the steering system, the braking system, etc...
From our point of view, the full vehicle model could be presented as four sub-models

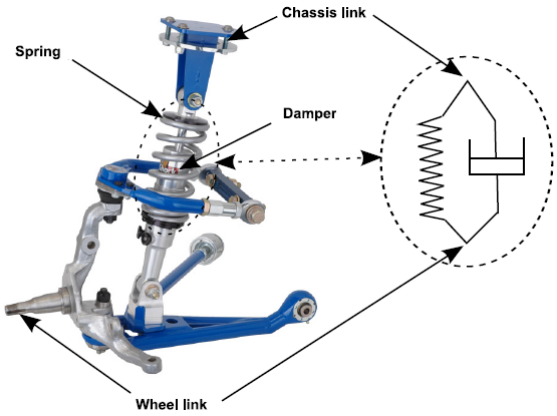


Figure 1.1 – Passive suspension system

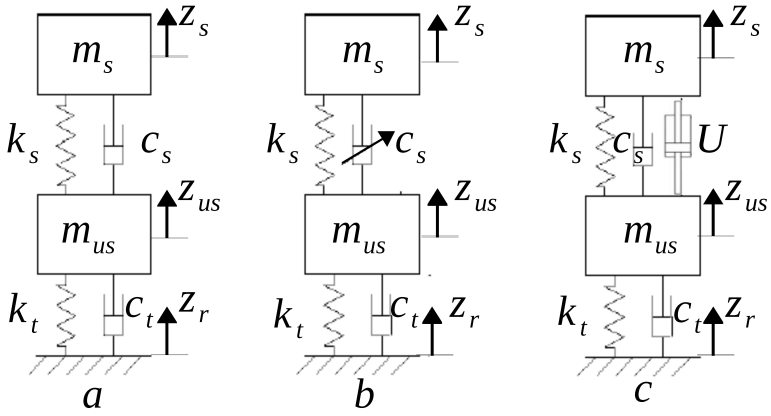


Figure 1.2 – Types of suspension system(a: passive; b: semi-active; c: active)

combined together to describe the full vehicle dynamics when moving on ground. These sub-models are:

- the vehicle vertical model which describes the suspension deflection, the tire deflection, and the sprung mass roll, pitch and heave motions;
- the vehicle longitudinal and lateral model (in the horizontal plan) which describes the longitudinal acceleration, the lateral acceleration and the vehicle yaw rate;
- the tire/road contact model;
- the wheels dynamics model.

### 1.1.1 Vertical Model

The vehicle vertical model describes a part of the vehicle dynamics, i.e. the suspension deflection, the wheels bounce, and the sprung mass roll, pitch and heave motions.

The suspension system relies the sprung and unsprung masses (chassis to wheel link). The classical vehicle suspension system is shown in Figure 1.1. It is formed by a spring and a damper with constant coefficients. The suspension system has two main goals: the first one is to isolate the vehicle chassis from an uneven ground in order to improve passenger's comfort; the second one is to provide good road-holding properties, in order to ensure passenger's safety. Indeed, the suspensions help the wheels to maintain a sufficient contact with the road in presence of irregularities and load transfer.
In the recent decades, automotive societies and researchers have had interest to improve passenger's comfort and the road-holding properties, either through the road profile estimation or through evolving the performance of the suspension system. Indeed, the road profile estimation and prediction represents a useful information that can be used in the feedback signals to adapt the behavior of the new controlled types of suspensions [Doumiati et al., 2011], [Doumiati et al., 2017], and [Imine et al., 2005]. From the other hand, there has been a development of new types of suspension systems, the semi-$ASus$ and the $ASus$ systems [Rajamani, 2012]. Figure 1.2.a shows the passive suspension system model formed by a spring and a damper which has a passive behavior due to its constant parameters (stiffness and damping coefficient). Generally, these parameters are selected by analyzing several evaluation criteria [Rajamani, 2012]. This type of suspensions lacks the capability of responding accurately to some frequency excitations and to adjust its behavior depending on the driving situation. Figure 1.2.b shows the semi-$ASus$ system model which has a variable damping coefficient making the suspension properties more flexible to handle both comfort and road holding objectives. Mainly, there are two types of semi-$ASus$: the variable-orifice damper and the magneto(electro)-rheological (MR) damper. In the the variable-orifice damper, the damping force of can be changed through controlling the diameter of the orifice in the piston. In the magneto(electro)-rheological (MR) damper, the fluid has rheological properties that can be changed with a controlled magnetic (electric) field, making the damping coefficient controllable. For more details about the semi-$ASus$ refer to [Guglielmino et al., 2008], and [Savaresi et al., 2010]. Figure 1.2.c shows the $ASus$ system model which is formed -in addition to the spring and the damper- by a controlled hydraulic or pneumatic actuator which adds to the system a new controlled force called the active force. This type of suspension system is the most reactive with the variation of the vehicle's dynamics, but the most expensive due to its cost and energy consumption.

#### 1.1.1.1 Quarter Vehicle Vertical Model

Figure 1.3 shows the quarter vehicle vertical model. When a vehicle moves, the suspension system and the tires undergo dynamical motions/vibrations. The equations that describe the system dynamics at the $ij$ ($i = \{f : front, r : rear\}$ and

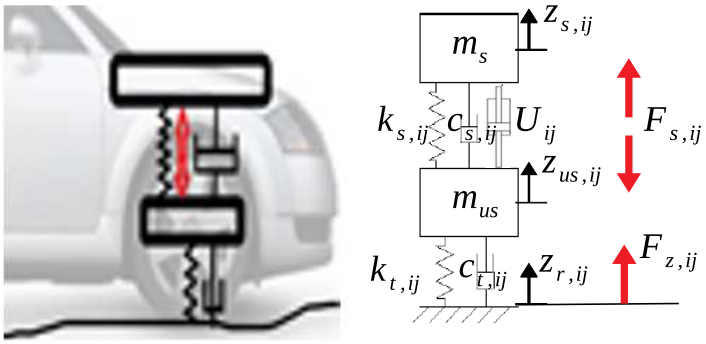


Figure 1.3 – Quarter vehicle vertical model

$j = \{r : right, l : left\}$) corner of the vehicle are:

$$F_{s,ij} = -K_{s,ij}(z_{s,ij} - z_{us,ij}) - C_{s,ij}(\dot{z}_{s,ij} - \dot{z}_{us,ij}) + U_{ij}, \tag{1.1}$$

$$\ddot{z}_{us,ij} = \frac{1}{m_{us,ij}}(F_{z,ij} - F_{s,ij}), \tag{1.2}$$

$$F_{z,ij} = -K_{t,ij}(z_{us,ij} - z_{r,ij}) - C_{t,ij}(\dot{z}_{us,ij} - \dot{z}_{r,ij}), \tag{1.3}$$

where $K_{t,ij}$, $C_{t,ij}$, $K_{s,ij}$, $C_{s,ij}$, $U_{ij}$, $F_{s,ij}$, and $F_{z,ij}$, are respectively, the tire stiffness coefficient, the tire damping coefficient, the suspension stiffness coefficient, the suspension damping coefficient, the actuator force of the $ASus$ system (active force), the total (passive+active) suspension force, and the vertical force on the tire of the $ij$ corner. $z_{s,ij}$ and $z_{us,ij}$ are respectively the vertical displacement of the sprung mass and the unsprung mass (wheel bounce). $z_{r,ij}$ and $g$ are respectively the vertical profile of the road and the gravitational constant. $z_{s,ij}$ and $z_{us,ij}$, with their time derivatives, are exogenous variables to this model, they are provided by the full vehicle vertical model developed in the next sub-section.

#### 1.1.1.2 Full Vehicle Vertical Model

In order to express the vertical displacement of each corner, and the roll, pitch and heave motions of the sprung mass at the center of gravity, the full vehicle vertical model is developed (see Figure 1.4).
Let $\theta$, $\phi$ and $z_s$ be respectively the roll, pitch and heave of the sprung mass. Geometrically, the vertical displacements of the vehicle corners $z_{s,ij}$ can be approximated by:

$$z_{s,fr} = z_s - t_f sin\theta - l_f sin\phi, \tag{1.4}$$

$$z_{s,fl} = z_s + t_f sin\theta - l_f sin\phi, \tag{1.5}$$

$$z_{s,rr} = z_s - t_r sin\theta + l_r sin\phi, \tag{1.6}$$

$$z_{s,rl} = z_s + t_r sin\theta + l_r sin\phi, \tag{1.7}$$

where $t_f$, $t_r$, $l_f$ and $l_r$ are respectively half front track, half rear track, wheelbase to the front and wheelbase to the rear.

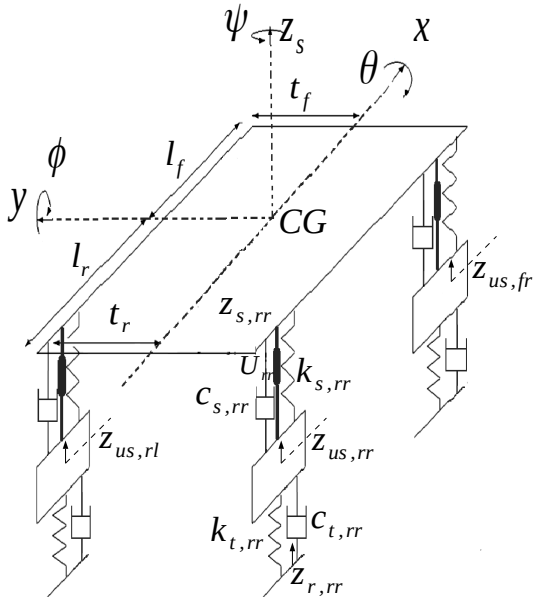


Figure 1.4 – Full vehicle vertical model

The vertical velocities of the vehicle corners $\dot{z}_{s,ij}$ are the time derivatives of the four above equations, such that:

$$\dot{z}_{s,fr} = \dot{z}_s - t_f\dot{\theta}cos\theta - l_f\dot{\phi}cos\phi, \tag{1.8}$$

$$\dot{z}_{s,fl} = \dot{z}_s + t_f\dot{\theta}cos\theta - l_f\dot{\phi}cos\phi, \tag{1.9}$$

$$\dot{z}_{s,rr} = \dot{z}_s - t_r\dot{\theta}cos\theta + l_r\dot{\phi}cos\phi, \tag{1.10}$$

$$\dot{z}_{s,rl} = \dot{z}_s + t_r\dot{\theta}cos\theta + l_r\dot{\phi}cos\phi. \tag{1.11}$$

The dynamic equations of the sprung mass i.e. the roll, pitch and heave (angular) accelerations ($\ddot{\theta}$, $\ddot{\phi}$, and $\ddot{z}_s$) can be modeled as:

$$\begin{aligned}\ddot{\theta} = \frac{1}{I_x + M_s h_\theta^2}[&(-F_{s,fr} + F_{s,fl})\, t_f + (-F_{s,rr} + F_{s,rl})\, t_r \\ &+ M_s\,(h_\theta\ cos\,(\theta) + z_s)\, a_y + M_s\,(h_\theta\ sin\,(\theta) + z_s)\, g],\end{aligned} \tag{1.12}$$

$$\begin{aligned}\ddot{\phi} = \frac{1}{I_y + M_s h_\phi^2}[&-(F_{s,fr} + F_{s,fl})\, l_f + (F_{s,rr} + F_{s,rl})\, l_r \\ &+ M_s\,(h_\phi\ cos\,(\phi) + z_s)\, a_x + M_s\,(h_\phi\ sin\,(\phi) + z_s)\, g],\end{aligned} \tag{1.13}$$

$$\ddot{z}_s = \frac{1}{M_s}(F_{s,fr} + F_{s,fl} + F_{s,rr} + F_{s,rl}), \tag{1.14}$$

where, $M_s$, $h_\theta$ and $h_\phi$ are respectively the sprung mass mass, the distance between the center of gravity of the sprung mass and the roll rotation center, and the distance between the center of gravity of the sprung mass and the pitch rotation center. $I_x$ and $I_y$ are respectively the moment of inertia of the sprung mass around $x$ axis and $y$ axis. $a_x$ and $a_y$ are considered as exogenous inputs to this model, they are calculated in the lateral and longitudinal vehicle model.

### 1.1.2 Longitudinal-Lateral Model

The longitudinal and lateral vehicle models can be derived by applying the second Newton law to the horizontal vehicle scheme shown in Figure 1.5. The governed equations are given by:

$$Ma_x = (F_{x,fl}\cos\delta_{fl} + F_{x,fr}\cos\delta_{fr} - F_{y,fl}\sin\delta_{fl} - F_{y,fr}\sin\delta_{fr} + F_{x,rl} + F_{x,rr}), \tag{1.15}$$

$$Ma_y = (F_{x,fl}\sin\delta_{fl} + F_{x,fr}\sin\delta_{fr} - F_{y,fl}\cos\delta_{fl} + F_{y,fr}\cos\delta_{fr} + F_{y,rl} + F_{y,rr}), \tag{1.16}$$

$$\begin{aligned} I_z\ddot{\psi} = &- t_f(F_{x,fl}\cos\delta_{fl} - F_{x,fr}\cos\delta_{fr} - F_{y-fl}\sin\delta_{fl} + F_{y,fr}\sin\delta_{fr}) \\ &+ l_f(F_{x,fl}\sin\delta_{fl} + F_{x,fr}\sin\delta_{fr} + F_{y,fl}\cos\delta_{fl} + F_{y,fr}\cos\delta_{fr}) \\ &- l_r(F_{y,rl} + F_{y,rr})) - t_r(F_{x,rl} + F_{x,rr})), \end{aligned} \tag{1.17}$$

where $a_x$, $a_y$, and $\ddot{\psi}$ are respectively the longitudinal acceleration, the lateral acceleration, and the yaw acceleration. $M$ is the total vehicle mass and $I_z$ is the moment of inertia of the vehicle around $z_s$ axis. $F_{x,ij}$ and $F_{y,ij}$ are respectively the longitudinal and lateral forces applied to the tire $ij$ as shown in Figure 1.7. These forces are determined (in the next sub-section) based on the tire/road contact properties and the vertical force $F_{z,ij}$ applied to the tire.
A virtual variable called "side-slip angle $\beta$" is an important variable used to determine the vehicle stability. The side-slip angle is the angle between the longitudinal direction of the vehicle and the speed vector $V$ of the vehicle at its center of gravity as shown in Figure 1.6. The side-slip velocity can be found by projecting the tires' lateral forces to the speed vector $V$ (Figure 1.5). The side-slip dynamics is given by the following equation:

$$\begin{aligned} \dot{\beta} = &\frac{1}{MV}(F_{x,fr}\sin(\delta_{fr} - \beta) + F_{x,fl}\sin(\delta_{fl} - \beta) + F_{y,fr}\cos(\delta_{fr} - \beta) \\ &+ F_{y,fl}\cos(\delta_{fl} - \beta) - (F_{x,rr} + F_{x,rl})\sin(\beta) + (F_{y,rr} + F_{y,rl})\cos(\beta)) - \dot{\psi}. \end{aligned} \tag{1.18}$$

When the vehicle operates in the linear region (lateral tire forces not saturated), the side-slip dynamics can be approximated by projecting the lateral acceleration $a_y$ to the longitudinal speed vector $V_x$ such as:

$$\dot{\beta} = \frac{a_y}{MV_x} - \dot{\psi}. \tag{1.19}$$

### 1.1.3 Tire/Road Contact Model

The tire is the interface between the vehicle and the road. It has a double functionality, the first one is its vertical functionality to handle a part of the vehicle mass taking into account the vehicle vertical dynamics and road perturbations. The second one is to transform the wheel rotation into planar vehicle motion due to the

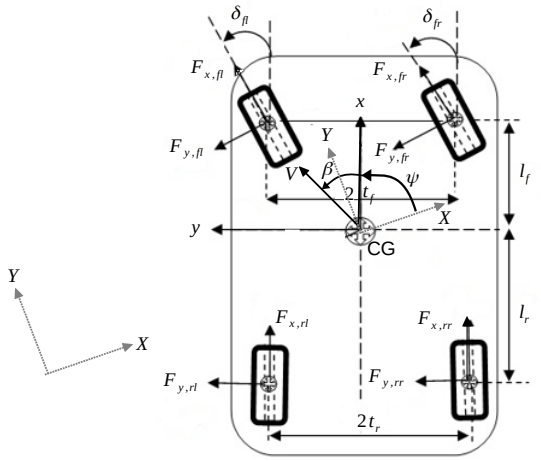


Figure 1.5 – Vehicle lateral/longitudinal model

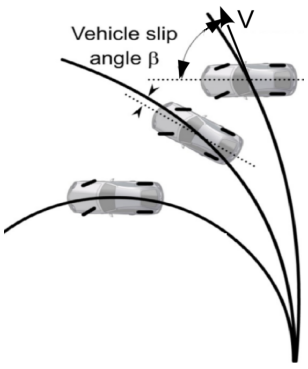


Figure 1.6 – Vehicle side-slip


Figure 1.7 – Tire forces

tire/road contact properties, by creating the lateral and longitudinal forces acting on the tires. These functionalities can be described by the tire vertical model and tire/road contact model.
In literature, the tire has different vertical models, some researchers model the tire as a spring and a damper with constant stiffness and damper coefficients, while others neglect the damping coefficients. Automotive societies and vehicle dynamics simulators as SCANeR Studio (OKTAL) model the tire as a spring and a damper with passive variable stiffness and damping coefficients, depending on the suspension deflection and its velocity. In this thesis, the tire is supposed a punctual mass at its center of gravity and modeled as a spring and a damper with constant stiffness and damping coefficients (see Figure 1.8).
On the same time, the literature is rich in tire/road contact models which aim at describing the lateral and longitudinal tire forces as nonlinear functions of the vertical load, tire properties, and road properties. Here, we cite the well-known models:

- analytical models which are developed from the basic theory of sliding and adherence constraints, taking into account tire parameters (material, pressure, rigidity) and the environment (temperature, road nature);
- Pacejka-Baker model known by its magic formula [Pacejka and Besselink, 1997];
- DUGOFF model [Dugoff et al., 1970];
- Burckhardt/Kiencke model [Kiencke, 1993];
- LuGrue model or Carlos Canudas-de-Wit model [Canudas-de Wit et al., 2003].

In this thesis, the DUGOFF model is adopted because of its simplicity and computational implementation where the tire longitudinal and lateral forces can

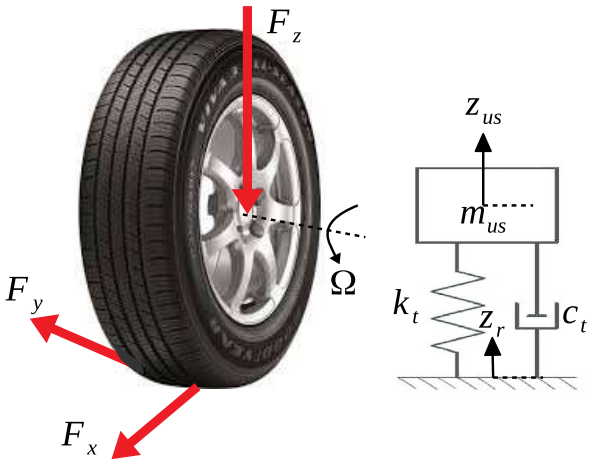


Figure 1.8 – Tire vertical model

be expressed as:

$$F_{x,ij} = C_\sigma \frac{\sigma_{x,ij}}{1-\sigma_{x,ij}} f(\lambda_{ij}), \tag{1.20}$$

$$F_{y,ij} = C_\alpha \frac{\tan(\alpha_{ij})}{1-\sigma_{x,ij}} f(\lambda_{ij}), \tag{1.21}$$

$$f(\lambda_{ij}) = \begin{cases} (2-\lambda_{ij})\lambda_{ij} & for \quad \lambda_{ij} < 1 \\ 1 & for \quad \lambda_{ij} > 1, \end{cases} \tag{1.22}$$

$$\lambda_{ij} = \frac{\mu F_{z,ij}(1-\sigma_{x,ij})}{2 \times \sqrt{(C_\sigma \sigma_{x,ij})^2 + (C_\alpha \tan(\alpha_{ij}))^2}}. \tag{1.23}$$

As these equations show, the lateral and longitudinal tire forces ($F_{y,ij}$ and $F_{x,ij}$) only depend on three parameters i.e. the longitudinal tire stiffness $C_\sigma$, the lateral tire stiffness (cornering finesses) $C_\alpha$, and the road adherence $\mu$. From DUGOFF model, $F_{y,ij}$ and $F_{x,ij}$ are nonlinear functions of the tire variables i.e. the longitudinal tire slipping $\sigma_{x,ij}$, the side slip angle of the tire $\alpha_{ij}$, and the vertical load applied on the tire $F_{z,ij}$. $\sigma_{x,ij}$ and $\alpha_{ij}$ are calculated in the wheels dynamics model.

### 1.1.4 Wheels Dynamics Model

The wheel side slip angle $\alpha_{ij}$ represents the deviated angle between the wheel speed vector and the wheel orientation as shown in Figure 1.9. $\alpha_{ij}$ of each wheel can be obtained based on the speed vector of the vehicle at its center of gravity and the

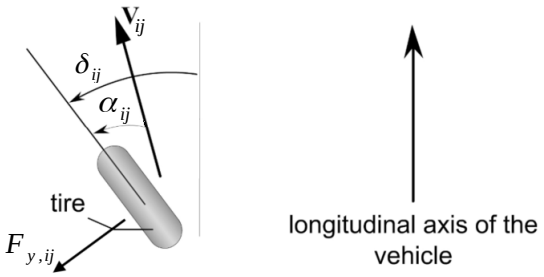


Figure 1.9 – Tire side-slip

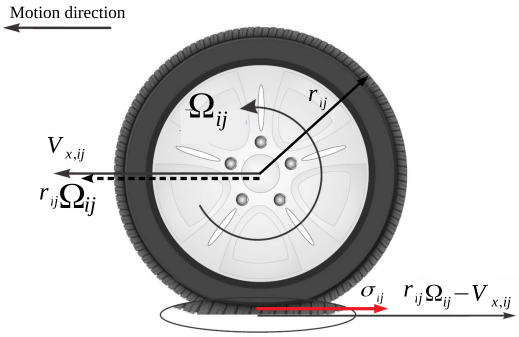


Figure 1.10 – Actual vs expected wheel speed

vehicle geometry, as given in the following equations:

$$\alpha_{fr} = \delta_{fr} - \arctan\left(\frac{V_y + l_f\dot{\psi}}{V_x + t_f\dot{\psi}}\right), \tag{1.24}$$

$$\alpha_{fl} = \delta_{fl} - \arctan\left(\frac{V_y + l_f\dot{\psi}}{V_x - t_f\dot{\psi}}\right), \tag{1.25}$$

$$\alpha_{rr} = -\arctan\left(\frac{V_y - l_r\dot{\psi}}{(V_x + t_r\dot{\psi}}\right), \tag{1.26}$$

$$\alpha_{rl} = -\arctan\left(\frac{V_y - l_r\dot{\psi}}{V_x - t_r\dot{\psi}}\right). \tag{1.27}$$

The longitudinal tire slipping represents the difference between the actual linear wheel speed in the longitudinal direction $V_{x,ij}$ at its center of gravity and the expected one $r_{ij}\Omega_{ij}$ due to its rotation (see Figure 1.10). The longitudinal tire slipping of the tire $ij$ is given by the following equation:

$$\sigma_{x,ij} = \begin{cases} \frac{r_{ij}\Omega_{ij} - V_{x,ij}}{r\Omega_{ij}} & acceleration \\ \frac{r_{ij}\Omega_{ij} - V_{x,ij}}{V_{x,ij}} & braking \end{cases} \tag{1.28}$$

where $r_{ij}$ is the effective tire radius and $\Omega_{ij}$ is its angular velocity. $\Omega_{ij}$ has the dynamics given in the following equation:

$$I_r\dot{\Omega}_{ij} = -r_{ij}F_{x,ij} + C_{m,ij} - C_{f,ij}, \tag{1.29}$$

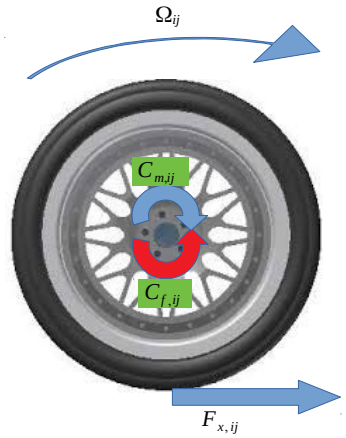


Figure 1.11 – Wheel dynamics

where $I_r$ is the moment of inertia around the wheel axis of rotation. $C_{m,ij}$ and $C_{f,ij}$ are respectively the motor and braking torques applied to the wheel as shown in Figure 1.11. $C_{m,ij}$ is transmitted from the motor to the wheels through the power transmission system, and $C_{f,ij}$ is generated by the braking system.
In this thesis, the motor and braking torques are considered as the inputs to the vehicle, neither the power transmission system nor the braking system are modeled, since we limit the study to the chassis dynamics. Similar for steering system, we directly consider the steering angle on the front wheels.

Before validating the full vehicle model, let develop the vehicle performance criteria based on the vehicle dynamics. Then the full vehicle model and the performance criteria will be validated using "SCANeR Studio Simulator".

## 1.2 Vehicle Dynamics Performance Criteria

Several performance criteria are already defined in sub-section 0.2.2. This sub-section provides analytical equations of the $LTR$, and the lateral $SI$ which evaluate the most critical features discussed in this thesis i.e. the rollover avoidance and the lateral stability.

$LTR$ reflects the vertical load transfer from the inside to the outside wheels w.r.t the corner (turn). the $LTR$ is defined in [Rajamani, 2012] and described in (1.30) by:

$$LTR = \frac{F_{zr} - F_{zl}}{F_{zr} + F_{zl}}, \tag{1.30}$$

where $F_{zr}$ and $F_{zl}$ are respectively the vertical forces on the right and left side wheels. The rollover is supposed to start when the vehicle inner wheels lift off from ground (even if in some cases the wheels can lift off and then come back to the ground, but the full nonlinear models cannot recover these special cases which create discontinuity in the tire/road contact model). Thus, the rollover starts when $F_{zl}$ or

$F_{zr}$ becomes zero, which means all the load is on the outer wheels. Hence, it occurs when the $LTR = \pm 1$. $LTR$ varies between $-1$ and 1. When $|LTR| > \overline{LTR}$, where $\overline{LTR}$ a positive constant higher threshold, a rollover risk is detected. Under a lower positive constant threshold $\underline{LTR}$, the vehicle is not subjected to a rollover risk.
The $LTR$ defined in (1.30) can be used only to evaluate the rollover risk a posterori by simulation, since the vertical tire forces are not measured in real time application. An estimation of $LTR$, when the roll dynamics is moderate, is given in (1.31) as a linear combination of the roll angle, its rate of change and the lateral acceleration [Yoon et al., 2007], [Rajamani, 2012], [Peng and Eisele, 2000]:

$$LTR = r_1\theta + r_2\dot{\theta} + r_3 a_y, \tag{1.31}$$

where $r_1$, $r_2$ and $r_3$ are identified depending on the vehicle parameters. The identified value of $r_1$ and $r_2$ are given later in Table 5.1, while $r_3 = 0$.
The estimated $LTR$ of (1.31) is used in this thesis to monitor the rollover risk. To do so, $\dot{\theta}$ is supposed to be measured by a gyrometer and given at the $CG$ of the vehicle, in real time control; $\theta$ is integrated from $\dot{\theta}$ ($\theta$ could be directly taken from the Inertial Measurement Unit IMU if available).

The lateral $SI$ reflects the orientation of the vehicle w.r.t its speed vector at the $CG$, and its rate of change. $SI$ is expressed in (1.32) as [Chen et al., 2016]:

$$SI = \left| q_1\beta + q_2\dot{\beta} \right|, \tag{1.32}$$

where $q_1$ and $q_2$ are identified depending on the vehicle parameters and road adherence $\mu$ to characterize the stable boundary of the $\beta - \dot{\beta}$ phase plane. $SI$ is normalized and varies between 0 and 1. For $SI \leq \underline{SI}$ (a predefined lower threshold depending on the vehicle and road parameters), the vehicle is in normal driving situations (stable region). Up to a predefined higher threshold $\overline{SI}$, the vehicle is considered in the critical lateral stability region, where active safety controllers have to be triggered to cover back the lateral stability of the vehicle. Beyond $\overline{SI}$ the vehicle operates in the unstable region.
In order to use the $SI$ criterion for monitoring, the side-slip angle $\beta$ (and its velocity $\dot{\beta}$) have to be estimated. Several observer approaches that suit the real time constraints implementation and vehicle dynamics have been proposed in literature to estimate $\beta$, e.g. an Extended Kalman Filter EKF based observer as done in [Chen et al., 2016] and [Doumiati et al., 2012].

## 1.3 Full Vehicle Model Validation

The full vehicle model serves to perform several driving scenarios in order to analyze the vehicle dynamics. This model is recommended when the professional simulators or real experimentation are not available. Indeed, in this thesis, some of the vehicle controllers are validated on the full vehicle model and others on the professional simulator "SCANeR Studio" (this issue is discussed more later). However, this section aims at validating the full vehicle model in order to show its accuracy. Thus, the ISO

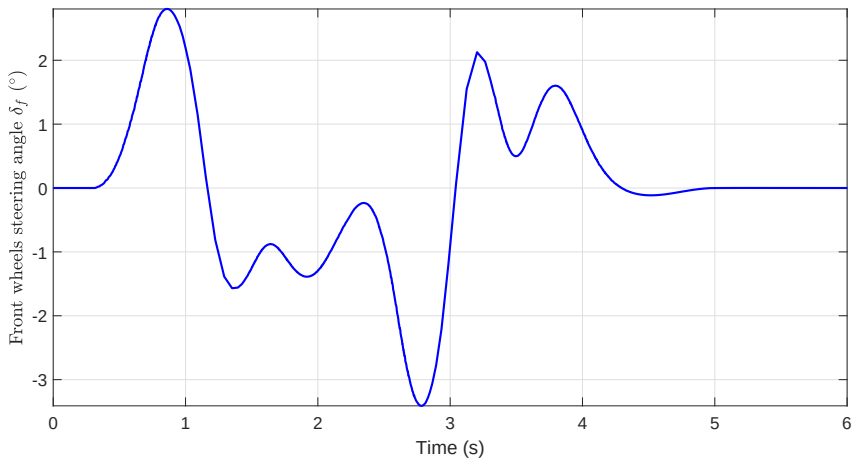


Figure 1.12 – Steering angle

3888 Double Lane Change ($DLC$) test at a constant speed of 100 $km/h$ is performed, where the results of the full vehicle model are compared to the professional simulator "SCANeR Studio". The vehicle parameters used for simulation are given in Table 2. Figure 1.12 shows the front wheels steering angle applied to both simulations, where at 100 $km/h$, it solicits the lateral and roll motions of the vehicle, making the vehicle operates in a moderate region in terms of lateral stability and load transfer. Figures 1.13, 1.14, and 1.15 respectively show and validate the solicitations of the vehicle yaw rate, the lateral acceleration, and the roll angle. The pitch angle and the vehicle heave are less solicited by this test as shown in Figures 1.16, and 1.17. Figures 1.18, 1.19, and 1.20 respectively show and validate the vertical, lateral, and longitudinal forces of all the vehicle tires. Figure 1.21 shows the longitudinal speed of the vehicle which remains constant 100 $km/h$. The longitudinal speed had to drop because of the friction of tires' with the road, but to perform the ISO test, the built-in longitudinal speed controller of the simulator adjusts the speed by introducing a motor torque on the wheels which is also applied to the full vehicle model. Figures 1.22, 1.23, and 1.24 respectively show and validate the side-slip angle, side-slip rate, and the $SI$ of the vehicle which operates in the moderate lateral stability region ($SI \approx 0.5$). Figure 1.25 shows and validates the $LTR$ which is also in the moderate range.

## 1.4 Bicycle Model

The vehicle bicycle model is a simplified version of the full vehicle model. It is usually used as the desired reference model when controlling/stabilizing the lateral vehicle motion. The bicycle model consists of merging each two wheels of the same axle together at the center of the axle as shown in Figure 1.26. The bicycle expresses the yaw rate and the side-slip angle of the vehicle at its center of gravity as the following:

$$\begin{aligned} I_z\ddot{\psi} &= F_{yf}l_f + F_{yr}l_r, \\ MV\left(\dot{\beta}+\dot{\psi}\right) &= F_{yf} + F_{yr}. \end{aligned} \tag{1.33}$$

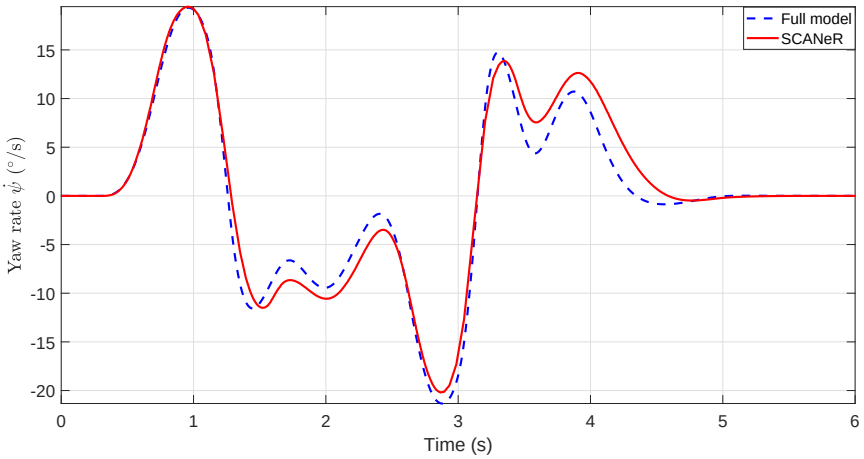


Figure 1.13 – Yaw rate

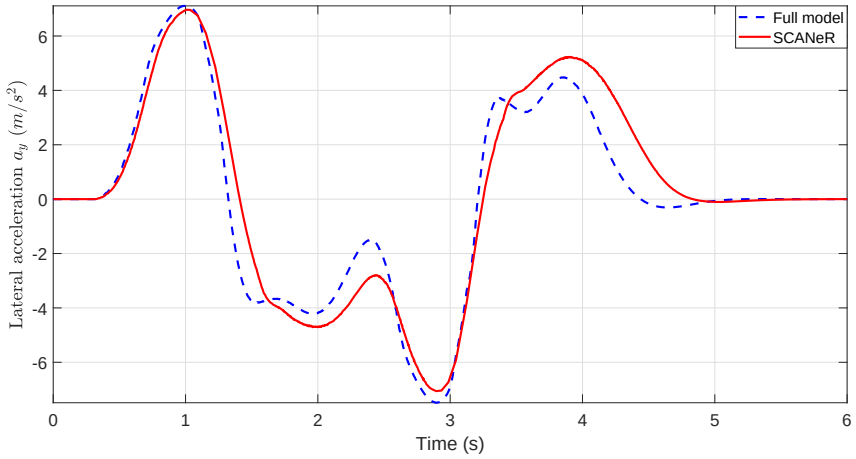


Figure 1.14 – Lateral acceleration

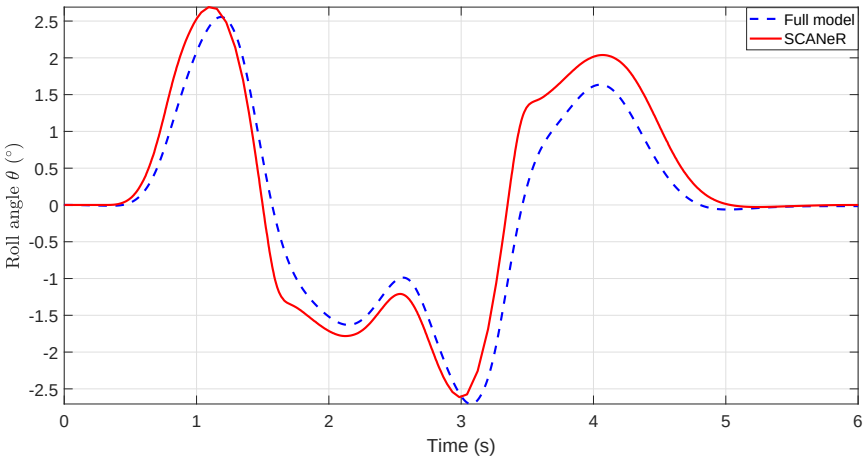


Figure 1.15 – Roll angle

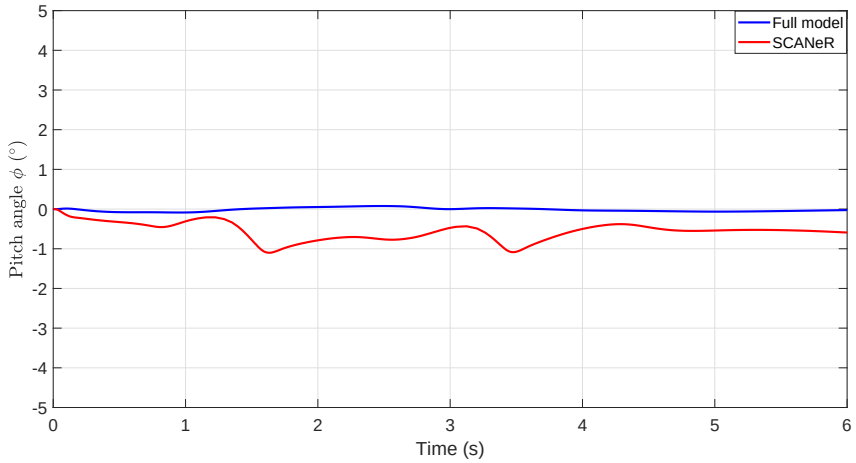


Figure 1.16 – Pitch angle

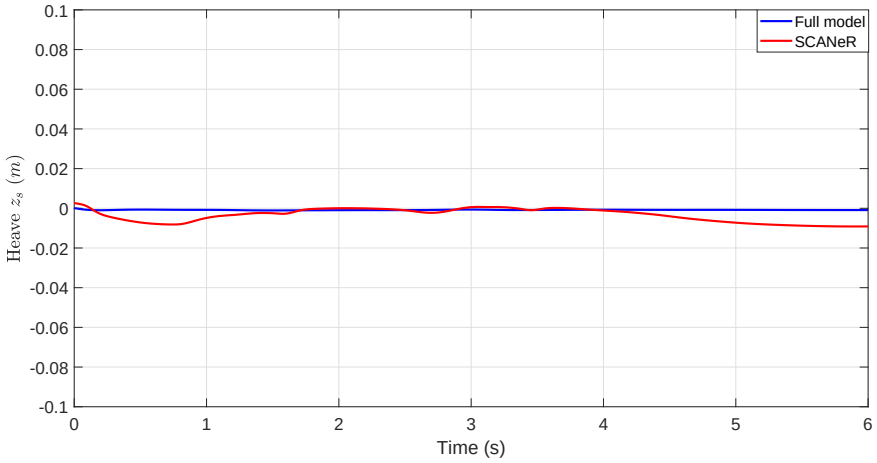


Figure 1.17 – Heave

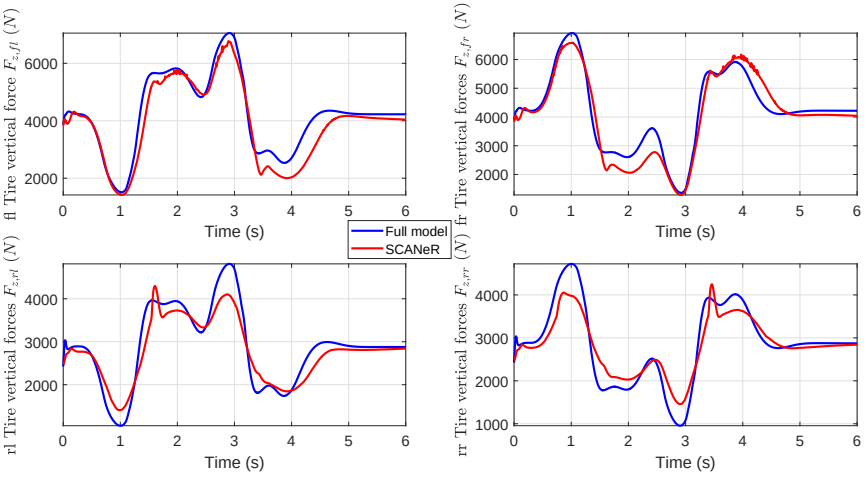


Figure 1.18 – Tire's Vertical forces

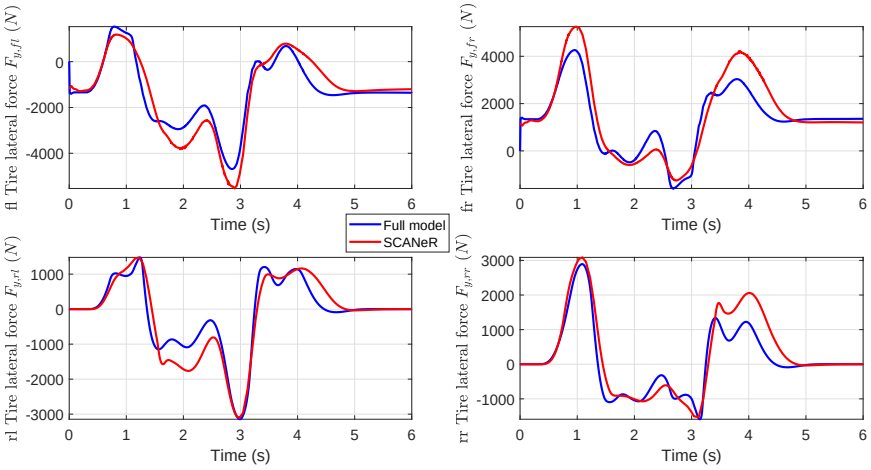


Figure 1.19 – Tire's lateral forces

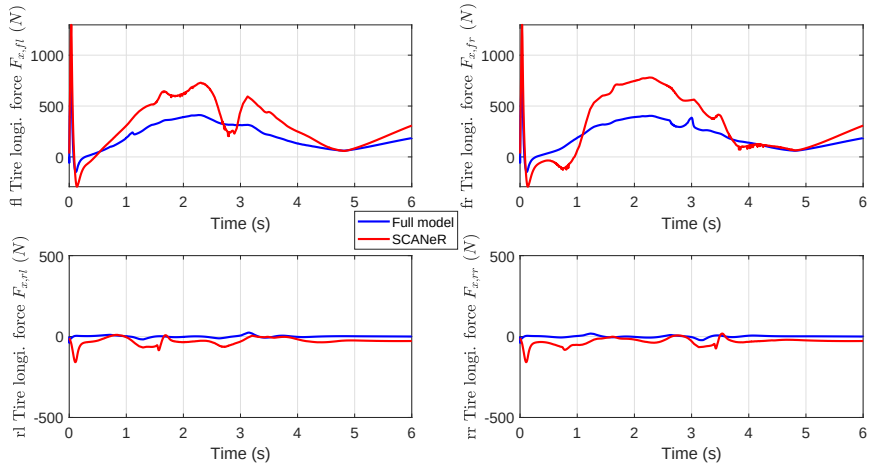


Figure 1.20 – Tire's longitudinal forces

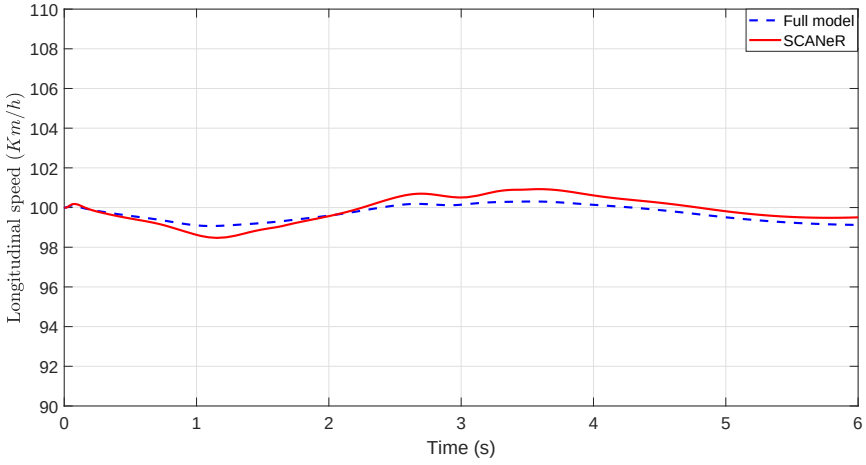


Figure 1.21 – Longitudinal speed

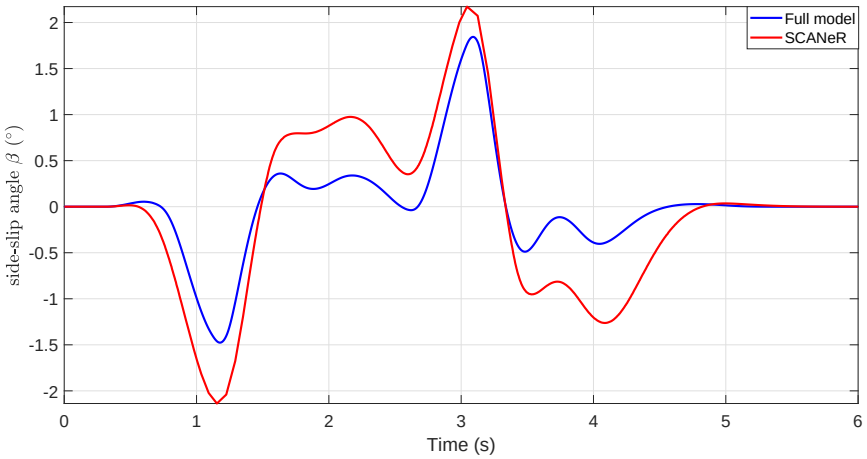


Figure 1.22 – Side-slip angle

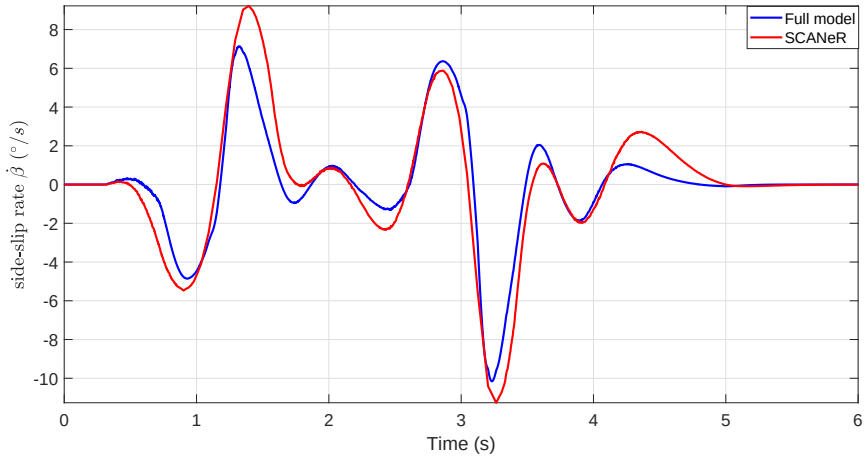


Figure 1.23 – Side-slip rate

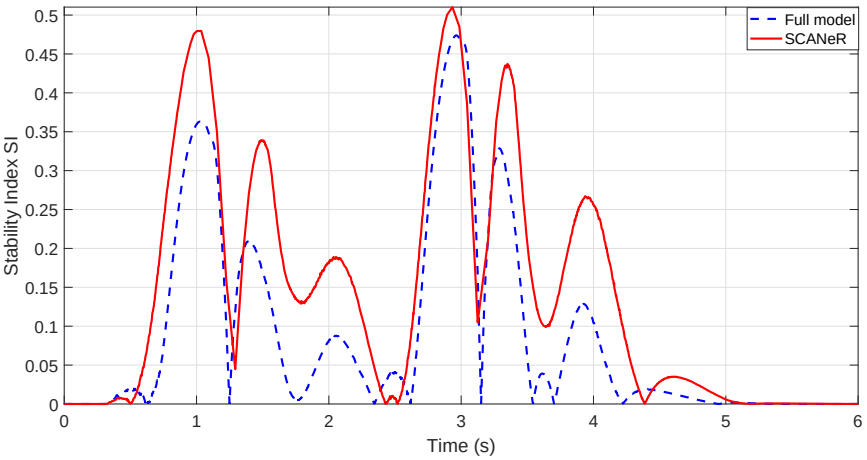


Figure 1.24 – Stability Index $SI$

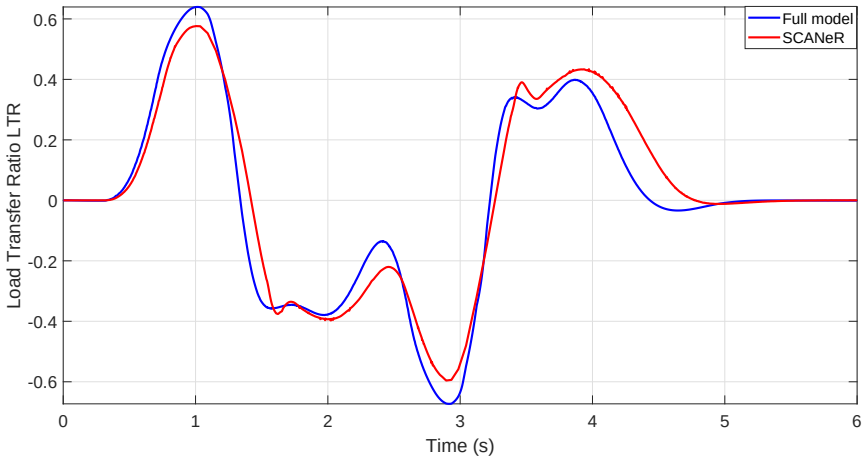


Figure 1.25 – Load transfer ratio $LTR$

$F_{yf}$ and $F_{yr}$ respectively represent the lateral force of the tire on the front axle and on the rear axle. $F_{yf}$ and $F_{yr}$ are supposed to be linear to the wheels side-slip angle such that:

$$\begin{aligned} F_{yf} &= \mu C_f \alpha_f, \\ F_{yr} &= \mu C_r \alpha_r, \end{aligned} \tag{1.34}$$

where $C_f$ and $C_r$ are respectively the double of the front and rear tires cornering stiffness. The wheels side-slip angles are found using the following equations:

$$\begin{aligned} \alpha_f &= -\beta - \frac{l_f \dot{\psi}}{V} + \delta_f, \\ \alpha_r &= -\beta + \frac{l_r \dot{\psi}}{V}, \end{aligned} \tag{1.35}$$

where $\delta_f$ is the front steering angle. Throughout of this thesis, $\delta_f$ could represent $\delta_d$ or $\delta_t$ (where $\delta_t = \delta_d + \delta_c$) depending on the context. To be noted also, the vehicle speed $V$ and the longitudinal vehicle speed $V_x$ are used equivalently when the vehicle

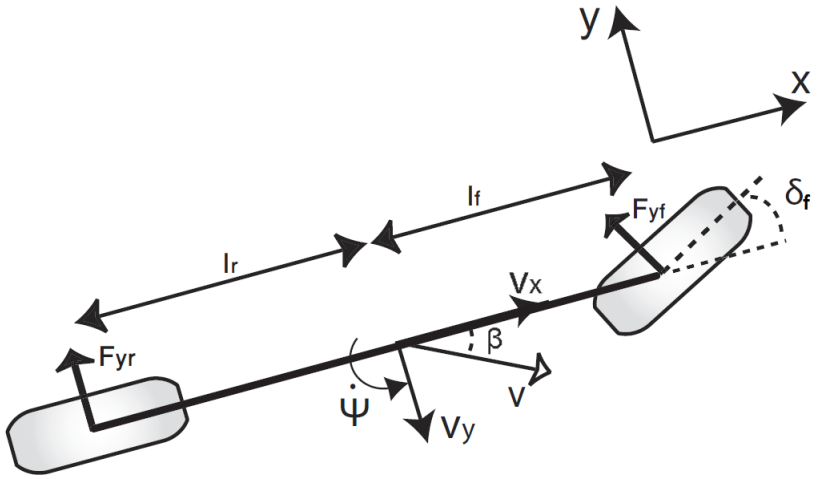


Figure 1.26 – Bicycle model

$$\dot{X} = \begin{bmatrix} \ddot{\psi} \\ \dot{\beta} \\ \dot{\theta} \\ \ddot{\theta} \end{bmatrix} = \underbrace{\begin{pmatrix} a_{11} & a_{12} & a_{13} & a_{14} \\ a_{21} & a_{22} & a_{23} & a_{24} \\ 0 & 0 & 0 & 1 \\ a_{41} & a_{42} & a_{43} & a_{44} \end{pmatrix}}_{A} \begin{bmatrix} \dot{\psi} \\ \beta \\ \theta \\ \dot{\theta} \end{bmatrix} + \underbrace{\begin{pmatrix} b_{u,11} \\ b_{u,21} \\ 0 \\ b_{u,41} \end{pmatrix}}_{B_1} \delta_f \tag{1.38}$$

motion is linear.
The state space representation of the bicycle model can be written as:

$$\begin{pmatrix} \ddot{\psi}_{bic} \\ \dot{\beta}_{bic} \end{pmatrix} = \begin{bmatrix} -\mu \frac{{l_f}^2 c_f + {l_r}^2 c_r}{I_z V_x} & \mu \frac{l_r c_r - l_f c_f}{I_z} \\ -1 + \mu \frac{l_r c_r - l_f c_f}{M {V_x}^2} & -\mu \frac{c_f + c_r}{M V_x} \end{bmatrix} \begin{pmatrix} \dot{\psi}_{bic} \\ \beta_{bic} \end{pmatrix} + \begin{bmatrix} \mu \frac{l_f c_f}{I_z} \\ \mu \frac{c_f}{M V_x} \end{bmatrix} \delta_f. \tag{1.36}$$

To be mention that the bicycle model does not consider any of the vehicle vertical motion i.e. wheels bounce, sprung mass motion, load transfer, etc...
The next section presents an extended bicycle model including the sprung mass roll dynamics due to its particular effect on the lateral motion behavior as will be shown in Chapter 5.

## 1.5 Extended Bicycle Model

The extended bicycle model is a coupled lateral-roll vehicle model. It is a linear simplified vehicle model which combines the vehicle yaw and side-slip to the roll motion. This model is suitable to analyze the effect of the roll motion control on the lateral stability of the vehicle. A frequency and time domain study is conducted in Chapter 3 to show this coupled-effect. The extended bicycle model is inspired from literature [Vu et al., 2017] as the following:

$$\begin{aligned} I_z \ddot{\psi} &= F_{yf} l_f + F_{yr} l_r + I_{xz} \ddot{\theta}, \\ MV \left( \dot{\beta} + \dot{\psi} \right) &= F_{yf} + F_{yr} + M_s h_\theta \ddot{\theta}, \\ \left( I_x + M_s h_\theta^2 \right) \ddot{\theta} &= M_s h_\theta V \left( \dot{\beta} + \dot{\psi} \right) + (M_s g h_\theta - K_\theta) \theta - C_\theta \dot{\theta}. \end{aligned} \tag{1.37}$$

As can be seen, the extended bicycle model is an improved version of the bicycle model where firstly the roll dynamics is described by a linear differential equation and secondly it is included into the lateral motion equations. By substituting (1.35) in (1.34), and then in (1.37), the state space representation of the extended bicycle model can be formalized as in (1.38), where $X = [\dot{\psi}, \beta, \theta, \dot{\theta}]^T$ is the state vector. The elements of the state matrix $A \in I\!R^{4\times4}$, and the input matrix $B_1 \in I\!R^{4\times1}$ are formalized in Appendix .1.

## 1.6 Vehicle Active Actuators

This section briefly introduces the active actuators of the $AFS$, $ADB$, and $ASus$ systems. This section serves later to generate the control actions demanded by the

controllers.

The $AFS$ system is formed by an electrical motor that generates the physical additive steering called "actuator control steering" $\delta_c^a$ that tracks the "control steering angle" $\delta_c$ provided by the controller. $AFS$ also provides the mechanical link between $\delta_c^a$ and $\delta_d$, the driver steering angle, where the total steering $\delta_t = \delta_c^a + \delta_d$. However, the actuator detailed model is not in the scope of this thesis (for more information refer to [Klier et al., 2004]).
In order to ensure that controller demand is achievable by the actuator, a simple actuator model is implemented into the control loops. $AFS$ actuator is modeled as:

$$\dot{\delta}_c^a = 2\pi f_5(\delta_c - \delta_c^a), \tag{1.39}$$

where $f_5$ is the actuator cut-off frequency. This actuator is bounded between $\left[-\delta_{c,max}^a, +\delta_{c,max}^a\right]$, where $\delta_{c,max}^a$ is the saturation of the $AFS$ actuator.

The $ADB$ can provide the corrective yaw moment $M_z$ of the $DYC$. In order to prevent direct interference with the $AFS$ on the front tires, the $ADB$ is generated by the rear Electro-Mechanical Brakes ($EMB$) (right $Tb_{rr}$ and left $Tb_{rl}$ braking torques) [Doumiati et al., 2013]. Thus, The $DYC$ torque $M_z$ is generated as a braking torque $T_{b,rj} = \frac{2r}{t_r} M_z$ at one of the rear wheels of radius $r$ (at the same instant), depending on the direction of $M_z$ [Doumiati et al., 2014].
The $EMB$ actuators providing $T_{b,rj}^a$ (that tracks $T_{b,rj}$) model is given by:

$$\dot{T}_{b,rj}^a = 2\pi f_6(T_{b,rj} - T_{b,rj}^a), \tag{1.40}$$

where $f_6$ is the actuator cut-off frequency. This actuator control is bounded between $[0, T_{b,max}^a]$, where $T_{b,max}^a$ is the saturation of the $EMB$ actuators.

The $ASus$ actuator is a spool valve controlled electro-hydraulic component. The spool valve control makes the $ASus$ providing at its output a force $U_{ij}^*$ that tracks $U_{ij}$ sent from the $ASus$ controller. Several works in literature have focused on the control of the electro-hydraulic actuators in order to track a desired force specified by an $ASus$ controller [Rajamani, 2012]. However, the control of the actuator valve is not in the scope of this thesis, for the details of the dynamics and the control of the actuator please refer to [Rajamani, 2012]. In this thesis, in order to have a feasible active suspension control input, a simple actuator model is used to deal with the actuator constraints. These constraints are mainly the response time (cut-off frequency $f$) and the saturation (maximal achievable force $U_{ij,max}$) of the actuator. The actuator model is given in (1.41).

$$\dot{U}_{ij}^* = 2\pi f * (min(U_{ij}, U_{ij,max}) - U_{ij}^*). \tag{1.41}$$

The actuators should be designed to be faster enough and capable to provide sufficient force, to control the vehicle dynamics (cut-off frequency $f$, and maximal active force $U_{ij,max}$). These characteristics are generally time-varying, while a proper selection of their mean values is done in [Chamseddine et al., 2006] where $f = 10\ Hz$ and $U_{ij,max} = 9800\ N$.

## 1.7 Conclusion

In this chapter, the vehicle dynamics is discussed. A full vehicle nonlinear model is presented and validated, and some other linearized models are exposed. The performance criteria are also quantified. Finally, the active actuators that are involved in this thesis are modeled. Next chapter reviews the control architectures and techniques used in the *GCC* field.

# *Review on Control Architectures and Techniques*

This chapter briefly reviews some of the control architectures and the robust and/or optimal control techniques existing in literature that are applied in *GCC* filed. We can identify two types of control architectures: multilayer centralized and multilayer decentralized. The reviewed control techniques are the essential keys for controllers' design in next chapters. Mainly, three advanced control techniques are used in this thesis: a Lyapunov-based control technique in the framework of Immersion and Invariance, the Super-Twisting Sliding Mode $STSM$ control technique, and the $\mathcal{H}_\infty$ control technique in the framework of the $LPV$ system.
Both the Lyapunov-based and the $STSM$ are nonlinear robust control techniques applied in the decentralized architectures for Single-Input-Single-Output ($SISO$) systems, while the $\mathcal{H}_\infty$ is a linear robust and optimal control technique applied in the centralized architectures for $MIMO$ systems.

## 2.1 Introduction

A crucial task in control system engineering is the choice of the most suitable control technique. One should carefully study the characteristics of the system to be controlled, i.e., the representativeness of the model (how much precise or uncertain), the complexity of this model (number of inputs/outputs, monovariable or multivariable, types of parameters(constant or variant), interconnection between dynamics (linear, nonlinear, ordinary and partial differential equations)), and the computational time for real world experiments.
As can be seen from the full vehicle model of Section 1.1, the vehicle is a complex multivariable nonlinear system, whose control is relatively difficult compared to other dynamical systems. The literature is rich in chassis control systems, either to control one, a part, or all the chassis variables through one or several control inputs. Therefrom comes the notion of decentralized and centralized control [Chen et al., 2016]. Indeed, in the decentralized control, the control researcher/engineer selects, for each set of control variables (one variable or more), one control input (generally, the most influencing one) and neglects the effect of the other inputs on the variables of interest. Then, for each combination (variables-input), a specific control technique is applied in order to achieve a precise reference/equilibrium tracking in presence of model uncertainties, neglected inputs, and eventual external perturbations. For

the case where only one variable is controlled through one input, this part of the control system is said $SISO$ or monovariable. The cooperation between the control inputs is generally achieved in a higher layer, the decision layer, which is responsible to determine the actual/future vehicle operation situation. Thus, the control architecture is said multilayer. On the opposite side, in the centralized control, the control inputs cooperate all together to control all the variables of interest. The controlled part of the control system is said $MIMO$ or multivariable. Meanwhile, a higher layer, the decision layer, monitors the vehicle situation to adjust the controller dynamics to the encountered situation.

## 2.2 Multilayer Centralized vs Multilayer Decentralized Control Architectures

The multilayer control architecture consists of decomposing the controller design into several layers as shown in Figure 2.1. After collecting all the vehicle operation information, including data from the sensors and the state estimators, the upper layer (decision layer) monitors the driver's intentions and the current vehicle state, then, it informs, through scheduling parameters, the middle layer about the encountered situation to adjust its behavior. By the way, the upper layer is designed to coordinate interactions amongst all the subsystem controllers. Thereafter, the control inputs are generated, by the middle layer (control layer), in order to achieve the desired vehicle states, depending on the architecture of this layer (centralized or decentralized). If the middle layer architecture is centralized (Figure 2.1.a), that means a single central controller generates the control inputs which cooperate all together to control all the variables of interest. If the middle layer architecture is decentralized (Figure 2.1.b), that means several controllers exist in the middle layer, where each controller generates only one control input which controls a part of the variables of interest. Finally, each of the individual lower layer (actuator layer) executes its local control objectives to control the vehicle dynamics.
Therefore, both the advantages and disadvantages are obvious. The centralized architecture has the advantages of controlling and observing all the subsystems in an integrated manner. This means, control actions are more precise, optimal, and less conflicting. However, the disadvantages cannot be ignored: the curse of dimensionality caused by the increasing number of subsystems results in tremendous design difficulties. Moreover, the failure of the centralized controller inevitably leads to a total failure of the whole chassis control system. Finally, when the centralized architecture needs to include more required subsystems, the entire centralized architecture has to be redesigned since the architecture lacks flexibility. In the decentralized architecture a number of benefits can be observed, amongst which are: facilitating the modular design of chassis control systems; favoring scalability, need less accurate model since interactions are neglected. On the other hand, it has disadvantages of not mastering model complexity and neglecting dynamics interactions which naturally lead to a non optimal control design.
This chapter focuses on the control techniques that can be enclosed in middle layer, especially in the $GCC$ filed. In literature, several control techniques are applied

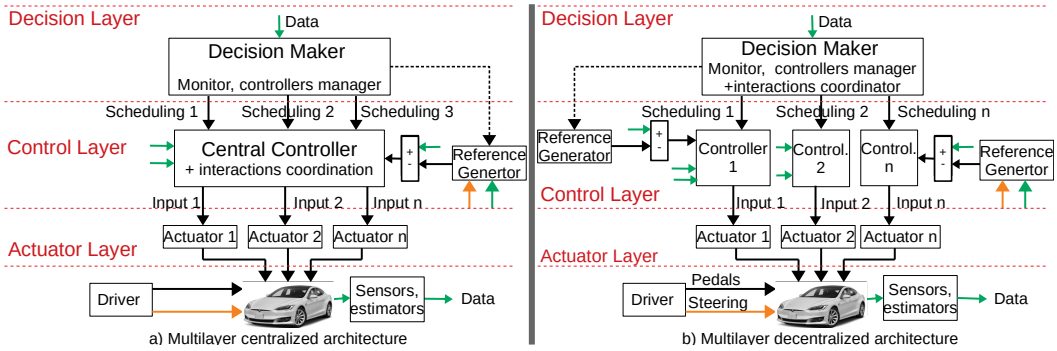


Figure 2.1 – Multilayer centralized and decentralized control architectures

in both centralized and decentralized architectures. Examples include linear and nonlinear model predictive control [Canale and Fagiano, 2008] [Falcone et al., 2007b] [Falcone et al., 2007a], random sub-optimal control [Chen et al., 2006], robust and optimal $\mathcal{H}_\infty$ and $LPV/\mathcal{H}_\infty$ control [Fergani et al., 2016b] [Doumiati et al., 2013] [Poussot-Vassal et al., 2009] [Gaspar et al., 2007], sliding mode [Li et al., 2008] [Chamseddine et al., 2006] [Chen et al., 2016] [Yoon et al., 2010], Immersion and Invariance control (Lyapunov-based) [Tagne et al., 2015], (adaptive) Fuzzy logic control [Wei et al., 2006] [Xiao et al., 2009], nonlinear (adaptive or fuzzy) PID [Pedro et al., 2013] [Moradi and Fekih, 2013], Inverse model control [Andreasson and Bünte, 2006], and artificial neural networks [Nwagboso et al., 2002].
Among these many control techniques, in this thesis, we have chosen to apply three advanced control techniques to the $GCC$: a Lyapunov-based control technique in the framework of Immersion and Invariance, the $STSM$ control technique, and the $\mathcal{H}_\infty$ control technique in the framework of the $LPV$ system. Both the Lyapunov-based and the $STSM$ are nonlinear robust control techniques applied in the decentralized architectures for $SISO$ systems, while the $\mathcal{H}_\infty$ is a linear robust and optimal control technique applied in the centralized architectures for the $MIMO$ systems. These control techniques are introduced in the following sections.

## 2.3 Lyapunov-Based Control Technique

Consider the second order system written as:

$$\ddot{x} = f(X,t) + g(X,t)u(t), \tag{2.1}$$

where $u$ is the control input, $X = [x, \dot{x}]^T \in \Re^2$ is the state vector, $f$ and $g$ are continuous functions, and $g$ is invertible.
Let the desired trajectory of the state vector $X$ is $X_{des} = [x_{des}, \dot{x}_{des}]^T \in \Re^2$.
Let $E = [e, \dot{e}]^T = X - X_{des} = [x - x_{des}, \dot{x} - \dot{x}_{des}]^T \in \Re^2$ is the state error vector.
The control objective is to converge the error vector $E$ to zero.
As the system has a relative degree 2 w.r.t the control input $u$, let define a new variable $z$ such as:

$$z = \dot{e} + k_1 e + k_2 \int_0^t e d\tau. \tag{2.2}$$

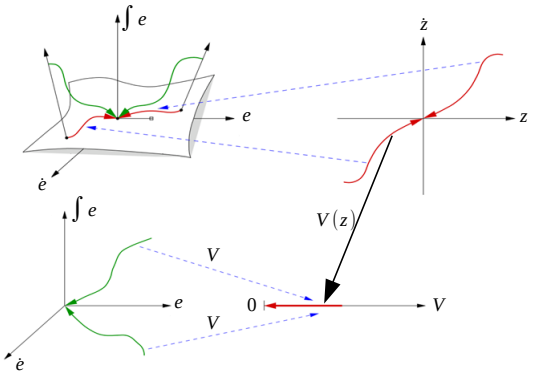


Figure 2.2 – Immersion and Invariance (modified from [Astolfi et al., 2007])

Based on Immersion and Invariance approach [Astolfi et al., 2007], the "off-the-manifold" variable $z$ has to converge to the target dynamics corresponding to $z = 0$ in the manifold as shown in Figure 2.2. In order to render the manifold attractive, i.e. to ensure the convergence of $z$ to zero, given that $z$ has a relative degree of 1 w.r.t the control input $u$, let define a positive definite Lyapunov candidate function as follows:

$$V(z) = \frac{1}{2}z^2, \tag{2.3}$$

$\dot{V}$ should be negative (Lyapunov stability conditions), thus,

$$\dot{V} = z\dot{z} \leq 0, \tag{2.4}$$

then, let:

$$\dot{z} = -\alpha z, \tag{2.5}$$

which makes (2.4) always negative if $\alpha > 0$. Thus:

$$\ddot{e} + k_1\dot{e} + k_2 e = -\alpha(\dot{e} + k_1 e + k_2 \int_0^t e d\tau), \tag{2.6}$$

where

$$\ddot{e} = \ddot{x} - \ddot{x}_{des} = f(X,t) + g(X,t)u(t) - \ddot{x}_{des}, \tag{2.7}$$

then, the control input $u$ can be found such as:

$$\begin{aligned} u = g^{-1}(X,t)[-f(X,t) + \ddot{x}_{des} - (\alpha + k_1)(\dot{x} - \dot{x}_{des}) \\ -(\alpha k_1 + k_2)(x - x_{des}) - \alpha k_2 \textstyle\int_0^t (x - x_{des}) d\tau]. \end{aligned} \tag{2.8}$$

$g^{-1}(X,t)$ and $-f(X,t)$ compensate all the dynamics of the system as a feed-forward command, beside the robust terms.
In the manifold, once $z = 0$, the error dynamics obey to the following equation:

$$\dot{e} + k_1 e + k_2 \int_0^t e d\tau = 0. \tag{2.9}$$

A sufficient condition to guarantee the convergence of $\dot{e}$, $e$, and $\int_0^t e d\tau$ to zero, is to have $k_1 > 0$ and $k_2 > 0$ (Routh-Hurwitz stability condition for a second order characteristic polynomial). Despite the fact that the convergence of $\int_0^t e d\tau$ to zero is not a necessary condition, its addition in $z$ helps to reduce the permanent steady-state error.

## 2.4 Super-Twisting Sliding Mode Control Technique

The Super-Twisting algorithm is a second order sliding mode control that handles a relative degree equal to one [Shtessel et al., 2014]. It generates the continuous control function that drives the sliding variable and its derivative to zero in finite time in the presence of smooth matched disturbances [Shtessel et al., 2014].
Consider the system written as:

$$\ddot{x} = f(X,t) + g(X,t)u(t), \tag{2.10}$$

where $u$ is the control input, $X = [x, \dot{x}]^T \in \Re^2$ is the state vector, and $f$, $g$ are continuous functions. Let the desired trajectory of the state vector $X$ is $X_{des} = [x_{des}, \dot{x}_{des}]^T \in \Re^2$, and let $E = [e, \dot{e}]^T = X - X_{des} = [x - x_{des}, \dot{x} - \dot{x}_{des}]^T \in \Re^2$ is the state error vector. Let us define a sliding variable $s$ of relative degree equal to one w.r.t the control input, such as:

$$s = \dot{e} + k\ e, \tag{2.11}$$

with a second derivative written as:

$$\ddot{s}(s,t) = \Phi(s,t) + \xi(s,t)\dot{u}(t), \tag{2.12}$$

where $\Phi(s,t)$ and $\xi(s,t)$ are unknown bounded functions.
The control objective is to achieve the convergence to the sliding surface defined as $s = 0$. Only the knowledge of $s$ is required in real time.
Suppose that there exist positive constants $S_0$, $b_{min}$, $b_{max}$, $C_0$, $U_{max}$ such that $\forall x \in \Re^2$ and $|s(x,t)| < S_0$, the system satisfies the following conditions:

$$\begin{cases} |u(t)| \leq U_{max}, \\ |\Phi(s,t)| < C_0, \\ 0 < b_{min} \leq |\xi(s,t)| \leq b_{max}. \end{cases} \tag{2.13}$$

The sliding mode control law, based on the Super-Twisting algorithm, is given by:

$$u(t) = u_1 + u_2 \begin{cases} u_1 = -\alpha_1 |s|^{\nabla} \text{sign}(s); \quad \nabla \in ]0,\ 0.5], \\ \dot{u}_2 = -\alpha_2 \text{sign}(s). \end{cases} \tag{2.14}$$

$\alpha_1$ and $\alpha_2$ are positive gains. The finite time convergence is guaranteed by the following conditions:

$$\begin{cases} \alpha_1 \geq \sqrt{\frac{4C_0(b_{max}\alpha_2 + C_0)}{b_{min}^2(b_{min}\alpha_2 - C_0)}}, \\ \alpha_2 > \frac{C_0}{b_{min}}. \end{cases} \tag{2.15}$$

The convergence is shown in Figure 2.3. The convergence analysis is given in [Utkin, 2013].
**Note :**
- The $STSM$ controller is known for its robustness against parameters uncertainties and disturbances. It converges to the sliding surface in finite time. However, it could

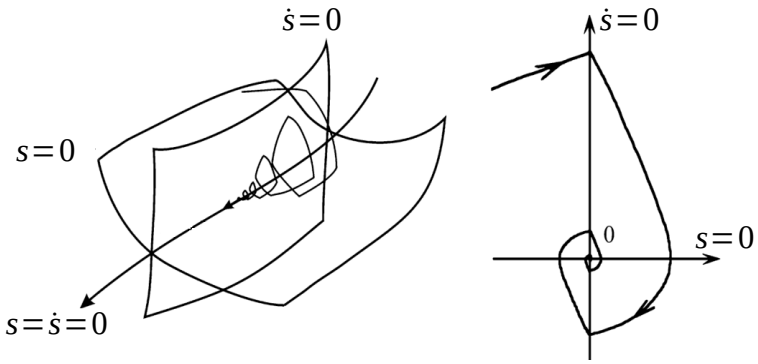


Figure 2.3 – Super-twisting sliding mode (modified from [Shtessel et al., 2014])

cause chattering once the equilibrium is reached. For that reason, the controller is made adaptive through approximating the function $sign(s)$ by $\frac{s}{|s|+\varepsilon}$, where $\varepsilon$ is a small positive value. The aim of such approximation is to attenuate the controller gains near to the sliding surface, and then reduce chattering; while maintaining the gains far away from the sliding surface to guarantee fast convergence.
- An equivalent input can be added as a feedforward control input to the $STSM$ control input (feedback) given in (2.14). This equivalent input compensates the dynamics of the system (when $f$ and $g$ are sufficiently well estimated) to make the sliding variable converges faster as in the Lyapunov based approach. The final control input becomes:

$$u(t) = g^{-1}(X,t)\left[-f(X,t) + \ddot{x}_{des} - k(\dot{x} - \dot{x}_{des}) - \alpha_1|s|^{\nabla}\frac{s}{|s|+\varepsilon} - \alpha_2\int_0^t \frac{s}{|s|+\varepsilon}d\tau\right]. \tag{2.16}$$

Once $s = 0$, the error dynamics obey to the following equation:

$$\dot{e} + ke = 0. \tag{2.17}$$

$\dot{e}$ and $e$ exponentially converge to zero if $k > 0$.

## 2.5 $LPV/\mathcal{H}_\infty$ Control Technique

For any system, the $\mathcal{H}_\infty$ control synthesis is a disturbance attenuation problem. It consists in finding a stabilizing controller that minimizes the impact of an input disturbances $w(t)$ on a (weighted) controlled output $z(t)$. Generally, the $\mathcal{H}_\infty$ control technique is applied to $LTI$ and $LPV$ systems. Figure 2.4 shows the plant $P(S)$ to be controlled, the input $W_i(S)$ and output $W_o(S)$ weighting dynamic functions, and the $\mathcal{H}_\infty$ controller $K_{\mathcal{H}_\infty}(S)$ to be synthesized ($S$ is the Laplace transformation). The open-loop system formed by the interconnection of $P(S)$, $W_i(S)$, and $W_o(S)$ is called the generalized plant $\Sigma_g(S)$. In this thesis, $P(S)$ represents an $LTI$ vehicle model, and $W_i(S)$ and $W_o(S)$ are scheduled $LPV$ filters. Thus, $\Sigma_g(S)$ is a $LPV$ system. The closed-loop system formed by the interconnection of $\Sigma_g(S)$ and $K_{\mathcal{H}_\infty}(S)$ is called $C_l(S)$.

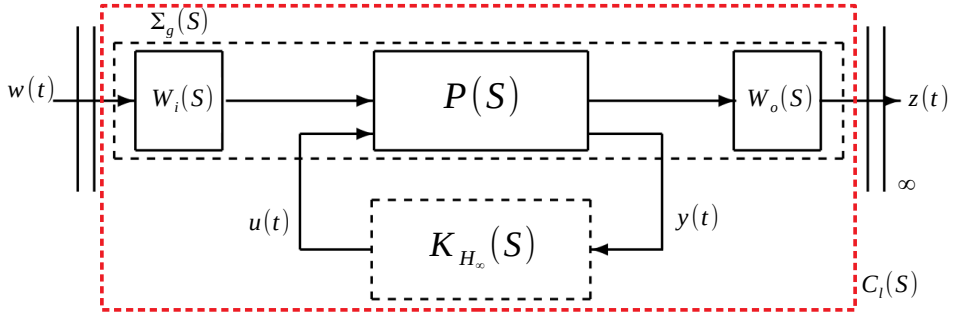


Figure 2.4 – $\mathcal{H}_\infty$ control architecture (modified from [Sename et al., 2013])

To understand the $\mathcal{H}_\infty$ control technique, let consider in a first time that the generalized system $\sum_g$ and the controller $K_{\mathcal{H}_\infty}$ are $LTI$. The $\mathcal{H}_\infty$ control design consists in finding the controller $K_{\mathcal{H}_\infty}$ that minimizes the $\mathcal{H}_\infty$ norm of the closed-loop system $C_l(S)$ as given in the following equation:

$$||C_l(S)||_\infty = sup_{\omega\in\Re}\bar{\sigma}(C_l(j\omega)) < \gamma, \tag{2.18}$$

where $\bar{\sigma}$ is the largest singular value, and $\gamma$ is the attenuation level. The $\mathcal{H}_\infty$ norm represents the maximal gain of the frequency response of the system. It is also called the worst case attenuation level in the sense that it measures the maximum amplification that the system can deliver on the whole frequency set. For $SISO$ (respectively $MIMO$) systems, it represents the maximal peak value on the Bode magnitude (respectively singular value) plot of $C_l(j\omega)$; in other words, it is the largest gain if the system is fed by harmonic input signal [Sename et al., 2013]. For more information on the $\mathcal{H}_\infty$ control refer to [Zhou et al., 1996], [Apkarian et al., 1995], and [Apkarian and Gahinet, 1995]. A useful summary is given in chapter 2 of the dissertation of [Poussot-Vassal, 2008].

Now, let consider a $LPV$ system defined by its generalized form $\sum_g$, such as:

$$\Sigma_g(\rho): \begin{bmatrix} \dot{x} \\ z \\ y \end{bmatrix} = \begin{bmatrix} A(\rho) & B_1(\rho) & B_2 \\ C_1(\rho) & D_{11}(\rho) & D_{12} \\ C_2 & D_{21} & 0 \end{bmatrix} \begin{bmatrix} x \\ w \\ u \end{bmatrix}, \tag{2.19}$$

where $x$ includes all the state variables of the system, $w$ is the exogenous input vector, $u$ represents the control inputs, $y$ is the measurement vector fed-back to the controller, $y_e$ is the exogenous output, and $z$ is the weighted controlled output vector. $A$, $B_1$, $B_2$, $C_1$, $C_2$, $D_{11}$, $D_{12}$, and $D_{22}$ are known matrices with finite dimensions. $\rho$ is the vector of the varying parameters, it is known and bounded. Without loss of generality, we treat the case where $\rho = \{\rho_1, \rho_2\}$, since it will serve for the next chapters.
The $LPV/\mathcal{H}_\infty$ problem consists in finding the controller $K_{LPV/\mathcal{H}_\infty}(\rho_1, \rho_2)$, scheduled by the parameters $\rho_1$ and $\rho_2$, such that:

$$K_{LPV/\mathcal{H}_\infty}(\rho): \begin{bmatrix} \dot{x}_c \\ u \end{bmatrix} = \begin{bmatrix} A_c(\rho) & B_c(\rho) \\ C_c(\rho) & 0 \end{bmatrix} \begin{bmatrix} x_c \\ y \end{bmatrix}, \tag{2.20}$$

which minimizes the $\mathcal{H}_\infty$ norm of the closed-loop $LPV$ system formed by the interconnection of equations (2.19) and (2.20).

***Problem resolution:*** $LMI$ ***based*** $LPV/\mathcal{H}_\infty$***:***

Thanks to the Bounded Real Lemma ($BRL$) extended to $LPV$ systems, this controller can be found. According to system (2.19) and via the change of basis expressed in [Scherer et al., 1997], a non conservative $LMI$ that expresses the same problem as the $BRL$ is formulated in (2.24) and solved by a Semi-Definite Program ($SDP$), while minimizing $\gamma$ for $\rho \in \Omega = [\underline{\rho_1}, \overline{\rho_1}]\ X\ [\underline{\rho_2}, \overline{\rho_2}]$.

The polytopic approach aims at finding $\widetilde{A}$, $\widetilde{B}$ and $\widetilde{C}$ at each vertex of the polytope described by $\rho \in \Omega$, by using a common Lyapunov function, i.e common $X > 0$ and $Y > 0$. Thus, the solution can be obtained by solving the system (2.21) at each vertex $\left\{\omega_1 = (\underline{\rho_1}, \underline{\rho_2}), \omega_2 = (\overline{\rho_1}, \underline{\rho_2}), \omega_3 = (\underline{\rho_1}, \overline{\rho_2}), \omega_4 = (\overline{\rho_1}, \overline{\rho_2})\right\}$ of the convex hull $\Omega$:

$$\left\{\begin{array}{lcl} C_c(\rho) & = & \widetilde{C}(\rho)M^{-T} \\ B_c(\rho) & = & N^{-1}\widetilde{B}(\rho) \\ A_c(\rho) & = & N^{-1}(\widetilde{A}(\rho) - YA(\rho)X - NB_c(\rho)C_2X \\ & - & YB_2(\rho)C_c(\rho)M^{-T})M^{-T} \end{array}\right. , \tag{2.21}$$

where $M(\rho)$ and $N(\rho)$ are defined by the user so that $M(\rho)N(\rho)^T = I - X(\rho)Y(\rho)$. See [Scherer et al., 1997] for more details on the computation solution.

According to the polytopic approach, the final controller, $K_{LPV/\mathcal{H}_\infty}(\rho_1, \rho_2)$, is a convex combination of the controllers synthesized at the vertices of the polytope [Apkarian et al., 1995] such as:

$$\begin{array}{r} K_{LPV/\mathcal{H}_\infty}(\rho_1, \rho_2) = \alpha_1 K_{\mathcal{H}_\infty}(\omega_1) + \alpha_2 K_{\mathcal{H}_\infty}(\omega_2) \\ +\alpha_3 K_{\mathcal{H}_\infty}(\omega_3) + \alpha_4 K_{\mathcal{H}_\infty}(\omega_4), \end{array} \tag{2.22}$$

where $\sum_{i=1}^{i=4} \alpha_i(\rho_1, \rho_2) = 1$; $\alpha_i(\rho_1, \rho_2) > 0$. The polytopic coordinates $\alpha_i(\rho_1, \rho_2)$ weight the controllers on the vertices to construct the final controller (see Figure 2.5). $\alpha_i(\rho_1, \rho_2)$ are instantly evaluated by the following equations (the Matlab function"*polydec*" (Robust Control Toolbox) is also useful to evaluate polytopes with more vertices):

$$\begin{array}{ll} \alpha_1 = \frac{\overline{\rho_1} - \rho_1}{\overline{\rho_1} - \underline{\rho_1}} . \frac{\overline{\rho_2} - \rho_2}{\overline{\rho_2} - \underline{\rho_2}}; & \alpha_3 = \frac{\overline{\rho_1} - \rho_1}{\overline{\rho_1} - \underline{\rho_1}} . \frac{\rho_2 - \underline{\rho_2}}{\overline{\rho_2} - \underline{\rho_2}}; \\ \alpha_2 = \frac{\rho_1 - \underline{\rho_1}}{\overline{\rho_1} - \underline{\rho_1}} . \frac{\overline{\rho_2} - \rho_2}{\overline{\rho_2} - \underline{\rho_2}}; & \alpha_4 = \frac{\rho_1 - \underline{\rho_1}}{\overline{\rho_1} - \underline{\rho_1}} . \frac{\rho_2 - \underline{\rho_2}}{\overline{\rho_2} - \underline{\rho_2}}. \end{array} \tag{2.23}$$

## 2.6 Conclusion

In this chapter, a differentiation between the multilayer centralized and decentralized architectures is provided. Some advanced control techniques are also evoked.

The power of the super-twisting algorithm, compared to the Lyapunov-based approach (Immersion and Invariance), is its robustness to modeling uncertainties (when the dynamics $f$ and $g$ are not well estimated and measured). Indeed, the

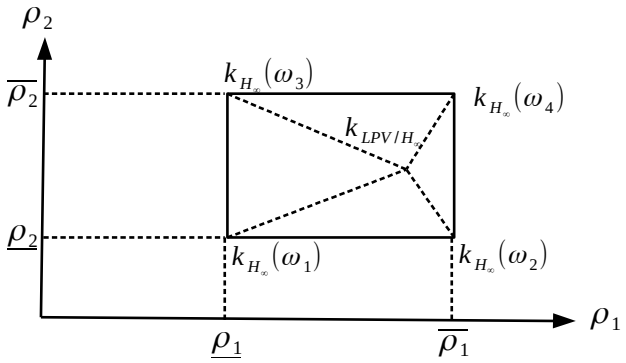


Figure 2.5 – Polytopic $LPV/\mathcal{H}_\infty$ controller

$$\begin{bmatrix} A(\rho)X + XA(\rho)^T + B_2\widetilde{C}(\rho) + \widetilde{C}(\rho)^T B_2^T & (*)^T & (*)^T & (*)^T \\ \widetilde{A}(\rho) + A(\rho)^T & YA(\rho) + A(\rho)^T Y + \widetilde{B}(\rho)C_2 + C_2^T\widetilde{B}(\rho)^T & (*)^T & (*)^T \\ B_1(\rho)^T & B_1(\rho)^T Y + D_{21}^T\widetilde{B}(\rho)^T & -\gamma I & (*)^T \\ C_1(\rho)X + D_{12}\widetilde{C}(\rho) & C_1(\rho) & D_{11}(\rho) & -\gamma I \end{bmatrix} < 0;$$

$$\begin{bmatrix} X(\rho) & I \\ I & Y(\rho) \end{bmatrix} > 0. \tag{2.24}$$

feedforward equivalent input is not mandatory to proove the closed-loop stability of the super-twisting algorithm. This feature is essential in $GCC$ because some of the vehicle and road parameters are time-varying. The comparison between the $STSM$ and the $LPV/\mathcal{H}_\infty$ is more difficult since they are both robust to uncertainties and disturbances. However, each of these two techniques has its pros and cons. The $STSM$ is simple to be applied since the controller gains can be easily adjusted for $SISO$ system, while the dynamics interconnection effects are neglected. In contrary, the $LPV/\mathcal{H}_\infty$ considers the dynamics interconnection effects through the generation of simultaneous control inputs, while the control objectives are not scalable. Later on, both architectures are compared together through performance simulation.
Next chapter discusses the effect of the roll motion control on the vehicle performance.

# *Effect of Roll Motion Control on Vehicle Performance*

This chapter discusses the effects of the roll control on the vehicle performance. Roll motion control is achieved through the generation of a virtual roll moment that can be allocated to the *ASus*, the semi-*ASus*, or the *ARB*. Rollover avoidance and lateral stability constitute the core analysis of this chapter to design two roll reference generators, one static and one dynamic. To do so, firstly, based on the time-domain equations of motion of the full-vehicle nonlinear model, a study on how the roll control can help the vehicle to avoid the rollover without deceleration or steering actions is done. Secondly, a frequency analysis of the lateral stability response to the steering input, with and without roll control is performed to extract the ranges of steering frequencies and amplitudes where the roll control could be useful. For this study, two lateral-roll Linear Time Invariant (*LTI*) vehicle models (without and with roll control) are compared. For simplicity and to serve the study, a *LQR* is developed to control the roll angle of the *LTI* model. Thirdly, three roll controllers, i.e., *LQR*, Lyapunov-based, and *STSM* are developed, validated and compared on the full vehicle nonlinear model using Matlab/Simulink. Finally, the capability limits of the roll control on rollover avoidance and lateral stability enhancement is deduced, and other performances like comfort, maneuverability, speed change, braking, longitudinal slipping, etc... are evaluated by simulation as a consequence of the roll motion control.
This chapter also provides a comparison between the roll angle control towards zero (the static reference), which can be achieved using either *ASus*, or semi-*ASus* or *ARB*, and roll angle control towards a new desired roll angle (dynamic reference function of the vehicle lateral acceleration), which can be only achieved using the *ASus*. A proposition to cooperate with other controllers in a *GCC* architecture is introduced at the end of this chapter.

## 3.1 Introduction

This introduction answers the question of why to study the effect of the roll motion control on the vehicle in a whole chapter. The answer is simply because the roll motion is involved in several vehicles performances e.g. rollover phenomenon, lateral stability, comfort... This involvement is deterministic especially in critical situations where the roll motion control can help other *ADAS* controllers (in a

*GCC* architecture) to achieve their objectives. The idea of this chapter is to make the (semi-)*ASus*, usually developed for ride comfort and road holding [Chamseddine et al., 2006],[Savaresi et al., 2010], intervene to achieve new functionalities supporting the other vehicle stability controllers aiming at avoiding rollover and maintaining lateral stability. This coordination makes the vehicle operates in a larger stable range, since for the same driving conditions, the different vehicle stability controllers will be less solicited.
The effect of the roll motion control on the rollover phenomenon is obvious, since the rollover problem is related to the roll motion and the lateral acceleration. This effect is detailed later in this chapter.
The effect of the roll motion control on the lateral stability is more complicated. The dynamics coupling between the vertical and lateral tire forces [Li et al., 2013] is an essential key to enhance the lateral stability. Several studies on the (semi-)*ASus* are conducted to explicitly try to enhance the lateral stability [Jin et al., 2016],[Vivas-Lopez et al., 2015],[Zhao et al., 2014],[Zulkarnain et al., 2012]. The basic idea is to prevent the saturation of tires lateral forces, which causes the vehicle to laterally skid when cornering, through controlling the vertical tires forces. That means, an inverse tire/road contact model should be evaluated, which is somehow difficult, especially in the nonlinear saturated regions. For that, researchers as [Vu et al., 2017],[Yao et al., 2017],[Fergani et al., 2016a] propose to control the vertical load transfer when cornering, or minimize the vertical displacements of the unsprung masses, as they are the most influencing factors on the lateral forces. However, this method may ensure a posterior enhancement on the lateral stability but not a prior demonstrated guaranty. One of this chapter objectives is to demonstrate, a priori, in the frequency domain, that the roll angle control can always enhance the lateral stability.

## 3.2 Roll Control Effect on Rollover Problem

### 3.2.1 Rollover Problem Formulation

Vehicle rollover is defined as 90° or more rotation of the vehicle around its longitudinal axis [Gillespie, 1992]. This phenomenon starts when two vehicle wheels of the same side lift off from ground. Equivalently, rollover risk can be also evaluated around the axis joining the other two wheels remaining on the ground. In spite of the fact that the rollover crash constitutes a small percentage of all road accidents (3%), it commits fatal injuries, nearly 33% of all deaths from passenger's vehicle crashes, according to the *NHTSA*, 2011 statistics. For this reason, rollover avoidance has become an important safety issue for many researchers and automotive societies. According to [Gillespie, 1992], there are two types of rollover: tripped and untripped rollover. Tripped rollover occurs due to an external force on the vehicle, like wheels impact with a curb or a pot hole, an accident with another vehicle, or even a violent wind. Untripped rollover occurs due to an excess in the lateral acceleration or due to the roll dynamics in a vehicle equipped with passive suspensions. For instance, untripped rollover occurs when performing a curved road with a sharp

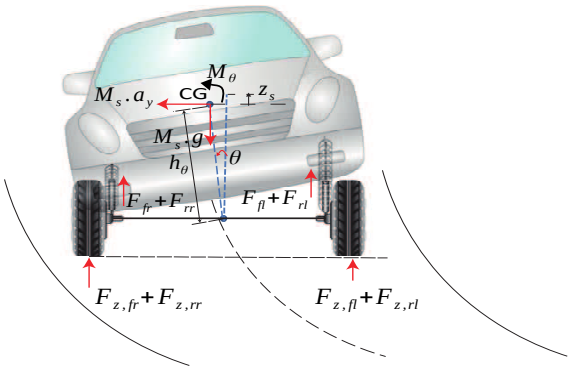


Figure 3.1 – roll motion (front view)

steering at high speed or undertaking a quick lane change. Despite the fact that the majority of rollovers are tripped rollovers, many studies have been developed to prevent untripped rollover, because it depends on the vehicle dynamics that can be quantified, unlike tripped rollover, which happens spontaneously, where prediction studies are still not well investigated.
From the full vehicle model, the roll motion is expressed as:

$$\begin{aligned}\ddot{\theta} = \frac{1}{I_x + M_s h_\theta^2}[&(-F_{s,fr} + F_{s,fl})\, t_f + (-F_{s,rr} + F_{s,rl})\, t_r \\ &+ M_s\,(h_\theta\ cos\,(\theta) + z_s)\, a_y + M_s\,(h_\theta\ sin\,(\theta) + z_s)\, g].\end{aligned} \tag{3.1}$$

The roll dynamics is equivalent to:

$$\begin{aligned}\ddot{\theta} = \frac{1}{I_x + M_s h_\theta^2}[&(-F_{fr} + F_{fl})\, t_f + (-F_{rr} + F_{rl})\, t_r \\ &+ M_s\,(h_\theta\ cos\,(\theta) + z_s)\, a_y + M_s\,(h_\theta\ sin\,(\theta) + z_s)\, g + M_\theta],\end{aligned} \tag{3.2}$$

as shown in Figure 3.1, where $F_{ij}$ is the passive suspension force on the vehicle corner $ij$, and $M_\theta$ is the active roll moment to be generated through the $ASus$ forces $U_{ij}$ such as:

$$M_\theta = (-U_{fr} + U_{fl})\, t_f + (-U_{rr} + U_{rl})\, t_r. \tag{3.3}$$

From the roll dynamics (3.2), the major variables that affect the induced roll angle are the passive suspension forces $F_{ij}$ and the lateral acceleration $a_y$. As the lateral acceleration becomes high when cornering, as the induced roll angle turns to the outside of the corner and the vehicle becomes subjected to a rollover risk. In order to avoid the rollover, the active roll moment $M_\theta$ should be generated to act on the roll motion.

### 3.2.2 Static Untripped Rollover

To better understand the rollover problem, let consider, in a first time, that the vehicle is a rigid body (without suspension system), for the reason to show the effect of the lateral acceleration alone on the vertical load transfer. In a second time, the effect of the induced roll motion in committing rollover, in a vehicle equipped

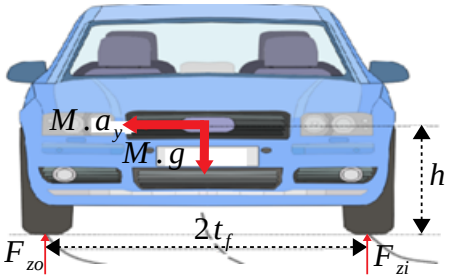


Figure 3.2 – Static rollover

with suspensions, is introduced. To carry out the lateral acceleration effect, suppose that the vehicle is subjected to a quasi-static lateral acceleration which varies slowly compared to the vehicle speed. This can be done through a steady steering at high speed, e.g. highway turn (see Figure 3.2).
The lateral acceleration $a_y$ applied on the vehicle center of gravity creates the d'Alembert's force (centrifugal force) $M.a_y$ which acts to turn the vehicle towards the outside of the turn, with the torque $Ma_yh$ acting on the axis formed by the outside wheels contact points with the ground. However, an opposite torque takes place to counterbalance the torque $Ma_yh$. It is performed by two vertical equal forces (in opposiste direction) distanced by $t_f$ forming a load transfer from inner to outer wheels, such as:

$$F_{zo} - F_{zi} = \frac{Ma_yh}{t_f}, \tag{3.4}$$

where $F_{zo}$ and $F_{zi}$ are respectively the outer and inner vertical forces formed by adding each two tire vertical forces in the same vehicle side. Taking the moments of all forces around the same axis (Newton's law), the equilibrium is maintained (before starting rollover) if:

$$Ma_yh - Mgt_f + F_{zi}2t_f = 0. \tag{3.5}$$

If the vehicle speed $V$ increases, or the radius of the turn $R$ decreases (the curvature increases), the lateral acceleration increases (for any rigid body: $a_y = V^2/R$ in a non-mobile frame). Increasing $a_y$ happens while guarantying equilibrium in (3.5), which is done by a natural decreasing of the other single variable $F_{zi}$, up to a certain amount of $a_y$ where $F_{zi}$ becomes 0, which represents inner wheels lift-off. Equation (3.5) becomes:

$$Ma_{y,lift-off}h - Mgt_f = 0, \tag{3.6}$$

where $a_{y,lift-off}$ is the minimal lateral acceleration that causes wheels lift-off. Hence:

$$a_{y,lift-off} = \frac{t_f}{h}g. \tag{3.7}$$

The factor $\frac{t_f}{h}$ is called Static Stability Factor ($SSF$). It is a constant value that depends on the vehicle geometry (around 1.2 for passengers cars, 1 for light trucks and 0.45 for heavy trucks [Gillespie, 1992]), that means heavy trucks rollover occurs at lower lateral accelerations.
This analysis to quantify the rollover risk is equivalent to the vertical $LTR$ defined in [Rajamani, 2012] and described in (1.30).

### 3.2.3 Dynamic Untripped Rollover

In real situations, due to the suspension system, the vehicle is not a simple rigid body. To study the motion roll effect on rollover, suppose that the vehicle has one degree of freedom represented by the roll angle $\theta$ between the suspended and unsuspended masses (see Figure 3.1). This means that the suspended mass center of gravity deviates by a positive angle $\theta$ (toward the outside) around the roll axis. Hereby, the moment of all forces around the axis joining outer wheels becomes:

$$M_s a_y h - M_s g(t_f - (h - h_r)sin\theta) + F_{zi} 2t_f = 0. \tag{3.8}$$

By analogy with previous analysis, under the assumption of small angles $sin\theta \approx \theta$, $a_{y,lift-off}$ becomes:

$$a_{y,lift-off} = \frac{t_f - (h - h_r)\theta}{h} g, \tag{3.9}$$

which means that $a_{y,lift-off}$ is reduced when considering the passive suspension system by approximately 5% [Gillespie, 1992]. Hence, comparing to a rigid body vehicle, the vehicle equipped with a passive suspension system starts rollover at lower lateral accelerations.
The transient response of $\theta$ is ignored in this analysis, while a roll overshoot may occur due to the developed roll dynamics. This overshoot adds to $\theta$ a small amount, which consequently, reduce $a_{y,lift-off}$ another 5%, and may cause vehicle to rollover when moving at a lower lateral acceleration. This analysis also ignores the lateral acceleration measurement error (accelerometer subjected to a roll motion), and other physical uncertainties causing rollover, like a vertical shift of the center of gravity, changes in tires and ground contact surfaces. In order to stay in a safe driving region, a safety factor of 0.7 of the total $a_{y,lift-off}$ expressed in (3.9) is proposed. A new variable is declared and denoted $a_{y,safe}$, where:

$$a_{y,safe} = 0.7 a_{y,lift-off} = 0.7 \frac{t_f - (h - h_r)\theta}{h} g \tag{3.10}$$

A lateral acceleration $a_y$ above $a_{y_{safe}}$ risks the vehicle inner wheels to lift off when cornering. Consequently, to avoid the rollover, the lateral acceleration $a_y$ should be maintained below this threshold.

### 3.2.4 Roll Reference Generation

To avoid the rollover, the $AFS$ and $ADB$ aim to reduce $a_y$, to maintain $a_y < a_{y_{safe}}$, while the $ASus$, semi-$ASus$ and $ARB$ aim, by controlling the roll angle, to elevate the maximal safe lateral acceleration $a_{y,safe}$. For instance, stiffening the suspensions using the semi-$ASus$ or the $ARB$ can reduce the vehicle roll angle towards zero. This procedure arises $a_{y,safe}$ as exhibits equation (3.10), which prevents the rollover to happen without the need to reduce $a_y$. The contribution that adds the $ASus$ system is the ability to continue turning the roll angle in the negative direction (to the inner side of the corner), that means $a_{y,safe}$ will be more shifted to a higher value. The choice of the desired roll angle $\theta_{des}$ is done as follows:
- At zero lateral acceleration (straight road), the desired roll angle is 0°.

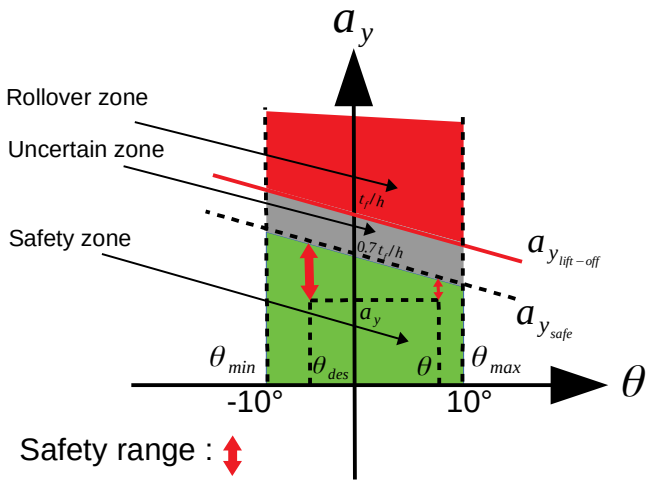


Figure 3.3 – Rollover risk evaluation

- At a lateral acceleration equal to the maximal static safe lateral acceleration threshold 0.7 $\frac{t_f}{h}$ $g$, the desired roll angle is equal to the maximal achievable roll angle 10° (vehicle design constraints).
- The map between $\theta_{des}$ and $a_y$ is supposed to be linear to make a smooth comfortable roll change rate. Thus, the desired roll angle $\theta_{des}$ is given as:

$$\theta_{des} = -\frac{10\frac{\pi}{180}}{0.7\frac{t_f}{h}g}a_y. \tag{3.11}$$

Figure 3.3 illustrates the safety range defined as the remoteness between the vehicle lateral acceleration and the maximal safe lateral acceleration which is a function of the vehicle roll angle. It also shows the effect of turning the vehicle roll angle $\theta$ towards $\theta_{des}$ of (3.11) in enlarging the safety range more than minimizing the roll angle towards zero ($\theta_{des} = 0$). However, a comparison is done in this chapter to compare both references.

## 3.3 Roll Control Effect on Lateral Stability

### 3.3.1 Frequency Analysis Setup

The analysis of the enhancement that the roll control brings on the lateral stability is not that much easy as for rollover avoidance, because the relation between the roll angle $\theta$ and the lateral stability quantified by the $SI$ criterion (function of the side-slip dynamics $\beta, \dot{\beta}$) is not static. This relation is rather governed by the dynamical differential equations of the vehicle. Therefore, this section analyzes, in the frequency and time domains, the effect of the roll control on the lateral stability.
The frequency analysis requires, in general, a linear model. Therefore, the extended bicycle model of (1.37), as a linear model describing the relation between the lateral and the roll dynamics, is augmented to include the active roll moment $M_\theta$ as the roll motion control input, and then it is used to make the study. The state-space representation of this model is given in (3.12). It is similar to that of the extended

$$\dot{X} = \begin{bmatrix} \ddot{\psi} \\ \dot{\beta} \\ \dot{\theta} \\ \ddot{\theta} \end{bmatrix} = \underbrace{\begin{pmatrix} a_{11} & a_{12} & a_{13} & a_{14} \\ a_{21} & a_{22} & a_{23} & a_{24} \\ 0 & 0 & 0 & 1 \\ a_{41} & a_{42} & a_{43} & a_{44} \end{pmatrix}}_{A} \begin{bmatrix} \dot{\psi} \\ \beta \\ \theta \\ \dot{\theta} \end{bmatrix} + \underbrace{\begin{pmatrix} b_{u,11} & b_{u,13} \\ b_{u,21} & b_{u,23} \\ 0 & 0 \\ b_{u,41} & b_{u,43} \end{pmatrix}}_{B_{1,3}} \begin{bmatrix} \delta_d \\ M_\theta \end{bmatrix} \tag{3.12}$$

bicycle model given in (1.38), with the simple addition of the control input $M_\theta$.
The elements of the matrices $A$ and $B_{1,3}$, given in Appendix .1, depend on several time-varying parameters such as: $V$, $\mu$, $C_f$, $C_r$, and $M_s$... However, the study is done for nominal/constant values of these parameters. Then, the study is enlarged to different vehicle speeds $V$, as it is the most varying one. Consequently, the state-space representation given in (3.12) is considered as a Linear Time-Invariant $LTI$ system.
The $LTI$ model gives an approximation of the real vehicle behavior in stable to mid-critical regions. Hence, as the vehicle is being controlled before loosing stability, this $LTI$ model is sufficient to study the effect of the roll control on the lateral stability. In fact, the risk of the vehicle to operate in the unstable region is minor, since other controllers like the $DYC$ in the $GCC$ structure are supposed to maintain the lateral stability. However, to analyze the effect of the roll control on the lateral stability when the vehicle operates in the unstable region, an extension of this study can be done using frequency response techniques for nonlinear systems like "Pseudo-Bode computation" [Nassirharand and Karimi, 2002].
The $LTI$ model (3.12) can be written as:

$$\dot{X} = AX + B_1\delta_d + B_3M_\theta, \tag{3.13}$$

where $B_1$ and $B_3$ are respectively the first and second colomun of $B1, 3$.
The objective is to compare the frequency response of the vehicle with a controlled roll motion as in (3.13), and a the vehicle without a roll controller ($M_\theta = 0$) as in (3.14):

$$\dot{X} = AX + B_1\delta_d. \tag{3.14}$$

Thus, let consider the state feedback $LQR$ control law:

$$M_\theta = -KX. \tag{3.15}$$

The optimal closed loop system becomes:

$$\dot{X} = (A - B_3K)X + B_1\delta_d, \tag{3.16}$$

which has the same form as (3.14), but with a controlled roll motion.
The optimization procedure consists in finding the control input $U = M_\theta$ which minimizes the performance index $J$:

$$J = \int_0^\infty (X^TQX + U^TRU)dt, \tag{3.17}$$

where $Q$ and $R$ are the weighting matrices.
The control purpose is to minimize the roll angle and roll velocity, by controlling

$M_\theta$. Thus, the performance index $J$ becomes:

$$J = \int_0^\infty (\rho_1 \theta^2 + \rho_2 \dot{\theta}^2 + M_\theta^2) dt, \tag{3.18}$$

where the weighting coefficients $\rho_1$ and $\rho_2$ are adjusted to promote the weight on the roll angle, while minimizing the energy of the control input.
The matrix gain $K$ has the form:

$$K = R^{-1} B_3^T P, \tag{3.19}$$

where the matrix $P$ is the solution of the *Algebric Riccati Equation*:

$$A^T P + PA - PB_3 R^{-1} B_3^T P + Q = 0. \tag{3.20}$$

The frequency response of the vehicle with roll controller (3.16) and the vehicle without roll controller (3.14) can be now compared. More specifically, the transfer functions of the $SI$ (as function of the side-slip dynamics) w.r.t the exogenous steering input are evaluated for both vehicles in the next sub-section.
**Note:**
The state feedback $LQR$ controller only serves to analyze the response of the vehicle. However, more efficient controllers are designed in Section 3.4.

### 3.3.2 Lateral Stability Frequency Analysis

#### 3.3.2.1 Steering Input

The steering input can be approximated (within a sample time) by a sinusoidal form with the amplitude $A$ and the frequency $\omega$ as in (3.21):

$$\delta_d = A \sin(\omega t). \tag{3.21}$$

The driver effective steering frequency $\omega$ is between $[0, 12.5]$ $rad/s$ as explained in [Heißing and Ersoy, 2010]. This range of frequencies is considered as the useful range needed to perform a maneuver. Beyond this range, the vehicle becomes non-sensitive to the steering angle [Heißing and Ersoy, 2010]. The reason of this limitation is that the vehicle yaw rate cannot respond to the demand of the steering angle amplitude when the steering rate (frequency) is too high. The driver, in the normal driving situations, can provide a steering in the frequency range $[0, 3]$ $rad/s$. Hence, the critical range of frequencies is when the driver perform a sudden steering with a frequency between $[3, 12.5]$ $rad/s$ which will be the range of the frequency response to be studied.
The effective steering amplitude $A$ depends on the vehicle speed and steering frequency. For the same steering frequency, as the vehicle speed becomes higher as the steering amplitude has to be maintained small, which is a natural tendency of the driver, this fact will be validated in the next section. In the frequency range $[3, 12.5]$ $rad/s$ and a speed range between $[80, 130]$ $km/h$, a steering amplitude between $[0, 0.1]$ $rad$ (approximately $[0°, 5°]$) is sufficient to make the study cover both normal and critical driving situations. Later, a discussion will be done to generalize for higher amplitudes.

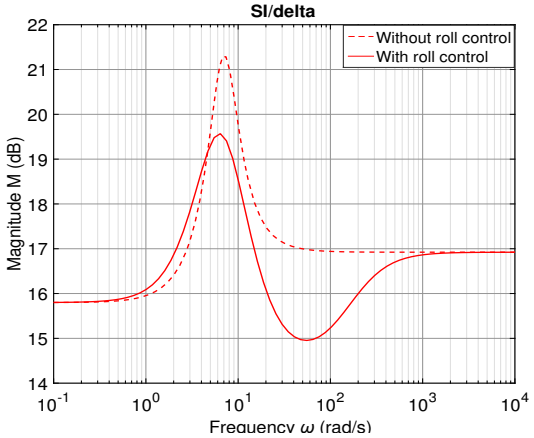


Figure 3.4 – Bode plot $SI/\delta_d$; $V = 100\ km/h$

#### 3.3.2.2 Frequency Response

To analyze the frequency response of the vehicle lateral stability w.r.t the steering input, the transfer functions $G^{SI}_{\delta_d}$ of both uncontrolled (3.14) and controlled (3.16) $LTI$ systems are evaluated in *Matlab* environment, and their bode diagrams at the vehicle speed $V = 100\ km/h$ are plotted in Figure 3.4. Both curves in Figure 3.4 represent the magnitude $M(\omega)$ of $G^{SI}_{\delta_d}$ in $(db)$ over the frequency range $\omega$ $[10^{-1}, 10^4]\ rad/s$ of $\delta_d$, that means, at any steering frequency $\omega$:

$$M(\omega) = 20 \log \left| \frac{SI}{\delta_d} \right|, \tag{3.22}$$

thus:

$$SI = A * 10^{\frac{M(\omega)}{20}}. \tag{3.23}$$

Equation (3.23) shows that for the same frequency $\omega$, the lateral $SI$ becomes greater as the steering amplitude $A$ increases. Thus, let $A$ be set at the maximum of the effective steering amplitude $A = 0.1\ rad$.
Equation (3.23) also shows that $SI$ becomes higher when $M(\omega)$ is higher. Consequently, the frequency response curve of the vehicle without roll control in Figure 3.4 shows that in the frequency range $[0, 3]\ rad/s$, the magnitude $M(\omega)$ of $G^{SI}_{\delta_d}$ is between $[15.8, 17]\ db$.This means that for $A = 0.1\ rad$, the $SI$ can reach $SI = 0.1 * 10^{(17/20)} = 0.7$, which demonstrates that in this frequency range, the driving situation is normal.
In the $[3, 12.5]\ rad/s$ frequency range, the magnitude response of $G^{SI}_{\delta_d}$ of the uncontrolled roll vehicle increases significantly, while controlling the roll angle remarkably reduces the response of $G^{SI}_{\delta}$. In this frequency range, for a high amplitude $(A = 0.1\ rad)$, the $SI$ of the uncontrolled roll vehicle exceeds $SI = 1$, while the controlled one establishes acceptable behavior.
In the frequency ranges $[3, 5]\ rad/s$ and $[11, 12.5]\ rad/s$, the curves are close to each other, meaning that the lateral stability enhancement is not as significant as in the frequency range $[5, 11]\ rad/s$, where the peak magnitude is located. It can be also deduced, that at least, the roll control does not deteriorate the lateral stability at

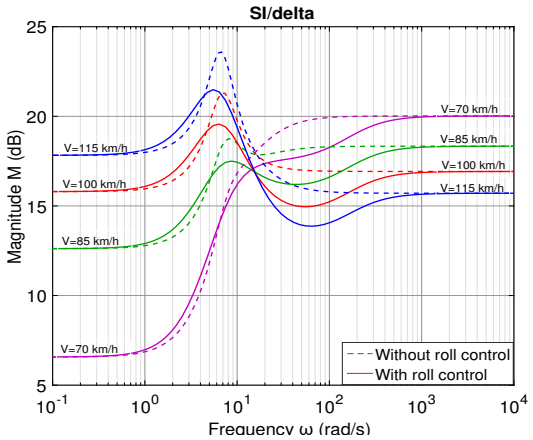


Figure 3.5 – Bode plot $SI/\delta_d$

any of these frequencies. That means, even if the roll controller is used for other objectives (like rollover avoidance, comfort...), it has no risk in deteriorating the lateral stability.
Beyond 12.5 $rad/s$, the magnitudes of both curves start decreasing, which means that the vehicle response to the steering becomes limited. Even if the roll control enhances well the lateral stability, however, as mentioned before, the vehicle will not be driven in this region.
In order to generalize for any speed, the frequency responses $G_{\delta_d}^{SI}$ of the controlled and uncontrolled vehicles are evaluated at different speeds $V = 70$, 85, 100, 115 $km/h$. The results are illustrated in Figure 3.5. This figure shows that at the speed $V = 70\ km/h$, both magnitude curves of $G_{\delta_d}^{SI}$ are low and approximately confounded in all the frequency range $[0, 12.5]\ rad/s$, that means even if the roll control can slightly reduce the $SI$, there is no need to control the roll motion, because $SI$ is already low. As the speed becomes higher, as the magnitude curves start at higher values, and the difference between both curves of each couple (at the same speed) starts to appear and becomes bigger (for $V \geq 85\ km/h$), especially in the critical frequency range $[5, 11]\ rad/s$.

### 3.3.3 Time-Domain Test

A time domain test is performed in order to show the study validity on the full vehicle model. For this task, the vehicle roll motion is controlled using the same $LQR$ controller developed before, but the vector $X$ and the speed $V$ are fed back from the full model. The chosen scenario consists of a sinusoidal steering input $\delta_d = 0.1 * \sin(6t)$ at the speed $V = 100\ km/h$. The results of the roll angle and the lateral stability comparison between both vehicles are shown in Figure 3.6. The figure confirms the frequency response study: when the roll induced angle is minimized, the lateral stability is enhanced.

To conclude, from the frequency response analysis, the major points to be highlighted are: regardless the steering amplitude value, the roll control could

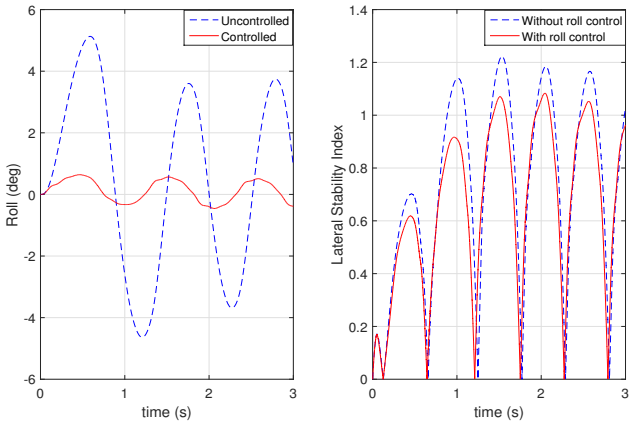


Figure 3.6 – Roll angle and $SI$ for $\delta_d = 0.1sin(6t)$; $V = 100\ km/h$

enhance the lateral stability if $SI \geq 0.7$; and at low $SI$ ($SI \leq 0.7$), there is no need to activate the roll controller for lateral stability purpose. It can be rather used for other purposes like rollover avoidance and passengers' comfort...

## 3.4 Roll Motion Controllers Design

This section is dedicated to design robust controllers to control the roll motion. The Lyapunov-based control technique described in Section 2.3 and the $STSM$ control technique described in Section 2.4 are used to develop the roll motion controllers. These robust control techniques are chosen to deal with the nonlinear behavior/dynamics of the vehicle. A performance comparison between the Lyapunov-based, the $STSM$, and the $LQR$ controllers is also performed.
As discussed before, the objectives of these controllers are either to converge the nonlinear roll motion $\theta$ given in (3.2) to zero or to $\theta_{des}$ given in (3.11). The controllers will be developed for a general reference $\theta_{des}$ of $\theta$, then, they will be tested for both references.
Let first define:

$$e_\theta = \theta - \theta_{des}, \tag{3.24}$$

the error between the actual and desired roll angles.

### 3.4.1 Lyapunov-Based Controller

The control objective is to converge the roll error variable $e_\theta$ (of relative degree 2 w.r.t the control input $M_\theta$) to zero. Let define the "off-the-manifold" variable $z_\theta$, such as:

$$z_\theta = \dot{e}_\theta + k_{1\theta} e_\theta + k_{2\theta} \int_0^t e_\theta d\tau. \tag{3.25}$$

Based on Immersion and Invariance approach [Astolfi et al., 2007], the "off-the-manifold" variable $z_\theta$ has to converge to the target dynamics corresponding to $z_\theta = 0$

in the manifold, where the roll error dynamics obey to the following equation:

$$\dot{e}_\theta + k_{1\theta} e_\theta + k_{2\theta} \int_0^t e_\theta d\tau = 0, \tag{3.26}$$

where $k_{1\theta} > 0$ and $k_{2\theta} > 0$ (Routh-Hurwitz stability condition for a second order characteristic polynomial).
In order to render the manifold attractive, i.e. to ensure the convergence of $z_\theta$ to zero, let define a positive definite Lyapunov candidate function as follows:

$$V_\theta = \frac{1}{2} {z_\theta}^2, \tag{3.27}$$

$\dot{V}_\theta$ should be negative (Lyapunov stability conditions), thus,

$$\dot{V}_\theta = z_\theta \dot{z}_\theta \leq 0, \tag{3.28}$$

then, let:

$$\dot{z}_\theta = -\alpha_\theta z_\theta, \tag{3.29}$$

which makes (3.28) always negative if $\alpha_\theta > 0$. Thus:

$$\ddot{e}_\theta + k_{1\theta}\dot{e}_\theta + k_{2\theta} e_\theta = -\alpha_\theta (\dot{e}_\theta + k_{1\theta} e_\theta + k_{2\theta} \int_0^t e_\theta d\tau), \tag{3.30}$$

where

$$\ddot{e}_\theta = \ddot{\theta} - \ddot{\theta}_{des}, \tag{3.31}$$

then substituting $\ddot{\theta}$ from (3.2) in (3.30), the control input $M_\theta$ can be found as in (3.32):

$$\begin{aligned} M_\theta = (I_x + M_s h_\theta^2)[-M_{\theta_{eq}} + \ddot{\theta}_{des} - (\alpha_\theta + k_{1\theta})(\dot{\theta} - \dot{\theta}_{des}) - (\alpha_\theta k_{1\theta} + k_{2\theta})(\theta - \theta_{des}) \\ - \alpha_\theta k_{2\theta} \int_0^t (\theta - \theta_{des}) d\tau], \end{aligned} \tag{3.32}$$

where

$$\begin{aligned} M_{\theta_{eq}} = \frac{1}{I_x + M_s h_\theta^2}[(-F_{fr} + F_{fl}) t_f + (-F_{rr} + F_{rl}) t_r \\ + M_s (h_\theta cos(\theta) + z_s) a_y + M_s (h_\theta sin(\theta) + z_s) g]. \end{aligned} \tag{3.33}$$

This control input means that the vehicle parameters should be well estimated and several variables need to be measured or estimated. Indeed, $-M_{\theta_{eq}}$ and $(I_x + M_s h_\theta^2)$ compensate all the dynamics of the roll angle expressed in (3.2) as a feed-forward command, beside the robust terms of the feedback on $e_\theta$, its time derivative and integral of equation (3.32). $\theta$, $\dot{\theta}$, and $a_y$, $z_s$ are measured by the Inertial Measurement Unit IMU, the suspension forces $F_{ij}$ could be estimated from suspensions' deflections. For the case where $\theta_{des}$ is zero, thus, $\dot{\theta}_{des}$ and $\ddot{\theta}_{des}$ are also zeros. For the case where $\theta_{des}$ is as in (3.11), thus, $\dot{\theta}_{des}$ and $\ddot{\theta}_{des}$ are the first and second derivatives of (3.11). $\dot{\theta}_{des}$ and $\ddot{\theta}_{des}$ are bounded to avoid sending high demand control to the actuators and to consider the driver feeling when turning.
Once the control input $M_\theta$ is generated, an allocation procedure on the $ASus$ forces $U_{ij}$ is proposed in Section 3.5.

### 3.4.2 Super-Twisting Second Order Sliding Mode Controller

A second controller has been developed based on the $STSM$ technique. Let define the sliding variable as follows:

$$s_\theta = \dot{e}_\theta + k_\theta e_\theta, \tag{3.34}$$

where $k_\theta > 0$. The variable $s_\theta$ has a relative degree of 1 w.r.t the control input $M_\theta$, thus the sliding mode super-twisting algorithm can be applied. Unlike the preceding Lyapunov controller, the integral term of $e_\theta$ has not been considered inside the variable $s_\theta$, because the super-twisting algorithm is a second order sliding mode, it contains an integral term on the sign of $s_\theta$ [Utkin, 2013]. $s_\theta$ has a relative degree equal to one, thus, based on the discussion given in Section 2.4, the control input can be given by:

$$M_\theta = -\alpha_\theta |s|^{0.5} \frac{s}{|s| + \varepsilon} - \beta_\theta \int_0^t \frac{s}{|s| + \varepsilon} d\tau, \tag{3.35}$$

where $\alpha_\theta$ and $\beta_\theta$ are positive gains verifying conditions (2.15). Only the knowledge of $s_\theta$ is required in real time. This means, there is no need to compensate the roll motion dynamics.
Once $s_\theta = 0$, the states $\theta$ and $\dot{\theta}$ exponentially converge to $\theta_{des}$ and $\dot{\theta}_{des}$ if $k_\theta > 0$. To be noted that the term $M_{\theta_{eq}}$ of (3.33) can be added to the control input $M_\theta$ of (3.35), as a feed-forward, to achieve a faster convergence towards the sliding surface. However, the performance shown later by simulations is performed while omitting this term.

## 3.5 Closed-Loop Control Architecture

The general closed loop control scheme is presented in Figure 3.7. The roll reference generator block represents the development given in (3.11). The switch block is manually actuated upon simulation to choose the desired roll reference. The roll controller block represents the three different control techniques: Linear Quadratic Regulation $LQR$, Lyapunov-based, and $STSM$. This block has the roll angle error and its first derivative as inputs, and $M_\theta$ as controller output. The control input $M_\theta$ has to be generated by the actuators forces or torques depending on the integrated technology. An example (but not restricted to) is the distribution of $M_\theta$ between the four active forces $U_{ij}$ of the $ASus$. This is done in the control allocation unit as described in (4.14):

$$\begin{aligned} U_{fl} &= 0.5 \tfrac{l_r}{l_f + l_r} \tfrac{M_\theta}{t_f}, \\ U_{fr} &= -0.5 \tfrac{l_r}{l_f + l_r} \tfrac{M_\theta}{t_f}, \\ U_{rl} &= 0.5 \tfrac{l_f}{l_f + l_r} \tfrac{M_\theta}{t_r}, \\ U_{rr} &= -0.5 \tfrac{l_f}{l_f + l_r} \tfrac{M_\theta}{t_r}. \end{aligned} \tag{3.36}$$

The choice of this distribution is done in order to avoid any influence on the pitch angle and the bounce displacement as shown in Figure 4.3.
The four forces in (4.14) have to be generated by the $ASus$ real physical actuators described in Section 1.6. To be noted, the controller gains are chosen to respect the

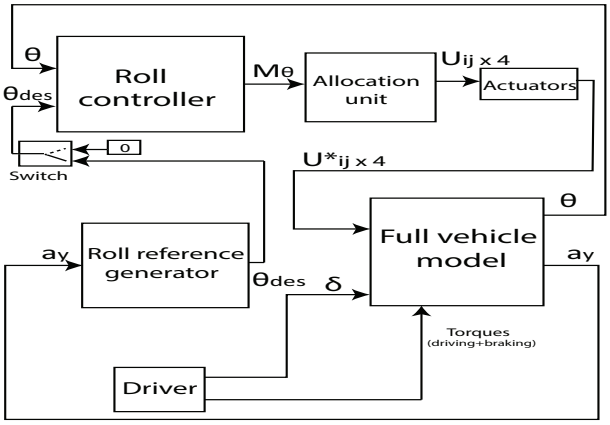


Figure 3.7 – Control scheme

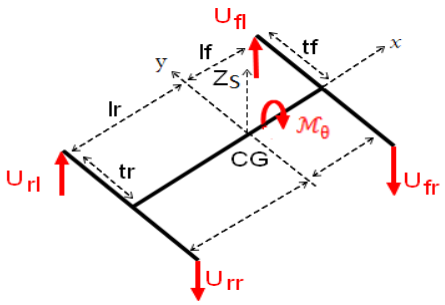


Figure 3.8 – Active forces distribution

actuator dynamics constraints. By this way, one guarantee that $U_{ij}$ passes through the actuator without being modified.

## 3.6 Controllers Validation and Performance Comparison

In this section, the proposed controllers will be validated on the simulation model (full vehicle model) because the *ASus* are not available on "SCANeR Studio" simulator. Indeed, the simulation model is efficient enough to validate the controllers, since it provides sufficient knowledge on the dynamical behavior of the vehicle.
To do so, the fishhook maneuver is the appropriate test to evaluate both the vehicle rollover risk and the lateral stability, because for the passengers cars, the lateral skidding happens around $0.8g$ lateral acceleration, while the rollover happens around $1.1g$ [Gillespie, 1992]. The fishhook maneuver represents a sharp steering in one direction, in a very short duration, then a similar steering in the opposite direction as shown in Figure 3.9.
The vehicle initial speed is $V = 130\ km/h$, while the throttle and the braking pedals are dropped.
As seen before, the roll controller is more useful above $SI = 0.7$ for lateral stability enhancement, and at high lateral acceleration for rollover avoidance. However, for now, as there is no decision layer to guaranty a stable switching, it will be activated

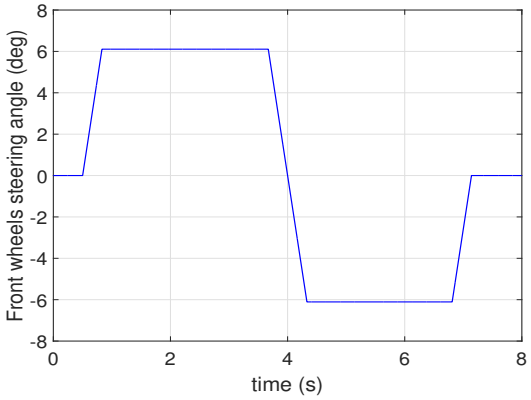


Figure 3.9 – Fishhook steering

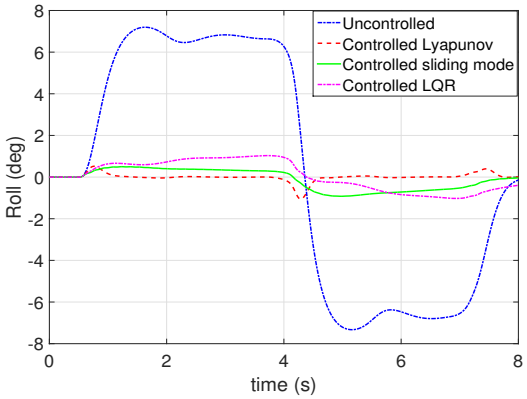


Figure 3.10 – Roll comparison ; $\theta_{des} = 0$

all the time without any switching constraint.
This section is divided into three parts: firstly, the static roll reference($\theta_{des} = 0$) will be considered, and then the dynamic one based on equation (3.11); finally, a performance comparison will be elaborated.

### 3.6.1 Controllers Validation (Static $\theta_{des}$)

Lyapunov-based, $STSM$ and $LQR$ controllers are compared in this section to evaluate their performances when minimizing the roll angle to $\theta_{des} = 0$.
Figure 3.10 shows the roll angle for a vehicle with passive suspensions (uncontrolled roll) which turns up to 7° in both directions. All the three controllers are efficient to control the roll angle toward zero. As a comparison, beside the robust terms of the feedback (3.32), the Lyapunov-based controller compensates all the dynamics of the roll angle as expressed in (3.33) to have this performance. That means, in real application, a strong knowledge (estimation, measurement, parameters exactitude, ideal modeling) on the components of $M_{\theta_{eq}}$ is needed. On the other side, the $STSM$ controller is efficient in controlling the roll angle by only the generation of the feedback from the roll angle and velocity (3.35), with no need to compensate the roll dynamics. This fact is due to the robustness of the $STSM$ control law.

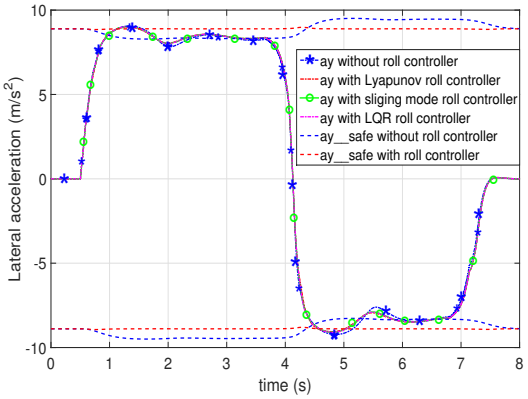


Figure 3.11 – ay comparison ; $\theta_{des} = 0$

This issue gives the sliding mode controller an advantage over the Lyapunov-based one especially in real-time application, where the estimated components could be imprecise, the vehicle parameters are uncertain, the model is not exact or perturbations occur on the system. The performance of the $LQR$ controller is also acceptable to control the roll angle towards zero.
Figure 3.11 shows the lateral acceleration of the uncontrolled roll vehicle which is approximately the same for all roll controllers. This means that the roll control does not affect the lateral acceleration to avoid rollover. In fact, the controller aims to elevate the maximal safe lateral acceleration expressed in (3.10), which depends on the roll angle. As the roll angle is minimized to zero, thus, the maximal safe lateral acceleration increases as shown in the same figure. Obviously, the roll control is not sufficient at higher lateral accelerations (higher speed and/or higher road curvature).

Figure 3.12 shows the lateral $SI$ of the uncontrolled roll vehicle which exceeds 0.7, while the controlled ones (by all the proposed controllers) enhance the lateral stability. Even if the enhancement is not sufficient, because the $SI$ remains above 0.7, the roll control to zero can be used to help the other controllers ($AFS$ and $DYC$) to avoid the lateral skidding in a $GCC$ strategy. Note that $SI$ will be more improved when controlling the roll motion towards the dynamic reference in the opposite direction.

### 3.6.2 Controllers Validation (Dynamic $\theta_{des}$)

In this section, the controllers performances will be evaluated when controlling $\theta$ to $\theta_{des}$ in the opposite direction expressed in (3.11).

Figure 3.13 shows the uncontrolled roll angle (same as in Figure 3.10), the desired one, and the controlled ones. The Lyapunov-based controlled one, and the $STSM$ controlled one accurately track the desired roll trajectory with a small error especially for the $STSM$ controller between 4 and 5 seconds, where the roll angle turns quickly. In fact, it is because the sliding mode controller has no knowledge on the roll dynamics. This transient behavior can be enhanced when considering the equivalent control input. The $LQR$ controller, as is synthesized to minimize the

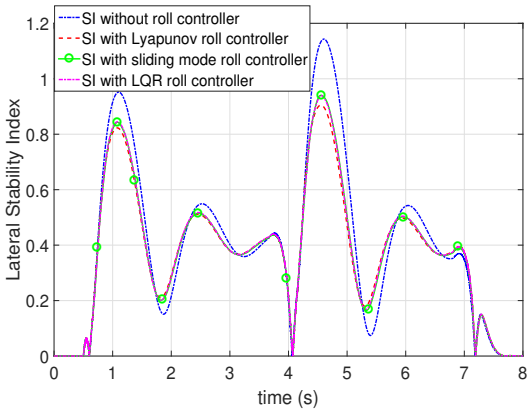


Figure 3.12 – $SI$ comparison ; $\theta_{des} = 0$

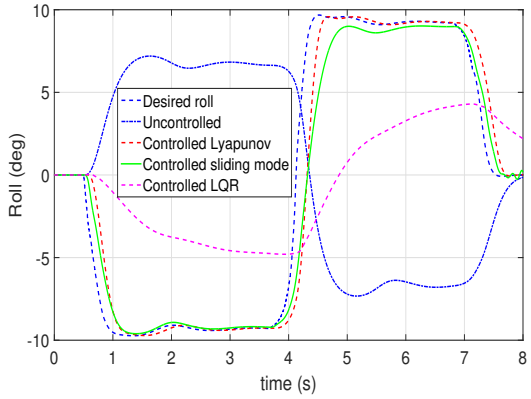


Figure 3.13 – Roll comparison ; $\theta_{des}$ opposite direction

roll angle to zero, not to minimize the error between the roll angle and its desired trajectory, it could not track the desired roll as is shown in the same figure. For this reason, in this subsection, the $LQR$ controller is not compared with the Lyapunov-based and $STSM$ controllers.

Figure 3.14 shows the approximately confounded lateral accelerations of the uncontrolled roll vehicle, and the controlled ones. It also shows the maximal safe lateral acceleration which increases more comparing to the case where the roll angle is minimized to zero. This issue drives away the rollover risk at this range of lateral acceleration.

Figure 3.15 shows the $LTR$ for the uncontrolled roll vehicle which increases up to 1 (respectively -1), that means, the vehicle is risked to rollover, while the $LTR$ for the controlled roll vehicles (both Lyapunov-based and sliding mode) is enhanced and reduced to 0.85 (respectively -0.85). Figure 3.16 shows the lateral $SI$ of the uncontrolled roll vehicle that exceeds the value 0.7 up to 1.2 which leads the vehicle to loose its lateral stability. This behavior can be explained by the high lateral acceleration which exceeds the lateral acceleration handling limit $\mu.g$ [Rajamani, 2012]. It can be also explained by the insufficiency of the inner tires lateral forces due to low vertical loads on these tires. Controlling the roll angle toward the inside wheels elevates these vertical forces, thus, the tire lateral forces become higher,

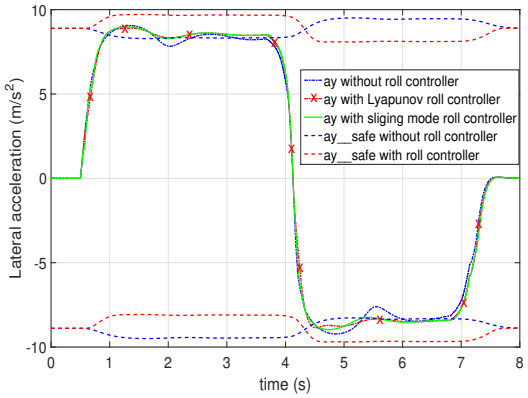


Figure 3.14 – ay comparison ; $\theta_{des}$ opposite direction

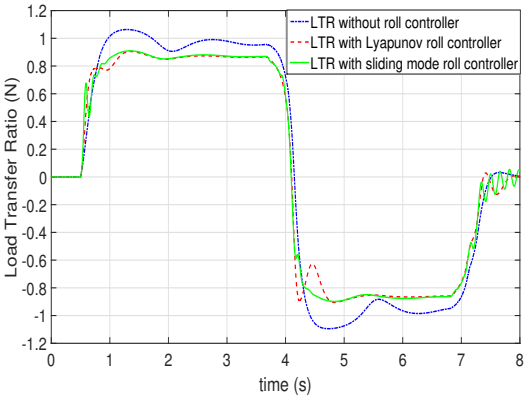


Figure 3.15 – $LTR$ comparison ; $\theta_{des}$ opposite direction

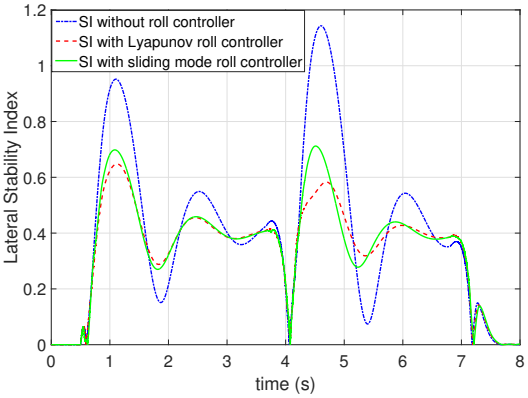


Figure 3.16 – $SI$ comparison ; $\theta_{des}$ opposite direction

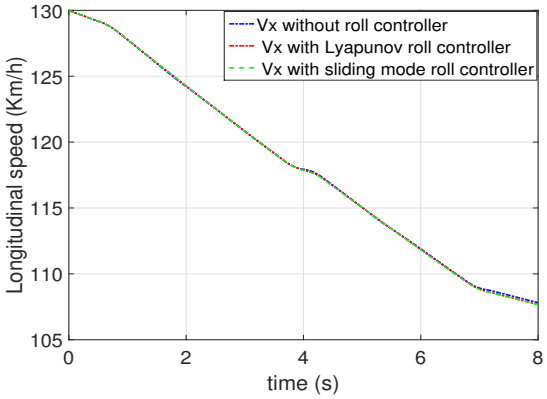


Figure 3.17 – Vx comparison ; $\theta_{des}$ opposite direction

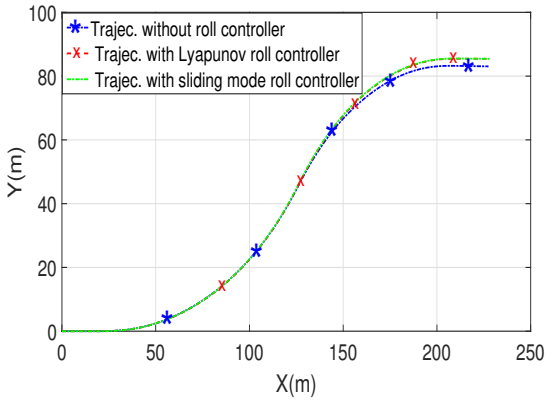


Figure 3.18 – Trajectory comparison ; $\theta_{des}$ opposite direction

which enhances the lateral stability as shown in the same figure. Hence, the $ASus$ system contributes in maintaining the vehicle lateral stability, especially after a sharp steering where the $SI$ is reduced to 0.7 (or less) by both roll controllers.
Figure 3.17 shows the vehicle longitudinal speed, it drops during all tests due to frictions and the aggressive steering at the same rate, that means the roll control dedicated to avoid rollover and lateral skidding has no effect on the vehicle speed, in contrary to other known stabilizing controllers like $ADB$ or simply normal braking [Rajamani, 2012].
Figure 3.18 shows the advantage of the roll control for lateral stability enhancement and rollover avoidance on the performed trajectories, where they are very close to each other comparing to other controllers like $AFS$ or $ADB$ dedicated to the same objectives as explained in [Rajamani, 2012].
Figure 3.19 shows the control inputs for both Lyapunov-based and sliding mode controllers which are in fact the $ASus$ forces provided by the actuators (after saturating and filtering). This figure shows that their maximal value is around 4000 $N$ which is feasible by the $ASus$ actuators without any saturation. This fact makes these developed forces realistic and can be implemented to the vehicle after controlling the $ASus$ actuators.

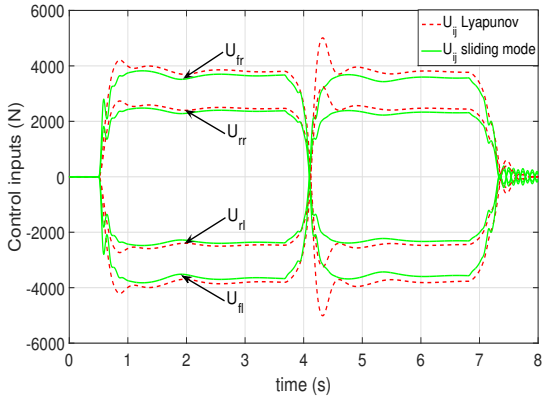


Figure 3.19 – Control inputs comparison ; $\theta_{des}$ opposite direction

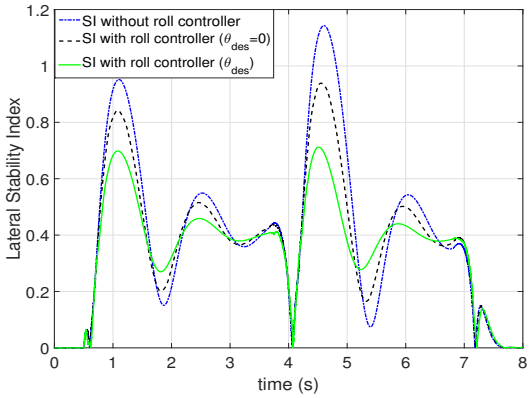


Figure 3.20 – $SI$ comparison; $\theta_{des} = 0$ vs $\theta_{des}$ opposite direction

### 3.6.3 Roll Reference Performance Comparison

Turning the roll angle in the opposite direction requires more energy than just minimizing it to zero, because it can be only achieved by the $ASus$ which consume more energy comparing to the semi-$ASus$ or the $ARB$. This fact has made from the $ASus$ a non preferable system to be integrated into series vehicles. However, the results of this chapter show the ability of the $ASus$ in maintaining the lateral stability and avoiding the rollover when turning the roll angle in the opposite direction. Figure 3.20 compares the $SI$ for the vehicle when controlling the roll angle toward zero and toward $\theta_{des}$ of eq. (3.11). This Figure also shows that the control of the roll angle in the opposite direction brings more enhancement on the lateral stability than just minimizing it to zero. Hence, it could contribute to reduce the energy consumption of other actuators used for lateral stability ($AFS$, $ADB$...).

## 3.7 Conclusion

This chapter has shown the enhancement that the vehicle roll control could bring on its lateral stability and rollover avoidance, either by turning it to zero or to a

new desired trajectory in the opposite direction. For rollover avoidance, the proof of this improvement is done in time domain, by means of defining the safe lateral acceleration threshold and analyzing it when controlling the roll angle. The proof of the improvement on the lateral stability is done in the frequency domain, by means of analyzing the frequency response of the lateral $SI$ w.r.t the steering input, in both cases, when the roll angle is controlled or not.
Lyapunov-based, $STSM$, and $LQR$ controllers have been developed to generate the roll moment which controls the roll angle. Controlling the roll in the opposite direction has demonstrated more advantages on the lateral stability and rollover avoidance compared to only minimizing the roll angle to zero.
In the context of $GCC$, the roll control can be activated for two objectives: first, when the lateral $SI$ becomes higher than $SI = 0.7$ (basing on the lateral stability enhancement), and second, when the $LTR$ becomes higher than $LTR = 0.8$ (basing on rollover avoidance enhancement). However, the controllers can be used all the time without these conditions because they do not deteriorate in any way neither the lateral stability nor the rollover avoidance. The advantages of these criteria could be to minimize the consumed energy, when a higher decision layer is proposed to coordinate the suspensions with other stabilizing systems, like the $AFS$ and the $DYC$, in the context of $GCC$.
Next chapter develops a decentralized architecture for the global chassis control, involving $AFS$, $DYC$, and $ASus$.

# Global Chassis Control Involving Active Front Steering, Direct Yaw Control and Active Suspensions - a Decentralized Architecture

This chapter investigates new achievements in *GCC*, involving *AFS*, *DYC*, and *ASus*, to improve the overall vehicle performance, i.e. the vehicle maneuverability, lateral stability, rollover avoidance, and ride comfort, in different driving situations. A decentralized multilayer control architecture is designed, tested, and validated on Matlab/Simulink using the "full vehicle model". The results show the effectiveness of the proposed architecture.

## 4.1 Introduction

The main goal of the *GCC* system developed in this chapter is to enhance the overall vehicle performance i.e. maneuverability, lateral stability, rollover avoidance, and ride comfort. Figure 4.1 depicts the general architecture of the proposed *GCC*. It consists of a multilayer control architecture, formed by three hierarchical layers. The lower layer is the actuator layer which represents the actuators implemented into the vehicle that generate their control inputs based on the orders sent from the middle layer (see Section 1.6). The middle layer is the control layer which is responsible to generate the control inputs that minimize the errors between the reference and actual vehicle state variables, i.e., yaw, side-slip, roll, pitch, and heave motions, regardless of the driving situation. Since the control architecture is decentralized, a heuristic solution is proposed by decoupling the control problem. The *STSM* robust control technique is applied to derive the control inputs, where the *AFS* control input minimizes only the error on the yaw rate, mainly to improve the maneuverability and enhance the lateral stability; the *DYC* control input is privileged to minimize only the error on the side-slip dynamics, mainly to guarantee the lateral stability of the vehicle; and the *ASus* control inputs minimize only the errors on the roll, pitch, and heave dynamics, mainly to improve the ride comfort, lateral stability, and rollover avoidance. The higher layer is the decision making layer which is developed to promote/attenuate the local objectives of the sub-controllers by monitoring the *SI* criterion, and a fuzzy-logic-based criterion developed in this

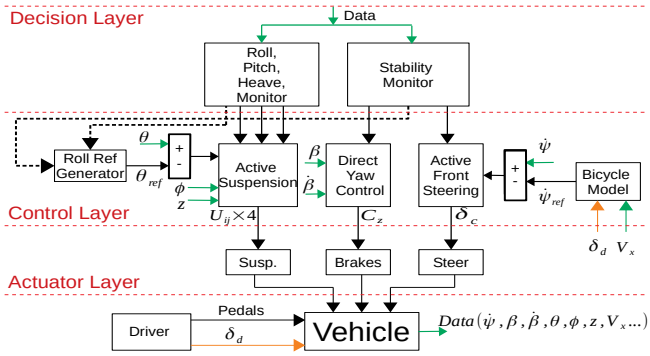


Figure 4.1 – Proposed $GCC$ scheme

chapter. The decision making layer generates weighted parameters which adjust the control reference trajectories to adapt the controllers dynamics and performances according to the driving conditions.

The contributions of this chapter are as follows:

- single-input single-output $STSM$ controllers are developed to control the $ASus$, the $DYC$, and the $AFS$ in the presence of modeling errors, external disturbances and exogenous inputs.
- new objectives are achieved by the $ASus$ controller, usually developed for ride comfort. It is exploited to improve the vertical stability (rollover avoidance) and lateral stability (lateral skidding avoidance). General improvements are also observed, e.g., the $DYC$ will be less solicited, the vehicle speed will less drop, and others...
- development of a decision layer that promotes/attenuates the local sub-controllers objectives. This layer monitors the dynamics of the vehicle, calculates and sends scheduled gains to the sub-controllers, based on fuzzy logic rules and a stability criterion to enhance the overall vehicle performance according to the driving conditions.

## 4.2 Global Chassis Control Controller Design

### 4.2.1 Control Synthesis Model

The full vehicle model has been already developed in Section 1.1. It is a complex nonlinear model which combines the vertical, lateral, longitudinal, and tire/road contact (Dugoff model) sub-models, in addition to four wheels angular dynamics, with a 26 state variables gathered in the state vector $X$ of (4.1).

$$X = [\theta, \dot{\theta}, \phi, \dot{\phi}, z_s, \dot{z}_s, z_{us,ij}, \dot{z}_{us,ij}, \omega_{ij}, x, \dot{x}, y, \dot{y}, \psi, \dot{\psi}, \beta, \dot{\beta}]^T. \tag{4.1}$$

In order to develop a $GCC$ controller, some dynamics of the full model (see Figure 4.2) are rewritten in the affine form to serve as a control synthesis model, such as:

$$\ddot{\theta} = g_\theta(X) + f_\theta(X)M_\theta, \tag{4.2}$$

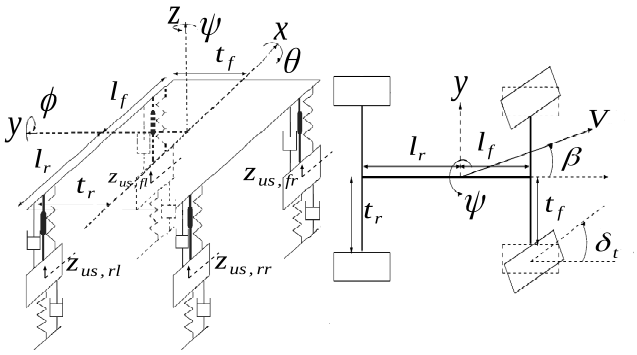


Figure 4.2 – Full vehicle model

$$\ddot{\phi} = g_{\phi}(X) + f_{\phi}(X)M_{\phi}, \tag{4.3}$$

$$\ddot{z}_s = g_z(X) + f_z(X)M_z, \tag{4.4}$$

$$\ddot{\psi} = g_{\dot{\psi}}(X) + f_{\dot{\psi},\delta}(X)\delta_t + f_{\dot{\psi},C_z}(X)C_z, \tag{4.5}$$

$$\ddot{\beta} = g_{\beta}(X) + f_{\beta,\delta}(X)\delta_t + f_{\beta,C_z}(X)C_z, \tag{4.6}$$

where $M_\theta$, $M_\phi$, and $M_z$ represent respectively the active roll torque, active pitch torque, and active heave force, as intermediate control inputs. These inputs have to be generated at a lower level control by physical actuators, e.g. the $ASus$ forces $U_{ij}$ integrated on four corners. $\delta_t = \delta_d + \delta_c$ is the total steering angle at the front wheels, where $\delta_d$ is the one provided by the driver and $\delta_c$ is the one provided by the $AFS$ controller. $C_z$ is the active yaw torque provided by the $DYC$ controller. $C_z$ has to be generated at a lower level control as an $ADB$ on the rear wheels. $g_q(X)$, $f_v(X)$, $f_{l,\delta}(X)$, and $f_{l,C_z}(X)$ where $q = \{v, l\}$, $v = \{\theta, \phi, z_s\}$ and $l = \{\dot{\psi}, \beta\}$ are the nonlinear functions of the full vehicle model detailed in Appendix .2.
Since the control synthesis model is nonlinear, where some functions are hard to be estimated in real time, and in presence of modeling errors and external disturbances, the $STSM$ robust control technique is relevant to design the $GCC$ controller, without compensating the vehicle dynamics.

## 4.2.2 Control Layer

### 4.2.2.1 Active Suspensions Controller

The common objectives of the $ASus$ widely developed in literature are improving the ride comfort and road holding [Savaresi et al., 2010], [Yoon et al., 2010] and [Akhmetov et al., 2010]. One contribution of this chapter is to emphasize new achievable enhancements on the global chassis performance through the coordinated integration of the $ASus$. These enhancements concern directly the rollover and the lateral stability. Hence, the other sub-controllers in the $GCC$ structure become less solicited, and consequently, the vertical and lateral stability ranges of the vehicle manipulation can be enlarged to more hard maneuvers.
Let first develop an $ASus$ controller dedicated to control the roll, pitch and heave

motions of the sprung mass, respectively described by equations (4.2), (4.3) and (4.4). A general form of these dynamics can be written as:

$$\ddot{v} = g_v(X) + f_v(X)M_v. \tag{4.7}$$

Each of these equations has a unique control input $M_v$, that acts only on the corresponding variable $v$. Thus, similar controllers with particular gains can be developed for all of these dynamics.
To control these dynamics, one can choose the $STSM$ control law known by its robustness to modeling errors and external disturbances. Let $v_{ref} = \{\theta_{ref}, \phi_{ref}, z_{ref}\}$ be the general reference trajectories to be tracked, and $\dot{v}_{ref} = \left\{\dot{\theta}_{ref}, \dot{\phi}_{ref}, \dot{z}_{s,ref}\right\}$ be their time derivatives.
The reference trajectories are determined based on several factors. The objective of ride comfort in literature is to minimize the roll, pitch and heave angles and velocities/accelerations [Savaresi et al., 2010], [Yoon et al., 2010] and [Akhmetov et al., 2010], thus, $v_{des} = \dot{v}_{des} = \{0, 0, 0\}$. As seen in Chapter 3, the roll control towards zero contributes to the enhancement of the lateral stability and rollover avoidance. To provide more enhancement on both objectives, the dynamic roll reference of Section 3.2.4 can be followed. Moreover, scheduling parameters are lately introduced, in the decision making layer, inside these reference trajectories to promote/attenuate the control objectives.
Let consider now the control towards general references $v_{ref}$. Thus, let:

$$e_v = v - v_{ref}, \tag{4.8}$$

be the error between the actual and reference state. Let:

$$s_v = \dot{e}_v + \lambda_v \, e_v, \tag{4.9}$$

be the sliding variable, chosen with a relative degree of 1 w.r.t the control input $M_v$ (the control input appears in the first time derivative of the sliding variable) to meet the super-twisting constraints. This means that the discontinuous function appears in the second derivative of the sliding variable such that:

$$\ddot{s}_v(s_v, t) = \Phi_v(s_v, t) + \xi_v(s_v, t)\dot{M}_v(t), \tag{4.10}$$

where $\Phi_v(s_v, t)$ and $\xi_v(s_v, t)$ are unknown bounded functions satisfying conditions of (2.13).
The sliding mode control input, based on the Super-Twisting algorithm, is given by:

$$M_v(t) = -\alpha_{v,1}|s_v|^{\tau_v} sign(s_v) - \alpha_{v,2}\int_0^t sign(s_v)d\tau, \tag{4.11}$$

where $\alpha_{v,1}$ and $\alpha_{v,2}$ are positive gains satisfying conditions of (2.15), and $\tau_v \in ]0, 0.5]$. The super-twisting algorithm guaranties the convergence of $s_v$ in a finite time to zero. Once $s_v = 0$, the states $v$ and $\dot{v}$ exponentially converge to $v_{ref}$ and $\dot{v}_{ref}$ respectively if $\lambda_v > 0$. The function $sign$ is smoothed by the approximation $sign(s_v) = \frac{s_v}{|s_v|+\varepsilon_v}$, where $\varepsilon_v > 0$.

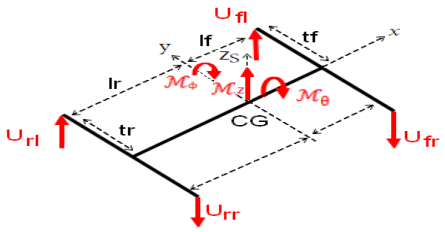


Figure 4.3 – Active forces distribution

Once the needed control inputs $M_\theta$, $M_\phi$, and $M_z$ are obtained to control $\theta$, $\phi$, and $z_s$, there are different ways to generate them by the $ASus$ forces on the four vehicle corners. An optimal allocation can be done by an optimization procedure. The optimal allocation has the advantage of tolerating the faults of the $ASus$. However, this is not treated in this thesis. Thus, we propose two simple allocation methods as the following:

**Pseudo-Inverse Matrix:**
From Figure 4.3, the virtual control inputs $M_\theta$, $M_\phi$, and $M_z$ can be written in function of the $ASus$ forces such as:

$$\begin{pmatrix} M_\theta \\ M_\phi \\ M_z \end{pmatrix} = \underbrace{\begin{bmatrix} -t_f & t_f & -t_r & t_r \\ -l_f & -l_f & l_r & l_r \\ 1 & 1 & 1 & 1 \end{bmatrix}}_{L} \begin{pmatrix} U_{fr} \\ U_{fl} \\ U_{rr} \\ U_{rl} \end{pmatrix}. \tag{4.12}$$

Thus, the $ASus$ forces $U_{ij}$ can be found by applying the pseudo-inverse matrix method, such as:

$$\begin{pmatrix} U_{fr} \\ U_{fl} \\ U_{rr} \\ U_{rl} \end{pmatrix} = \left(L^T.L\right)^{-1} L^T \begin{pmatrix} M_\theta \\ M_\phi \\ M_z \end{pmatrix} \tag{4.13}$$

The pseudo-inverse matrix method may hold singularities in the solution, thus, another constraint could be added to make a square matrix $L$, or a geometrical distribution method can be applied.

**Geometrical distribution:**
This methods consists of generating for each dynamics the needed control input, by doing a geometrical distribution between the four suspensions, while maintaining no effect on the other two dynamics, as given in (4.14) (see Figure 4.3).

$$\begin{aligned} U_{fl} &= 0.5\tfrac{l_r}{l_f+l_r}\tfrac{M_\theta}{t_f} - 0.5\tfrac{M_\phi}{l_f+l_r} + 0.5\tfrac{l_r}{l_f+l_r}M_z, \\ U_{fr} &= -0.5\tfrac{l_r}{l_f+l_r}\tfrac{M_\theta}{t_f} - 0.5\tfrac{M_\phi}{l_f+l_r} + 0.5\tfrac{l_r}{l_f+l_r}M_z, \\ U_{rl} &= 0.5\tfrac{l_f}{l_f+l_r}\tfrac{M_\theta}{t_r} + 0.5\tfrac{M_\phi}{l_f+l_r} + 0.5\tfrac{l_f}{l_f+l_r}M_z, \\ U_{rr} &= -0.5\tfrac{l_f}{l_f+l_r}\tfrac{M_\theta}{t_r} + 0.5\tfrac{M_\phi}{l_f+l_r} + 0.5\tfrac{l_f}{l_f+l_r}M_z. \end{aligned} \tag{4.14}$$

#### 4.2.2.2 Active Front Steering Controller

The maneuverability or steer-ability means having a linear relation between the steering provided by the driver and the achieved vehicle yaw rate. The objective of the $AFS$ controller is to enhance the steer-ability, thus, converging the real vehicle yaw rate to a reference one linear to the steer angle provided by the driver. The linear relation can be derived from the bicycle model exposed in Section 1.4, which represents a stable and ideal motion of the vehicle, where the tires lateral forces are supposed to be linear to the tires side-slip angles. From the other side, the $AFS$ controller will be promoted/attenuated based on the decision layer. Thus, the yaw rate reference trajectory $\dot{\psi}_{ref}$ is related to the bicycle model given in Section 1.4 and to the scheduling parameters of the decision layer. The explicit relation will be given later in Section 4.2.3.
The $AFS$ can also enhance the lateral stability of the vehicle. As the lateral stability is related to the lateral acceleration $a_y$, the authors in [Rajamani, 2012] propose to maintain $a_y$ below a threshold depending on the maximal possible adherence (4.15), by saturating $\dot{\psi}_{ref}$, as described in (4.16).

$$a_y \simeq \ V_x(\dot{\psi} + \dot{\beta}) \leq \mu \ g, \tag{4.15}$$

$$\dot{\psi}_{ref,max} = 0.85\mu \ g/V_x, \tag{4.16}$$

where $\mu$ is the road adherence coefficient and $g$ is the gravity constant.
Let consider for now that the objective of the $AFS$ is to converge the vehicle yaw rate $\dot{\psi}$, whose dynamics is described in (4.5), to a general reference one $\dot{\psi}_{ref}$.
Since the yaw equation (4.5) does not reflect the vehicle real yaw dynamics, because it is a simplified linear representation, and since some vehicle parameters are hard to be instantly estimated like $\mu$, the $STSM$ robust control technique is applied here without compensating the yaw dynamics. For simplicity, the corrective yaw torque control input is omitted in the $AFS$ controller design ($C_z = 0$). This assumption makes from the $STSM$ controller a heuristic solution. This issue is resolved in the next chapter when adopting the $MIMO$ $\mathcal{H}_\infty$ optimal control technique.
Thus, let define the sliding variable as follows:

$$s_{\dot{\psi}} = e_{\dot{\psi}} = \dot{\psi} - \dot{\psi}_{ref}. \tag{4.17}$$

The variable $s_{\dot{\psi}}$ has a relative degree of 1 w.r.t the control input $\delta_c$. Thus,

$$\ddot{s}_{\dot{\psi}}(s_{\dot{\psi}}, t) = \Phi_{\dot{\psi}}(s_{\dot{\psi}}, t) + \xi_{\dot{\psi}}(s_{\dot{\psi}}, t)\dot{\delta}_c(t). \tag{4.18}$$

$\Phi_{\dot{\psi}}(s_{\dot{\psi}}, t)$ and $\xi_{\dot{\psi}}(s_{\dot{\psi}}, t)$ are unknown bounded functions satisfying conditions of (2.13). By the same reasoning applied above, the $STSM$ control input $\delta_c$ can be formulated as (4.19):

$$\delta_c = -\alpha_{\dot{\psi},1} \left| s_{\dot{\psi}} \right|^{\tau_{\dot{\psi}}} sign(s_{\dot{\psi}}) - \alpha_{\dot{\psi},2} \int_0^t sign(s_{\dot{\psi}}) d\tau. \tag{4.19}$$

This algorithm guarantees the convergence of $s_{\dot{\psi}}$ to zero in a finite time, if the gains $\alpha_{\dot{\psi},1}$ and $\alpha_{\dot{\psi},2}$ satisfy the same convergence conditions of (2.15), and $\tau_{\dot{\psi}} \in ]0,\ 0.5]$.

Since $s_{\dot{\psi}}$ is formed only by the error on the yaw rate, thus, $\dot{\psi}$ converges in finite time towards $\dot{\psi}_{ref}$.

This control strategy enhances the maneuverability of the vehicle and maintain the lateral acceleration below the lateral-skidding threshold $\mu.g$. However, the lateral stability also depends on the vehicle side-slip angle $\beta$ and its rate of change $\dot{\beta}$. Thus, this control strategy enhances without guarantee the lateral stability, especially when these variables are solicited enough to destabilize the vehicle. To resolve the problem, the first intuitive solution is to introduce the control of $\beta$ and $\dot{\beta}$ in the objectives of the $AFS$ controller. However, the yaw torque provided by the steering in the critical range of lateral stability is not enough to stabilize the vehicle since the lateral tires forces will be saturated. Alternatively, the $DYC$ controller using differential rear braking is known to be effective to control $\beta$ and $\dot{\beta}$, while it has the disadvantages of: decelerating the vehicle, long-term wheels wear, and driver discomfort. Thus, it is recommended to actuate the $DYC$ controller only under critical situations.

#### 4.2.2.3 Direct Yaw Control Controller:

The objective of the $DYC$ controller is to control the side-slip angle $\beta$ and its rate of change $\dot{\beta}$ when the vehicle is under critical driving situations by generating a corrective yaw torque. The physical actuators to create the yaw torque are selected to be the rear $EMB$. This choice prevents direct interference with the $AFS$ on the front tires [Doumiati et al., 2013].
In this subsection, the $DYC$ controller will be developed as a decentralized controller, i.e. to control $\beta$ and $\dot{\beta}$ whatever the driving situation is. Later, in the decision layer, the $DYC$ controller will be activated based on the decision rules.
Similar to the case of the $AFS$, the $STSM$ control law is adopted to control $\beta$ and $\dot{\beta}$ of (4.6) respectively towards the reference trajectories $\beta_{ref}$ and $\dot{\beta}_{ref}$. These general reference trajectories are related to the bicycle model given in Section 1.4 and to the scheduling parameters of the decision layer. The explicit relation will be given later in Section 4.2.3.This control is done through generating the corrective yaw torque $C_z$ as the control input while omitting $\delta_c$. Thus, let:

$$e_\beta = \beta - \beta_{ref}, \tag{4.20}$$

be the error between the actual and reference side-slip angles. Let the corresponding sliding variable be:

$$s_\beta = \dot{e}_\beta + \lambda_\beta \, e_\beta. \tag{4.21}$$

The sliding variable has a relative degree of 1 w.r.t the control input $C_z$. By the same reasoning as before, the super-twisting algorithm guarantees the convergence of $s_\beta$ to zero in a finite time. Thus, $\beta$ and $\dot{\beta}$ exponentially converge to $\beta_{ref}$ and $\dot{\beta}_{ref}$ if $\lambda_\beta > 0$. Finally, the $STSM$ control input $C_z$ is given in (4.22) by:

$$C_z = -\alpha_{\beta,1} \left|s_\beta\right|^{\tau_\beta} sign(s_\beta) - \alpha_{\beta,2} \int_0^t sign(s_\beta) d\tau, \tag{4.22}$$

where $\alpha_{\beta,1}$ and $\alpha_{\beta,2}$ satisfy conditions of (2.15), and $\tau_\beta \in ]0,\ 0.5]$.

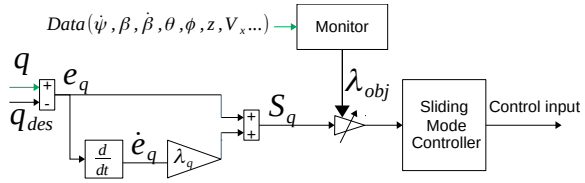


Figure 4.4 – Scheduled controller

### 4.2.3 Decision Layer

A decision layer will be developed in this section to coordinate the $GCC$ sub-controllers. The main idea is to promote/attenuate the control objectives by multiplying each sliding variable by a scheduling gain $\{\lambda_{obj}\} = \{\lambda_{\dot{\psi}}, \lambda_\beta, \lambda_\theta, \lambda_\phi, \lambda_z\}$ as depicted in Figure 4.4. Each of $\lambda_{obj}$ varies between 0 and 1. As much $\lambda_{obj}$ approaches to 1, as the control objective is promoted, vice-versa, the control objective is completely attenuated when $\lambda_{obj}$ approaches to 0.

In order to maintain the stability of each $STSM$ controller, these scheduling parameters have to be endogenous in the sliding variables. This can be done through introducing these scheduling parameters inside the reference trajectories. As mentioned before, $\dot{\psi}_{ref}$, and $\beta_{ref}$ depend on the bicycle model and the weighting gains sent from the decision layer, while $\theta_{ref}$, $\dot{\theta}_{ref}$, $\phi_{ref}$, $\dot{\phi}_{ref}$, $z_{ref}$, $\dot{z}_{ref}$ are to be minimized and depend on the weighting gains sent from the decision layer. Thus, let define the different trajectory references such as:

$$\begin{aligned}
\dot{\psi}_{ref} &= \lambda_{\dot{\psi}}\ \dot{\psi}_{bic} + (1 - \lambda_{\dot{\psi}})\ \dot{\psi}, \\
\beta_{ref} &= \lambda_\beta \beta_{bic} + (1 - \lambda_\beta)\beta, \\
\theta_{ref} &= \lambda_\theta 0 + (1 - \lambda_\theta)\theta, \\
\dot{\theta}_{ref} &= \lambda_\theta 0 + (1 - \lambda_\theta)\dot{\theta}, \\
\phi_{ref} &= \lambda_\phi 0 + (1 - \lambda_\phi)\phi, \\
\dot{\phi}_{ref} &= \lambda_\phi 0 + (1 - \lambda_\phi)\dot{\phi}, \\
z_{s,ref} &= \lambda_z 0 + (1 - \lambda_z) z_s, \\
\dot{z}_{s,ref} &= \lambda_z 0 + (1 - \lambda_z)\dot{z}_s.
\end{aligned} \tag{4.23}$$

When $\lambda_{obj}$ approaches to 1, the corresponding reference trajectory becomes equal to the bicycle trajectory (for $\dot{\psi}$ and $\beta$), and equal to 0 (for $\theta$, $\phi$, and $z_s$). Thus, the corresponding controller is promoted to control the corresponding variable. When $\lambda_{obj}$ approaches to 0, the reference trajectory becomes equal to the actual vehicle one, thus, the control of the corresponding variable is attenuated since the corresponding sliding variable is vanished.

Consequently, the different sliding variables become equivalent to:

$$\begin{aligned}
s_{\dot{\psi}} &= \dot{\psi} - \dot{\psi}_{ref} = \lambda_{\dot{\psi}}\ (\dot{\psi} - \dot{\psi}_{bic}), \\
s_\beta &= \beta - \beta_{ref} = \lambda_\beta(\beta - \beta_{bic}), \\
s_\theta &= (\dot{\theta} - \dot{\theta}_{ref}) + k_\theta(\theta - \theta_{ref}) = \lambda_\theta[\dot{\theta} + k_\theta\theta], \\
s_\phi &= (\dot{\phi} - \dot{\phi}_{ref}) + k_\phi(\phi - \phi_{ref}) = \lambda_\phi[\dot{\phi} + k_\phi\phi], \\
s_z &= (\dot{z}_s - \dot{z}_{s,ref}) + k_z(z_s - z_{s,ref}) = \lambda_z[\dot{z}_s + k_z z_s].
\end{aligned} \tag{4.24}$$

These new forms of sliding variables mean that the actual state variables are forced to converge to the extended bicycle reference model (for $\dot{\psi}$ and $\beta$), and to 0 (for $\theta$, $\phi$, and $z_s$), only if the scheduling gains are high (close to 1). In this case, we say that the control objective is promoted. Otherwise, the control objective is attenuated (relaxed) and the state variables remain without control.
**Note:** The modification of the sliding variables by the multiplication with the scheduling gains maintains the closed-loop stability of the individual $AFS$ and $DYC$ since these gains are introduced in the reference trajectories.

The decision layer monitors all controllers objectives based on monitoring criteria (data) and a set of coordination rules defined in the following, then, it calculates and sends instantly the exact value of $\lambda_{obj}$ to attenuate/promote the corresponding objective.

#### 4.2.3.1 Active Front Steering and Direct Yaw Control Coordination Rules:

The criteria by which the $AFS$ and $DYC$ are coordinated is the lateral $SI$. The coordination rules are as follows:
* If the vehicle situation is normal $SI \leq \underline{SI}$, then the $AFS$ controller should be promoted to improve the maneuverability. In this range, the $DYC$ controller is disabled.
* If the vehicle operates in the unstable region $SI \geq \overline{SI}$, then the $DYC$ controller should be promoted to enhance the lateral stability. In this range, the $AFS$ controller has a poor effect to enhance the lateral stability, thus, it may not be actuated.
* In the critical region $\underline{SI} \leq SI \leq \overline{SI}$, the $AFS$ and $DYC$ should be attenuated/promoted smoothly and continuously in this range which can be done by a sigmoid function.
Based on these rules, the scheduling gains $\lambda_{\dot{\psi}}$ and $\lambda_{\beta}$ can be given in function of $SI$ as:

$$\begin{aligned} \lambda_{\beta} &= \frac{1}{1+e^{-\frac{8}{\overline{SI}-\underline{SI}}(SI-\frac{\overline{SI}+\underline{SI}}{2})}}, \\ \lambda_{\dot{\psi}} &= 1-\lambda_{\beta}. \end{aligned} \tag{4.25}$$

These functions are plotted in Figure 4.5.

#### 4.2.3.2 Active Suspensions Coordination/Actuation Rules:

The proposed $ASus$ controller will participate in the $GCC$ by achieving three main objectives: roll control, pitch control and heave control. To reduce the excessive actuation of the $ASus$, while maintaining good ride and stability (vertical and lateral) qualities, the following supervision rules will promote/attenuate these objectives:

* Since the natural tendency of the driver is to turn his body towards the inside of the corner to encounter the induced roll motion, thus, controlling the roll angle towards the inside of the corner (in the opposite direction of the induced roll

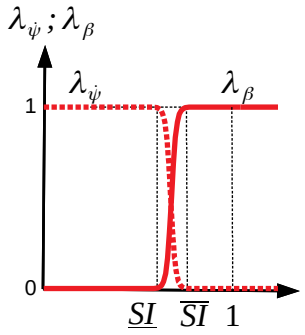


Figure 4.5 – $AFS$ and $DYC$ coordination functions

motion) improves the driver comfort. Hence, the roll control objective can always be promoted to follow the dynamic reference $\theta_{des}$ expressed in (3.11), or at-least to follow the static reference 0 in order to remove the induced roll motion feeling. By this procedure, the ride comfort (in terms of roll motion) and the stability (lateral and vertical) will be enhanced regardless of any monitoring criteria. Thus, $\lambda_\theta = 1$ whatever the vehicle situation is.

* The pitch control objective has to be attenuated/promoted depending on the severity of braking/acceleration, to reduce the use of the $ASus$ while maintaining good ride quality (in terms of pitch motion). Thus, only the harsh and considerable pitch motion has to be minimized by making $\lambda_\phi$ approaches to 1 to promote the pitch control objective. As much the pitch motion becomes soft, as $\lambda_\phi$ approaches to 0 to attenuate the pitch control objective.
One suggests treating $\lambda_\phi$ as a fuzzy-scheduling gain which attenuates/promotes the pitch control objective, based on the pitch angle error of (4.8) and its rate of change. The pitch angle error and its rate of change are applied to the Fuzzy Logic Controller ($FLC$) as inputs, and the fuzzy-scheduling gain $\lambda_\phi$ is the output. The reason of choosing the $FLC$ for the decision-making process is due to its simplicity to make the relation between the needed control input and the controlled variables in an intuitive way. Five fuzzy sets are defined for each input, and three for the output such as:
$e_\phi, \dot{e}_\phi \in \{NB\ (Negative\ Big),\ NS\ (Negative\ Small),\ ZE\ (Zero), PS\ (Positive\ Small),\ PB\ (Positive\ Big)\}$; and $\lambda_\phi \in \{PS,\ PM(Positive\ Medium),\ PB\}$. The normalized Membership Functions (MFs) of fuzzification of the controller inputs and defuzzification of the controller output are respectively given in Figures 4.6, 4.7 and 4.8. To determine the fuzzy controller output $\lambda_\phi$ for the given fuzzy controller inputs $e_\phi$ and $\dot{e}_\phi$, the decision matrix of the linguistic control rules is designed and presented in Table 4.1. These fuzzy sets, membership functions, and the linguistic rules are usually determined based on an expert knowledge of the system by performing several simulations. Finally, to defuzzify the result/output, the "*Mamdani centroid fuzzy inference method*" is used [[Reznik, 1997]].

* The heave control objective attenuation/promotion can be done in a similar manner to the pitch control objective. That means, a fuzzy-scheduling gain $\lambda_z$ can be obtained to regulate the degree of achievement of the heave control objective

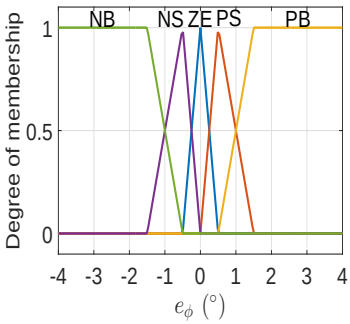


Figure 4.6 – Fuzzy sets of the input $e_\phi$

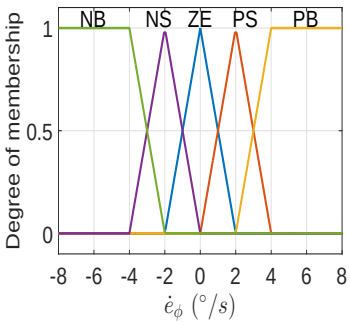


Figure 4.7 – Fuzzy sets of the input $\dot{e}_\phi$

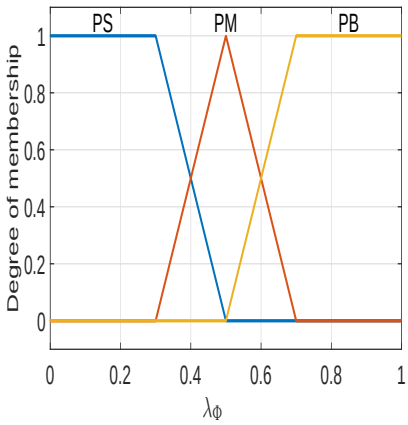


Figure 4.8 – Fuzzy sets of the output $\lambda_\phi$

Table 4.1 – Fuzzy rules decision matrix

| $\lambda_\phi$ | | $\dot{\mathbf{e}}_\phi$ | | | | |
|---|---|---|---|---|---|---|
| | | **NB** | **NS** | **ZE** | **PS** | **PB** |
| $\mathbf{e}_\phi$ | **NB** | PB | PB | PM | PM | PS |
| | **NS** | PB | PM | PS | PS | PM |
| | **ZE** | PM | PS | PS | PS | PM |
| | **PS** | PM | PS | PS | PM | PB |
| | **PB** | PS | PM | PM | PB | PB |

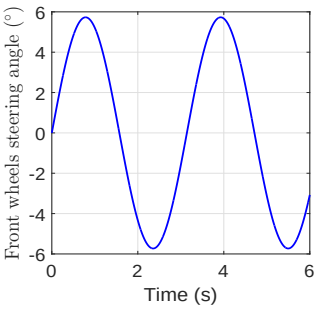


Figure 4.9 – Front wheels steering

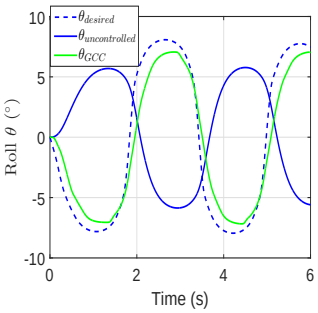


Figure 4.10 – Roll angle control

depending on the harshness of this motion. However, this is not done in this thesis since the literature is rich in controlling the heave motion as mentionned before.

## 4.3 Global Chassis Control Validation and Simulation

In this section, the proposed $GCC$ system will be validated through two simulation tests using Matlab/Simulink. The simulation model of the full vehicle is developed and validated on the professional vehicle simulator "SCANeR Studio" [Chokor et al., 2016] and [Chokor et al., 2017].
The first test is a sine steer (Figure 4.9) at 100 $km/h$ initial speed. This test solicits the vehicle yaw and lateral motions, as well as the roll motion. The uncontrolled (induced), desired and controlled roll angles are shown in Figure 4.10. The lateral $SI$, without controlling the vehicle, increases to reach more than $SI = 1$ as shown in Figure 4.11. That means, the vehicle has lost its lateral stability. The $AFS$ controller alone (dedicated to the maneuverability) can reduce the $SI$ to 1 as shown in the same figure. However, this improvement is not sufficient. The coordinated $AFS$ and $DYC$ controller can maintain the lateral stability under $SI = 0.8$. This improvement is obtained thanks to the torque $C_z$ generated by the $DYC$ that stabilizes the side slip angle $\beta$ and its rate of change $\dot{\beta}$. The addition of the roll control to the $GCC$ structure (by the $ASus$) can enhance more the lateral stability by reducing the peak value of $SI$ ($SI = 0.8$) to less than 0.7. The lateral stability can be alternatively studied in the "$\beta - \dot{\beta}$ phase plane" shown in Figure 4.12. The boundaries are for $SI = 1$. As much $\beta - \dot{\beta}$ relation is near the ideal one -calculated from the bicycle reference model-, as the lateral stability is more enhanced. It can be noticed that the uncontrolled vehicle exceeds the boundaries, while the $GCC$ controller is the nearest one to $\beta - \dot{\beta}$ reference. The vehicle yaw rate is shown in Figure 4.13. In the ranges below the saturation of the yaw rate reference, the uncontrolled vehicle is somehow far away from the yaw rate reference. Meanwhile, all the adopted strategies ($AFS$, $AFS + DYC$, and the $GCC$) converge to the desired yaw rate. This means that the maneuverability is enhanced regardless of the adopted strategy. When the vehicle yaw rate becomes too much high, the control objective attempts to saturate the yaw rate in order to simultaneously enhance the lateral stability and avoid the nonlinear relation between the yaw rate and the driver steering. The $AFS$ is shown

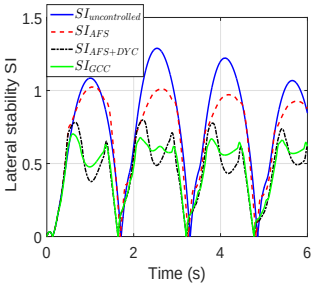


Figure 4.11 – Lateral Stability Index $SI$

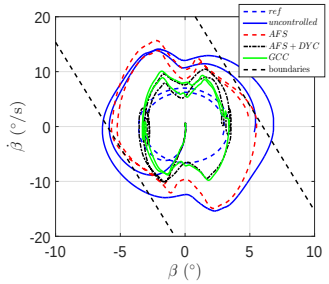


Figure 4.12 – $\beta$-$\dot{\beta}$ phase plane

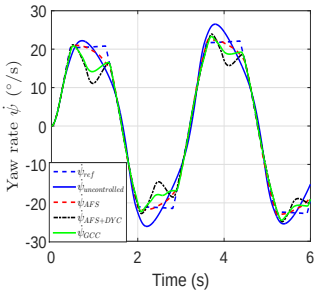


Figure 4.13 – Yaw rate comparison

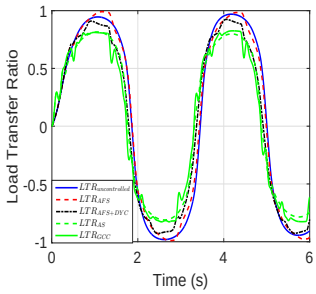


Figure 4.14 – Load Transfer Ratio $LTR$

to be the most effective controller in making the vehicle yaw rate converges to the desired saturated one. The $DYC$, by the braking effect to stabilize the vehicle, tends to reduce its kinetic energy, which is reflected by a reduction of the yaw rate. When adding the roll control (by means of $ASus$) to the $GCC$ system to enhance the stability, the $DYC$ controller becomes less solicited, and thus, the yaw rate re-approaches to the desired one.

Figure 4.14 shows the $LTR$ of the uncontrolled vehicle and the different control strategies. The results show that the $LTR$ is the best when the $GCC$ strategy is adopted compared to other strategies. It can also be noticed that activating the $AFS$ alone has a drawback on the $LTR$. The fact is because the vertical stability is not considered in the development of the $AFS$ controller.

Divers comfort enhancements are noticed when adding the roll control to the $GCC$ system. One observes that:

- The $ADB$ on the rear wheels, provided by the $AFS + DYC$ controller to stabilize the vehicle, are reduced as shown in Figure 4.15. The justification is that the $ASus$ contributes to the stabilization process. According to the same figure, the Root Mean Square ($RMS$) of the braking torques are reduced by 47% on the rear left wheel and by 36% on the rear right wheel. The $RMS$ reflects the dissipated energy by the braking actuator, which has an impact on its life time. The peak values of both braking are also considerably reduced by 53% and 30% respectively.
- The vehicle speed drop caused by the braking is less reduced as shown in Figure 4.16.
- The critical longitudinal slipping of the rear tires caused by the $ADB$ are limited as shown in Figure 4.17. Consequently, the $ABS$ control system (supposed to be integrated into the chassis) will be less solicited.

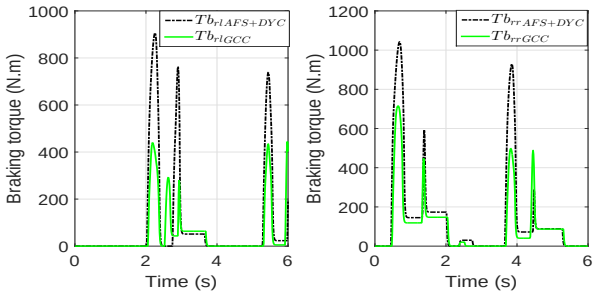


Figure 4.15 – Active Brake torques

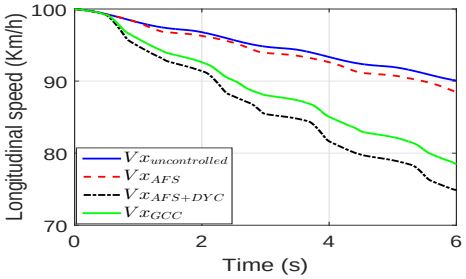


Figure 4.16 – Longitudinal speed

The second test represents a smooth medium accelerating followed by a sharp and hard braking as shown in Figure 4.18. The smooth/sharp acceleration/braking solicits the pitch rate, while the medium/hard value solicits the pitch angle, which are respectively represented by the uncontrolled vehicle in Figs. 4.19 and 4.20. The *ASus* controller eliminates the pitch angle and rate motion almost entirely, while the *GCC* controller only reduces the high values of the pitch angle and rate to ensure a soft pitch motion. The control inputs of the four *ASus* are depicted in Figure 4.21. The *RMS* value of the total input is reduced by 22%.

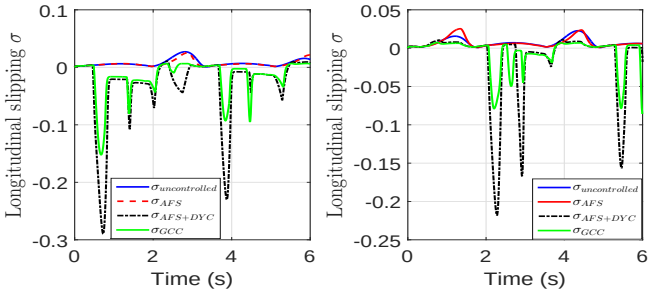


Figure 4.17 – Longitudinal slipping

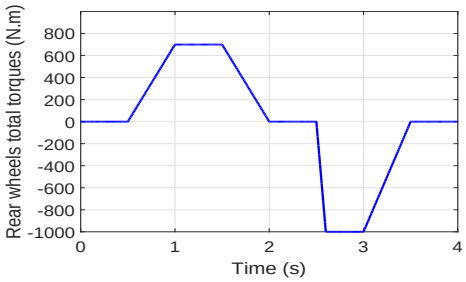


Figure 4.18 – Total driver torques on rear wheels

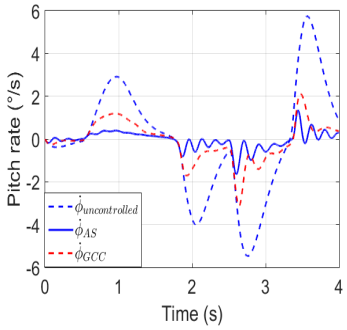


Figure 4.19 – Pitch rate comparison

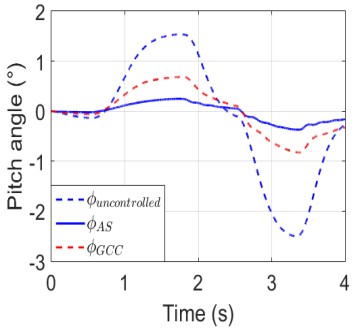


Figure 4.20 – Pitch angle comparison

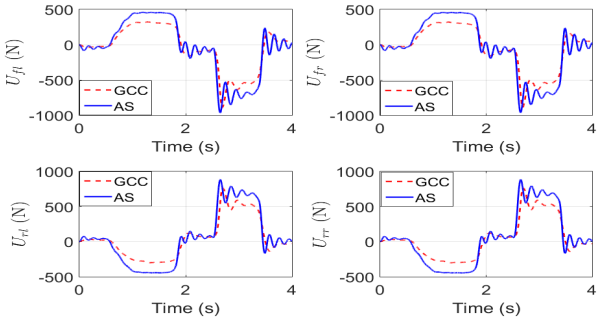


Figure 4.21 – *ASus* control inputs comparison

## 4.4 Conclusion

In this chapter, a Multilayer *GCC* system that coordinates the *AFS*, *DYC*, and *ASus* has been developed. It consists of a decision layer and control layer. The decision layer supervises the control layer which contains three main sub-controllers (*AFS*, *DYC*, and *ASus*) dedicated to improve local performances. The decentralized architecture is used to develop the control layer where each controller is developed based on the *STSM* control technique. The supervision can be divided into two categories: 1– monitor the overall vehicle performance by coordinating the interactions between the different control objectives (reinforce the favorable interactions and restrain the detrimental ones); 2– reduce the use of the *ASus* to involve only the undesirable motions of ride comfort. The *GCC* strategy has been validated by simulation results.

Next chapter develops and compares a Multilayer centralized and decentralized global chassis control architectures, involving $AFS$, $DYC$.

# *Centralized and Decentralized Global Chassis Control Architectures, Involving Active Front Steering and Direct Yaw Control*

In the previous chapters, we showed how the roll control can enhance the lateral stability and vertical stability of the vehicle in a $GCC$ architecture. The roll control has been achieved through the $ASus$ which have several disadvantages like cost, energy consumption and vehicle oversize. From the other side, as mentioned before, lots of work have been developed in literature to control the roll motion through the $AFS$. Thus, it is important to study how to achieve the roll control without the need to include the $ASus$ actuators in a $GCC$ architecture.

## 5.1 Introduction

This chapter investigates new achievements in $GCC$, involving only the $AFS$ and $DYC$, to improve the overall vehicle performance, i.e. the vehicle maneuverability, lateral stability and rollover avoidance, in different driving situations. Two multilayer control architectures, each formed by three hierarchical layers, are developed, validated and compared. The lower layer represents the actuators implemented into the vehicle which generate their control inputs based on the orders sent from the middle layer (see Section 1.6). The middle layer is the control layer which is responsible to generate the control inputs that minimize the errors between the desired and actual vehicle yaw rate, side-slip angle, and roll angle, regardless of the driving situation. The control layer is the main difference of the proposed architectures, where one centralized and one decentralized controllers are developed. In the centralized architecture, the novelty with respect to other works in the field of chassis control is that one single $MIMO$ optimal controller generates the optimal additive steering angle provided by the $AFS$ and the optimal $ADB$ provided by the $DYC$ to minimize -at once- all the vehicle state errors (yaw rate, side-slip angle, and roll angle). The optimal $\mathcal{H}_\infty$ control technique based on offline Linear Matrix Inequality ($LMI$) optimal solutions, in the framework of $LPV$ systems, is applied

to synthesize the controller.
In the decentralized architecture, a heuristic solution is proposed by decoupling the control problem where the $STSM$ robust control technique is applied to derive the $AFS$ control input which minimizes only the errors on the yaw rate, and the roll angle. Similarly, the $DYC$ control input is privileged to minimize only the error on the side-slip angle.
The higher layer of both architectures is the decision making layer which instantly monitors two criteria laying on lateral stability and rollover risks. Then, it generates two weighted parameters which adapt the controller(s) dynamics and performance(s) according to the driving conditions in order to improve the vehicle's maneuverability, lateral stability and rollover avoidance. Both control architectures are tested and validated on the professional simulator "SCANeR Studio". Simulation shows that both architectures are relevant to the $GCC$. The centralized one is optimal, complex and overall closed-loop stability is guaranteed, while the decentralized one does not guarantee the overall closed-loop stability, but it is intuitive, simple, and robust.
Chapter's contributions with respect to literature are:

- a new centralized control structure, which combines the yaw rate control, the side-slip angle control, and the roll control, in one single centralized controller, ensuring internal stability when switching between maneuverability, lateral stability and rollover avoidance objectives;

- a new decentralized control structure, which facilitates the $GCC$, by decoupling the control problem, into two sub-control problems, such as: $AFS$ is responsible on the control of the yaw rate, and the roll angle; $DYC$ is responsible on the control of the side-slip angle. Despite of the decoupling procedure, high maneuverability, lateral stability and rollover avoidance performances are guaranteed;

- a comparison between both approaches using SCANeR Studio simulator.

To do so, the extended bicycle model of (1.37) is modified to include the control and exogenous inputs, then, it is used as the control synthesis model. Based on this model, the $MIMO\ LPV/\mathcal{H}_\infty$ centralized controller structure is formalized, while detailing the control objectives represented as variable-weighted filters, to find the $LPV/\mathcal{H}_\infty$ controller which guarantees $\mathcal{H}_\infty$ performances between the exogenous inputs and the controlled variables, based on offline $LMI$ optimization, in the framework of the polytopic approach. Then, we present, in a decentralized architecture, both the $STSM$ based $AFS$ and $DYC$ controllers, as model-based controllers, where the control inputs are saturated and filtered a-posteriori. The decision layer of both the centralized and decentralized control architectures are also presented. The $SI$ (1.32) and the estimated $LTR$ (1.31) are used as the performance criteria to evaluate the lateral stability and rollover risks. Finally, we test and validate both architectures thanks to the co-simulation between Simulink and SCANeR Studio simulator.

$$\dot{X} = \begin{bmatrix} \ddot{\psi} \\ \dot{\beta} \\ \dot{\theta} \\ \ddot{\theta} \end{bmatrix} = \underbrace{\begin{pmatrix} a_{11} & a_{12} & a_{13} & a_{14} \\ a_{21} & a_{22} & a_{23} & a_{24} \\ 0 & 0 & 0 & 1 \\ a_{41} & a_{42} & a_{43} & a_{44} \end{pmatrix}}_{A} \underbrace{\begin{bmatrix} \dot{\psi} \\ \beta \\ \theta \\ \dot{\theta} \end{bmatrix}}_{X} + \underbrace{\begin{pmatrix} b_{u,11} & b_{u,12} \\ b_{u,21} & b_{u,22} \\ 0 & 0 \\ b_{u,41} & b_{u,42} \end{pmatrix}}_{B_{1,2}} \underbrace{\begin{bmatrix} \delta_d + \delta_c \\ M_z \end{bmatrix}}_{U} + \underbrace{\begin{pmatrix} b_{d,11} & 0 & 0 \\ 0 & b_{d,22} & 0 \\ 0 & 0 & 0 \\ 0 & 0 & b_{d,43} \end{pmatrix}}_{B_d} \underbrace{\begin{bmatrix} M_{d,\dot{\psi}} \\ F_{d,y} \\ M_{d,\theta} \end{bmatrix}}_{D};$$

$$y = X. \tag{5.2}$$

$$\dot{X}_{bic} = \begin{bmatrix} \ddot{\psi}_{bic} \\ \dot{\beta}_{bic} \\ \dot{\theta}_{bic} \\ \ddot{\theta}_{bic} \end{bmatrix} = \underbrace{\begin{pmatrix} a_{11} & a_{12} & a_{13} & a_{14} \\ a_{21} & a_{22} & a_{23} & a_{24} \\ 0 & 0 & 0 & 1 \\ a_{41} & a_{42} & a_{43} & a_{44} \end{pmatrix}}_{A} \underbrace{\begin{bmatrix} \dot{\psi}_{bic} \\ \beta_{bic} \\ \theta_{bic} \\ \dot{\theta}_{bic} \end{bmatrix}}_{X_{bic}} + \underbrace{\begin{pmatrix} b_{u,11} \\ b_{u,21} \\ 0 \\ b_{u,41} \end{pmatrix}}_{B_1} \underbrace{\begin{bmatrix} \delta_d \end{bmatrix}}_{U_{bic}}; \tag{5.3}$$

$$y_{bic} = X_{bic}.$$

## 5.2 Control Synthesis Model

The control synthesis model, denoted by "Plant P", is a linear vehicle model, which combines the coupled lateral and roll motions, while considering the control and exogenous inputs. This model suits the control problem of this work and it is given by the following system:

$$Plant\ P: \begin{cases} I_z\ddot{\psi} = F_{yf}l_f + F_{yr}l_r + I_{xz}\ddot{\theta} + M_z + M_{d,\dot{\psi}}, \\ MV\left(\dot{\beta} + \dot{\psi}\right) = F_{yf} + F_{yr} + M_s h_\theta \ddot{\theta} + F_{d,y}, \\ \left(I_x + M_s h_\theta^2\right)\ddot{\theta} = M_s h_\theta V\left(\dot{\beta} + \dot{\psi}\right) + \left(M_s g h_\theta - K_\theta\right)\theta \\ \qquad\qquad -C_\theta\dot{\theta} + M_{d,\theta}, \end{cases} \tag{5.1}$$

where $\dot{\psi}$, $\beta$, and $\theta$ are respectively the vehicle yaw rate, the vehicle side-slip angle, and the suspended mass roll angle. $M_{d,\dot{\psi}}, F_{d,y}, M_{d,\theta}$ represent the external disturbances and modeling errors respectively on the vehicle yaw rate, the lateral motion (side-slip angle) and the roll motion. $M_z$ is the active yaw moment to be generated, and $\delta_c$ the $AFS$ input is inside $F_{yf}$. The remaining notations of these equations and the vehicle parameters used for simulation are given in Tables 1 2. Even though these equations are valid when the vehicle operates in the stable region (no rollover or lateral stability risks), they are sufficient and recommended to synthesize a robust controller.

Similar to Section 1.4, the state space representation of the *Plant P* can be formalized as in (5.2), where $X = [\dot{\psi}, \beta, \theta, \dot{\theta}]^T$ is the state vector, $U = [\delta_c, Mz]^T$ is the vector of control inputs, $D = [M_{d,\dot{\psi}}, F_{d,y}, M_{d,\theta}]^T$ is the vector of exogenous inputs. The elements of the state matrix $A \in I\!R^{4\times4}$, the input matrices $B_{1,2} \in I\!R^{4\times2}$ and $B_d \in I\!R^{4\times3}$ are formalized in Appendix .1.

The objective in this chapter is to control the yaw, side-slip, and roll motions only by using the $AFS$ and $DYC$ actuators. This means that the vehicle is under-actuated, and the desired trajectories should be coherent to each other, because one actuator can not achieve contradictory objectives at the same time. Thus, the state space representation of the extended bicycle linear model (1.38) (re-written

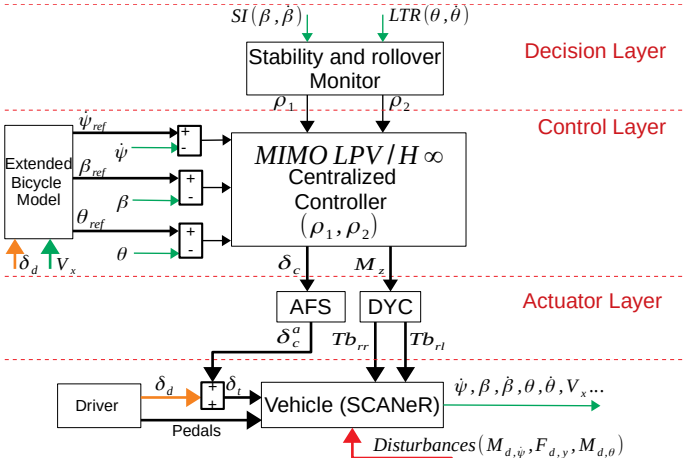


Figure 5.1 – Centralized $GCC$ architecture

with the suffix "bic" in (5.3)) is used to generate the "bicycle trajectory vector" $X_{bic} = [\dot{\psi}_{bic}, \beta_{bic}, \theta_{bic}, \dot{\theta}_{bic}]^T$. These trajectories are coherent to each other, feasible and represent the ideal stable states of the vehicle. The same saturation of 4.16 is done here on $\dot{\psi}_{bic}$, to maintain the adherence between the tires and the road.
Without loss of similarity, the trajectories provided by the extended bicycle model are used as the reference trajectories in the centralized approach, while they are slightly modified in the decentralized approach in order to introduce the weighting parameters. This issue is more developed later.

## 5.3 Centralized vs Decentralized Control Architectures

### 5.3.1 Overview

#### 5.3.1.1 Centralized Approach

The global centralized multilayer control architecture is shown in Figure 5.1. In the control layer, the controlled variables i.e. the vehicle yaw rate $\dot{\psi}$, the vehicle side-slip angle $\beta$, and the suspended mass roll angle $\theta$ are fed-back from "SCANeR Studio" vehicle and are controlled/optimized together by the optimal $MIMO\ LPV/\mathcal{H}_\infty$ centralized controller, to simultaneously enhance the vehicle maneuverability, the lateral stability and the rollover avoidance. Trajectories' references $\dot{\psi}_{ref}$, $\beta_{ref}$, and $\theta_{ref}$ of the controlled variables are exactly the ones generated by the Extended Bicycle Model 5.3. Two endogenous time-varying scheduling gains/parameters $\rho_1$ and $\rho_2$ schedule the $MIMO\ LPV/\mathcal{H}_\infty$ controller objectives. A decision maker (in the higher layer) monitors the vehicle situation and instantly sends the values of the scheduling parameters, based on lateral stability ($SI$) and rollover ($LTR$) criteria. Based on all these information, the $MIMO\ LPV/\mathcal{H}_\infty$ centralized controller generates the control steering angle $\delta_c$ and the corrective yaw moment $M_z$ as the control inputs, while considering actuators constraints (saturation and cut-off

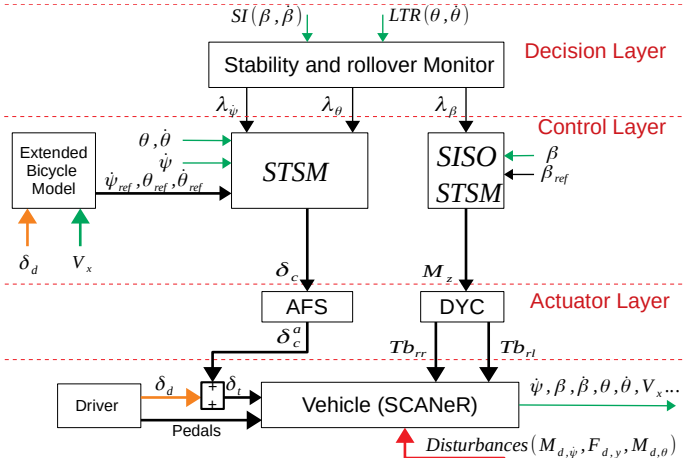


Figure 5.2 – Decentralized $GCC$ architecture

frequencies), to maintain the overall closed-loop stability.

#### 5.3.1.2 Decentralized Approach

The global decentralized multilayer control architecture is shown in Figure 5.2. The main difference w.r.t the centralized one is in the control layer, where each control input is generated by neglecting the other. Intuitively, $AFS$ control input $\delta_c$ is devoted to control the yaw rate $\dot{\psi}$ and the roll angle $\theta$, while $DYC$ control input $M_z$ is privileged to control side-slip angle $\beta$, to restrain the braking actuation. It will be proven later, it is proven that each standalone controller is stable by itself, while the overall closed-loop stability problem arises because of the decoupling of control problem. However, this procedure represents a heuristic solution to facilitate the controller development complexity, by benefiting from the robustness of the super-twisting algorithm. For more simplicity, actuators constraints are not considered in the controller structure, while a posterior filter is implemented to make the control inputs feasible. The decision layer is similar in structure to the one of the centralized approach. Based on the vehicle dynamics monitoring criteria, this layer generates three weighting gains $\lambda_{\dot{\psi}}$, $\lambda_{\beta}$ and $\lambda_{\theta}$. The goal of these gains is to promote/attenuate the $STSM$ controllers depending on the driving situation. These gains will be introduced into the reference trajectories, by modifying the extended bicycle model trajectories, to maintain each standalone controller stability.

### 5.3.2 Control Layers

In this sub-section, a detailed description of the control layer of both the centralized and decentralized $GCC$ architectures is presented.

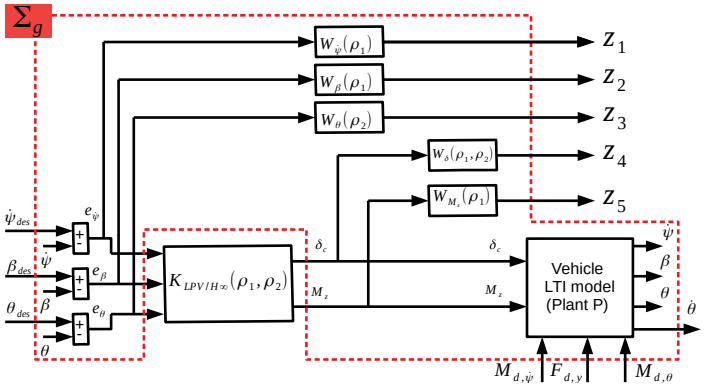


Figure 5.3 – Control layer architecture

#### 5.3.2.1 Centralized Control Layer Synthesis: $LPV/\mathcal{H}_\infty$ Controller

The control layer architecture is drawn in Figure 5.3. As a standard $\mathcal{H}_\infty$ structure, it contains the controller $K_{LPV/\mathcal{H}_\infty}(\rho_1, \rho_2)$ to be synthesized, and the generalized plant $\sum_g$, where $\rho_1(SI)$ and $\rho_2(LTR)$ are two endogenous weighted parameters calculated by the decision making monitor to adapt the controller dynamics and performances according to the driving conditions.

The controller $K_{LPV/\mathcal{H}_\infty}(\rho_1, \rho_2)$ has as inputs the errors between the desired trajectories and the actual ones of the yaw rate $e_{\dot\psi}$, the side-slip angle $e_\beta$, and the roll angle $e_\theta$. Since the $\mathcal{H}_\infty$ approach is a model-based robust control technique, the actual yaw rate, side-slip angle, and roll angle are calculated based on a $LTI$ vehicle model of (5.2) ($Plant\ P$).

$Plant\ P$ of the generalized plant $\sum_g$ is expressed in (5.2). It has $\delta_c$ and $M_z$ as control inputs; $M_{d,\dot\psi}$, $F_{d,y}$, and $M_{d,\theta}$ as disturbances (exogenous inputs); and the actual yaw rate $\dot\psi$, side-slip angle $\beta$, and roll angle $\theta$ as outputs to be controlled. The remaining subsystems of $\sum_g$ i.e. the weighting functions $W_{\dot\psi}(\rho_1)$, $W_\beta(\rho_1)$, $W_\theta(\rho_2)$, $W_\delta(\rho_1, \rho_2)$, and $W_{M_z}(\rho_1)$ of Figure 5.3 are defined to characterize the performance objectives $Z_1$, $Z_2$, and $Z_3$ and the actuators' constraints $Z_4$, and $Z_5$ (Dynamics of the actuators, given in Subsection 1.6, are neglected during the controller design process). The general form of these weights [Doumiati et al., 2014] is given by the following (numerical values are given in Section 5.4, since they depend on the simulated vehicle and integrated actuators):

- $W_{\dot\psi}(\rho_1)$ weights the yaw rate control objective:

$$W_{\dot\psi}(\rho_1) \quad = \quad \rho_1 \frac{s/M_1 + 2\pi f_1}{s + 2\pi f_1 A_1}, \tag{5.4}$$

where $M_1$ is sufficiently high for a large robustness margin, and $A_1$ is the tolerated tracking error on $e_{\dot\psi}$. $W_{\dot\psi}(\rho_1)$ is shaped to reduce the yaw rate error in the range of frequencies below a roll-off frequency $f_1$ where the vehicle operates [Heißing and Ersoy, 2010]. $W_{\dot\psi}(\rho_1)$ is linearly parametrized by the varying parameter $\rho_1$, where $\rho_1 \in \left\{\underline{\rho_1} \leq \rho \leq \overline{\rho_1}\right\}$ ($\underline{\rho_1}$ and $\overline{\rho_1}$ are constants representing the lower and higher values of $\rho_1$). When $\rho_1 = \overline{\rho_1}$, the performance objective $e_{\dot\psi}$ is prioritized (maneuverability is enhanced), on the contrary, when $\rho_1 = \underline{\rho_1}$, $e_{\dot\psi}$ is relaxed (lateral stability becomes

a priority).
- $W_\beta(\rho_1)$ weights the side-slip angle control objective:

$$W_\beta(\rho_1) = \frac{1}{\rho_1}\frac{s/M_2 + 2\pi f_2}{s + 2\pi f_2 A_2}. \tag{5.5}$$

$M_2$, $A_2$ and $f_2$ have similar meanings as $M_1$, $A_1$ and $f_1$. $W_\beta(\rho_1)$ is designed similarly to $W_{\dot{\psi}}(\rho_1)$. The main difference is that $W_\beta(\rho_1)$ is inversely dependent on the varying parameter $\rho_1$. This is because the lateral stability is more prioritized than maneuverability in critical situations. This issue is explained later in the decision layer.
- $W_\theta(\rho_2)$ weights the roll angle control objective according to a scheduling parameter $\rho_2$:

$$W_\theta(\rho_2) = \rho_2\frac{s/M_3 + 2\pi f_3}{s + 2\pi f_3 A_3}. \tag{5.6}$$

$M_3$, $A_3$ and $f_3$ have similar meanings as $M_1$, $A_1$ and $f_1$. $W_\theta(\rho_2)$ is linearly parametrized by the varying parameter $\rho_2$, where $\rho_2 \in \left\{\underline{\rho_2} \leq \rho_2 \leq \overline{\rho_2}\right\}$ ($\underline{\rho_2}$ and $\overline{\rho_2}$ are constants representing the lower and higher values of $\rho_2$). When $\rho_2 = \overline{\rho_2}$, the performance objective $e_\theta$ is prioritized (rollover avoidance is a priority). On the contrary, when $\rho_2 = \underline{\rho_2}$, $e_\theta$ is relaxed (rollover is not a risk).
- $W_\delta(\rho_1, \rho_2)$ weights the steering control input, $\delta_c$:

$$\begin{aligned} W_\delta(\rho_1,\rho_2) &= (\frac{1}{\rho_1} + \frac{1}{\rho_2})G_\delta^0\frac{(s/2\pi f_4 + 1)(s/2\pi f_5 + 1)}{(s/\alpha 2\pi f_5 + 1)^2}, \\ G_\delta^0 &= \frac{(\Delta_f/\alpha 2\pi f_5 + 1)^2}{(\Delta_f/2\pi f_4 + 1)(\Delta_f/2\pi f_5 + 1)}, \\ \Delta_f &= 2\pi(f_4 + f_5)/2, \end{aligned} \tag{5.7}$$

where $[f_4, f_5]$ is the filter bandwidth. This filter forces the steering system to act at frequencies higher than the driver ones ($f_4$), to avoid driver annoyance, and lower than the actuator cut-off frequency ($f_5$). This filter design is inspired from [Doumiati et al., 2014]. The novelty here is the dependency of $W_\delta(\rho_1, \rho_2)$ on $\rho_1$ and $\rho_2$, which allows to relax (promote) or penalize the steering depending on all possible situations. For instance, when rollover stability risk occurs, $AFS$ is relaxed/promoted to maintain vertical stability.
- $W_{M_z}(\rho_1)$ weights the braking control input, $M_z$:

$$W_{M_z}(\rho_1) = \rho_1 10^{-5}\frac{s/(2\pi f_6) + 1}{s/(\kappa 2\pi f_6) + 1}, \tag{5.8}$$

where $f_6$ is the braking actuator cut-off frequency and $\kappa$ to handle the braking actuator limitations (see [Doumiati et al., 2013]). When $\rho_1 = \overline{\rho_1}$, the braking input is penalized, on the contrary, when $\rho_1 = \underline{\rho_1}$, the braking control signal is relaxed. This design will be related to the vehicle lateral stability.
The controlled outputs $Z_1$, $Z_2$, $Z_3$, $Z_4$, and $Z_5$ have to be minimized for any exogenous input. To do so, the powerful $\mathcal{H}_\infty$ control technique is applied here. See [Sename et al., 2013] and [Gu et al., 2005] for more information about the robust $LPV/\mathcal{H}_\infty$ theory.

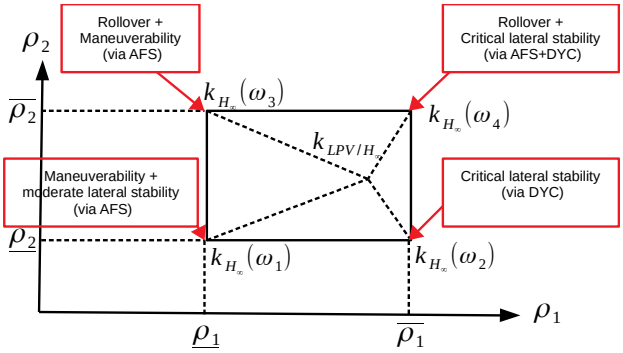


Figure 5.4 – Controller - Polytopic approach

Interconnection between $\sum_g$ subsystems is done using "*sysic*" Matlab function (Robust Control Toolbox). Since the generalized plant $\sum_g$ is *LPV* [Apkarian et al., 1995], it can be formulated as:

$$\Sigma_g(\rho): \begin{bmatrix} \dot{x} \\ z \\ y \end{bmatrix} = \begin{bmatrix} A(\rho) & B_1(\rho) & B_2(\rho) \\ C_1(\rho) & D_{11}(\rho) & D_{12}(\rho) \\ C_2 & D_{21} & 0 \end{bmatrix} \begin{bmatrix} x \\ w \\ U \end{bmatrix}, \tag{5.9}$$

where $\rho = \{\rho_1, \rho_2\}$, $x$ includes the state variables of *Plant* $P$ and of the weighting functions, $w = [\dot{\psi}_{ref}, \beta_{ref}, \theta_{ref}, M_{d,\dot{\psi}}, F_{d,y}, M_{d,\theta}]^T$ is the exogenous input vector, $U = [\delta_c, M_z]^T$ represents the control inputs, $y = [\dot{\psi}, \beta, \theta]^T$ is the measurement vector fedback to the controller, $y_e = [\dot{\theta}]^T$ is the exogenous output, and $z = [Z_1, Z_2, Z_3, Z_4, Z_5]^T$ is the weighted controlled output vector.
Note that the matrices $B_2$, and $D_{12}$ depend on $\rho$, which is not compatible with $\mathcal{H}_\infty$ requirements for polytopic systems. However, this issue is relaxed using some filter on the control input [Apkarian and Gahinet, 1995].

***Problem resolution:** LMI based LPV/$\mathcal{H}_\infty$:*
The *LMI* based *LPV*/$\mathcal{H}_\infty$ problem consists in finding the controller $K_{LPV/\mathcal{H}_\infty}(\rho_1, \rho_2)$, scheduled by the parameters $\rho_1$ and $\rho_2$, such that:

$$K_{LPV/\mathcal{H}_\infty}(\rho): \begin{bmatrix} \dot{x}_c \\ u \end{bmatrix} = \begin{bmatrix} A_c(\rho) & B_c(\rho) \\ C_c(\rho) & 0 \end{bmatrix} \begin{bmatrix} x_c \\ y \end{bmatrix}, \tag{5.10}$$

which minimizes the $\mathcal{H}_\infty$ norm of the closed-loop *LPV* system formed by the interconnection of equations (5.9) and (5.10). The *LPV*/$\mathcal{H}_\infty$ controller of (5.10) can be found using the development given in Section 2.5.
According to the polytopic approach, the final controller, $K_{LPV/\mathcal{H}_\infty}(\rho_1, \rho_2)$, is a convex combination of the controllers synthesized at the vertices of the polytope [Apkarian et al., 1995] such as:

$$\begin{aligned} K_{LPV/\mathcal{H}_\infty}(\rho_1, \rho_2) = \alpha_1 K_{\mathcal{H}_\infty}(\omega_1) + \alpha_2 K_{\mathcal{H}_\infty}(\omega_2) \\ +\alpha_3 K_{\mathcal{H}_\infty}(\omega_3) + \alpha_4 K_{\mathcal{H}_\infty}(\omega_4), \end{aligned} \tag{5.11}$$

as shown in Figure 5.4, where each vertex represents an objective (more discussion is given in Section 5.3.3.1).

$$\dot{X} = \begin{bmatrix} \ddot{\psi} \\ \dot{\beta} \\ \dot{\theta} \\ \ddot{\theta} \end{bmatrix} = \underbrace{\begin{pmatrix} a_{11} & a_{12} & a_{13} & a_{14} \\ a_{21} & a_{22} & a_{23} & a_{24} \\ 0 & 0 & 0 & 1 \\ a_{41} & a_{42} & a_{43} & a_{44} \end{pmatrix}}_{A} \underbrace{\begin{bmatrix} \dot{\psi} \\ \beta \\ \theta \\ \dot{\theta} \end{bmatrix}}_{X} + \underbrace{\begin{pmatrix} b_{u,11} \\ b_{u,21} \\ 0 \\ b_{u,41} \end{pmatrix}}_{B_1} \underbrace{\begin{bmatrix} \delta_c \end{bmatrix}}_{U1} + \underbrace{\begin{pmatrix} b_{d,11} & 0 & 0 \\ 0 & b_{d,22} & 0 \\ 0 & 0 & 0 \\ 0 & 0 & b_{d,43} \end{pmatrix}}_{B_d} \underbrace{\begin{bmatrix} M_{d,\dot{\psi}} \\ F_{d,y} \\ M_{d,\theta} \end{bmatrix}}_{D};$$
$$y = X. \tag{5.12}$$

$$\dot{X} = \begin{bmatrix} \ddot{\psi} \\ \dot{\beta} \\ \dot{\theta} \\ \ddot{\theta} \end{bmatrix} = \underbrace{\begin{pmatrix} a_{11} & a_{12} & a_{13} & a_{14} \\ a_{21} & a_{22} & a_{23} & a_{24} \\ 0 & 0 & 0 & 1 \\ a_{41} & a_{42} & a_{43} & a_{44} \end{pmatrix}}_{A} \underbrace{\begin{bmatrix} \dot{\psi} \\ \beta \\ \theta \\ \dot{\theta} \end{bmatrix}}_{X} + \underbrace{\begin{pmatrix} b_{u,12} \\ b_{u,22} \\ 0 \\ b_{u,42} \end{pmatrix}}_{B_2} \underbrace{\begin{bmatrix} M_z \end{bmatrix}}_{U2} + \underbrace{\begin{pmatrix} b_{d,11} & 0 & 0 \\ 0 & b_{d,22} & 0 \\ 0 & 0 & 0 \\ 0 & 0 & b_{d,43} \end{pmatrix}}_{B_d} \underbrace{\begin{bmatrix} M_{d,\dot{\psi}} \\ F_{d,y} \\ M_{d,\theta} \end{bmatrix}}_{D};$$
$$y = X. \tag{5.13}$$

#### 5.3.2.2 Decentralized Control Layer Synthesis: Super-Twisting Sliding Mode Controllers

In an intuitive way, the decentralized approach decouples the control problem into two sub-problems: $AFS$ is responsible on the control of the vehicle yaw rate $\dot{\psi}$ and the roll angle $\theta$ by neglecting the effect of the $DYC$ on these dynamics when developing the controller; $DYC$ which is effective to control both the vehicle yaw rate and the side-slip angle, is privileged to control only the side-slip angle $\beta$ to limit its intervention, in order to prevent long braking duration which decelerates the vehicle, annoys the driver and causes long term tires wearing. To be noted also, as a consequence of the $AFS$ controller, the side-slip angle is enhanced in the low-to-mid range of lateral stability, while it becomes ineffective at high critical lateral dynamics.

The $STSM$-based $AFS$ control synthesis model (5.12) is similar to (5.2), while considering $M_z = 0$, and thus, reducing $B_{1,2}$ to its first column. The driver steering input $\delta_d$ is neglected in the synthesis model, and then it is considered as a feed-forward of the entire system.

The $STSM$-based $DYC$ control synthesis model (5.13) is similar to (5.2), while considering $\delta_c = 0$, and thus, reducing $B_{1,2}$ to its second column. The driver steering input $\delta_d$ is also neglected in the synthesis model, and then it is considered as a feed-forward of the entire system.

Under these assumptions, a robust control technique, which deals with modeling uncertainties and decoupling phenomenon, is needed. Thus, the $STSM$ control technique, which is one of the most powerful robust control techniques that suit this control problem is chosen.

Consider the affine system form written as:

$$\ddot{X} = f(X,t) + g(X,t)u(t), \tag{5.14}$$

where $X = [\dot{\psi}, \beta, \theta, \dot{\theta}]^T$, and $f(X,t) = AX$. In the case of the $AFS$ controller synthesis $g(X,t) = B_1$ and $u = \delta_c$ as can be seen from (5.12). In the case of the $DYC$ controller synthesis $g(X,t) = B_2$ and $u = M_z$ as can be seen from (5.13).
Let define $E = [e_{\dot{\psi}}, e_\beta, e_\theta, \dot{e}_\theta]^T = [\dot{\psi} - \dot{\psi}_{ref}, \beta - \beta_{ref}, \theta - \theta_{ref}, \dot{\theta} - \dot{\theta}_{ref}]^T$ the error vector between the actual and the desired states. $\dot{\psi}_{ref}$, $\beta_{ref}$, $\theta_{ref}$, and $\dot{\theta}_{ref}$ depend on the extended bicycle model and the weighting gains sent from the decision layer. Their expressions are given later in this section.
Let define three sliding variables as the following:

$$\begin{aligned} &s_{\dot{\psi}} = e_{\dot{\psi}} = \dot{\psi} - \dot{\psi}_{ref}, \\ &s_\beta = e_\beta = \beta - \beta_{ref}, \\ &s_\theta = \dot{e}_\theta + k_\theta\, e_\theta = (\dot{\theta} - \dot{\theta}_{ref}) + k_\theta(\theta - \theta_{ref}), \end{aligned} \tag{5.15}$$

where $s_{\dot{\psi}}$ (resp. $s_\theta$) has a relative degree of 1 w.r.t the control input $\delta_c$ since $b_{u,11}$ (resp. $b_{u,41}$) is not zero as can be seen in the $AFS$ synthesis model of (5.12). Similarly, $s_\beta$ has a relative degree of 1 w.r.t the control input $M_z$ since $b_{u,11}$ is not zero as can be seen in the $DYC$ synthesis model of (5.13). $k_\theta$ is a positive constant gain which determines the time convergence of the state errors $\dot{e}_\theta$ and $e_\theta$.
Since the $AFS$ is responsible of the control of both state variables $\dot{\psi}$ and $\theta$, let define a new sliding variable $s_{\dot{\psi},\theta}$ such that:

$$s_{\dot{\psi},\theta} = c_1 s_{\dot{\psi}} + c_2 s_\theta, \tag{5.16}$$

where $c_1$ and $c_2$ are positive constant weights relatively scaling the sliding variables $s_{\dot{\psi}}$ and $s_\theta$.
$s_{\dot{\psi},\theta}$, and $s_\beta$ to be controlled respectively by the $AFS$ and the $DYC$, have their control inputs appear in their first derivatives (relative degree 1). This means their second derivative can be written as:

$$\ddot{s}(s,t) = \Phi(s,t) + \xi(s,t)\dot{u}(t) \tag{5.17}$$

where $\Phi(s,t)$ and $\xi(s,t)$ are unknown bounded signals.
The control objective is to achieve the convergence to the sliding surface defined by $s = 0$. Only the knowledge of $s$ is required in real time.
Based on Section 2.4, the $STSM$ control inputs of the $AFS$ and the $DYC$ are respectively given by:

$$\begin{aligned} \delta_c &= -\alpha_{\delta,1}|s_{\dot{\psi},\theta}|^{\tau_\delta} sign(s_{\dot{\psi},\theta}) - \alpha_{\delta,2}\int_0^t sign(s_{\dot{\psi},\theta})d\tau, \\ M_z &= -\alpha_{M_z,1}|s_\beta|^{\tau_{M_z}} sign(s_\beta) - \alpha_{M_z,2}\int_0^t sign(s_\beta)d\tau, \end{aligned} \tag{5.18}$$

where $\alpha_{\delta,1}$ and $\alpha_{\delta,2}$ (resp. $\alpha_{M_z,1}$ and $\alpha_{M_z,2}$) are positive gains satisfying conditions of (2.15). $\tau_\delta$ and $\tau_{M_z}$ are constants in the interval ]0, 0.5]. The function $sign$ is smoothed by the approximation $sign(s) = \frac{s}{|s|+\varepsilon}$, where $\varepsilon$ is a positive small value.
The $STSM$ control inputs guarantee the convergence of $s_{\dot{\psi},\theta}$ and $s_\beta$ in a finite time to zero. Once $s_\beta = 0$, this means that the state $\beta$ is converged to $\beta_{ref}$. Once $s_{\dot{\psi},\theta} = 0$, this means that $s_{\dot{\psi}} = 0$ and $s_\theta = 0$ because the state matrix $A$ is Hurwitz (all eigenvalues in the left half plane). Thus, $\dot{\psi}$ converges to $\dot{\psi}_{ref}$ and $\dot{e}_\theta + k_\theta\, e_\theta \to 0$,

which means that $\theta$ (resp. $\dot{\theta}$) exponentially converges to $\theta_{ref}$ (resp. $\dot{\theta}_{ref}$) if $k_\theta > 0$.

As mentioned before, $\dot{\psi}_{ref}$, $\beta_{ref}$, $\theta_{ref}$, and $\dot{\theta}_{ref}$ depend on the extended bicycle model and the weighting gains sent from the decision layer. Thus, let define

$$\begin{aligned} \dot{\psi}_{ref} &= \lambda_{\dot{\psi}}\ \dot{\psi}_{bic} + (1-\lambda_{\dot{\psi}})\ \dot{\psi}, \\ \beta_{ref} &= \lambda_\beta \beta_{bic} + (1-\lambda_\beta)\beta, \\ \theta_{ref} &= \lambda_\theta \theta_{bic} + (1-\lambda_\theta)\theta, \\ \dot{\theta}_{ref} &= \lambda_\theta \dot{\theta}_{bic} + (1-\lambda_\theta)\dot{\theta}, \end{aligned} \tag{5.19}$$

where $\lambda_{\dot{\psi}}(SI)$, $\lambda_\beta(SI)$ and $\lambda_\theta(LTR)$ are the scheduling gains which vary between 0 and 1. Their instant values are sent from the decision layer depending on the vehicle situation. When one of these gains approaches to 1, this means that the corresponding reference trajectory is equal to the one of the extended bicycle model, thus, the corresponding controller is promoted to control the corresponding variable. When it approaches to 0, this means that the reference trajectory is equal to the actual vehicle one, thus, the control of the corresponding variable is attenuated since the corresponding sliding variable is vanished.
Consequently, the sliding variables of (5.15) become equivalent to:

$$\begin{aligned} s_{\dot{\psi}} &= \dot{\psi} - \dot{\psi}_{ref} = \lambda_{\dot{\psi}}\ (\dot{\psi} - \dot{\psi}_{bic}), \\ s_\beta &= \beta - \beta_{ref} = \lambda_\beta(\beta - \beta_{bic}), \\ s_\theta &= (\dot{\theta} - \dot{\theta}_{ref}) + k_\theta(\theta - \theta_{ref}) = \lambda_\theta[(\dot{\theta} - \dot{\theta}_{bic}) + k_\theta(\theta - \theta_{bic})], \end{aligned} \tag{5.20}$$

These new forms of sliding variables mean that the actual state variables are forced to converge to the extended bicycle reference model only if the scheduling gains are high (close to 1). In this case, we say that the control objective is promoted. Otherwise, the control objective is attenuated (relaxed) and the state variables remain without control.
**Note:** The modification of the sliding variables by the multiplication with the scheduling gains maintains the closed-loop stability of the individual $AFS$ and $DYC$ since these gains are introduced in the reference trajectories.

### 5.3.3 Decision Layers

#### 5.3.3.1 Centralized Approach: $\rho_1$ and $\rho_2$ Calculations

Once the control layer is developed, the decision layer is responsible to monitor the driving situations.
For $SI \leq \underline{SI}$, the vehicle is in normal driving situations, thus, the $AFS$ is promoted for maneuverability purpose. It also enhances the lateral stability up to a moderate level. In this range, $DYC$ is penalized. When the vehicle reaches critical lateral stability $SI \geq \overline{SI}$, then the $DYC$ is promoted to enhance the lateral stability. Based on this analysis, the scheduled gain $\rho_1$ is designed to feed the $LPV/\mathcal{H}_\infty$ controller sufficient knowledge about the weights to be promoted or attenuated. A "*sigmoid*" function (5.21) (see Figure 5.5.a) governs the relation between $\rho_1$ and $SI$, to ensure a continuous and a relatively smooth variation of $\rho_1$.

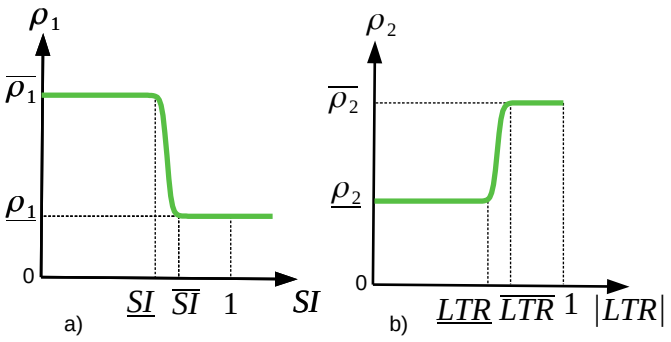


Figure 5.5 – Scheduling parameters

$$\rho_1 = \overline{\rho_1} - \frac{\overline{\rho_1} - \underline{\rho_1}}{1 + e^{-\frac{8}{\overline{SI}-\underline{SI}}(SI - \frac{\overline{SI}+SI}{2})}}. \tag{5.21}$$

When $|LTR| > \overline{LTR}$, where $\overline{LTR}$ a positive constant threshold, a rollover risk is detected, and thus, the controller is informed by the scheduling parameter $\rho_2$, to handle this risk. To ensure a smooth transition of $\rho_2$, a lower positive constant threshold $\underline{LTR}$ is defined. A "*sigmoid*" function (5.22) (see Figure 5.5.b) governs the relation between $\rho_2$ and $|LTR|$.

$$\rho_2 = \underline{\rho_2} + \frac{\overline{\rho_2} - \underline{\rho_2}}{1 + e^{-\frac{8}{\overline{LTR}-\underline{LTR}}(|LTR| - \frac{\overline{LTR}+\underline{LTR}}{2})}}. \tag{5.22}$$

#### 5.3.3.2 Decentralized Approach: $\lambda_{\dot{\psi}}$, $\lambda_\beta$ and $\lambda_\theta$ Calculations

Similar to the decision layer of the centralized approach, the decision layer of the decentralized approach monitors all the control objectives based on monitoring criteria ($SI$ and $LTR$), then, it calculates and sends instantly the values of $\lambda_{\dot{\psi}}$, $\lambda_\beta$ and $\lambda_\theta$ to attenuate/promote the corresponding control objective depending on the vehicle situation.
$\lambda_{\dot{\psi}}$ approaches to 1 when the vehicle maneuverability is the control objective. This means when $SI \leq \underline{SI}$. In this case, $\lambda_\beta$ approaches to 0 since no lateral stability risk is detected. When $SI \geq \overline{SI}$, $\lambda_{\dot{\psi}}$ approaches to 0 because the vehicle maneuverability is not a priority, while $\lambda_\beta$ approaches to 1 since the lateral stability risk is high. A "*sigmoid*" function (5.23) (Figure 5.6.a) governs the relation between $\lambda_{\dot{\psi}}$ (resp. $\lambda_\beta$) and $SI$, to ensure a continuous and a relatively smooth variation of $\lambda_{\dot{\psi}}$ and $\lambda_\beta$.

$$\begin{aligned} \lambda_\beta &= \frac{1}{1+e^{-\frac{8}{\overline{SI}-\underline{SI}}(SI - \frac{\overline{SI}+SI}{2})}}, \\ \lambda_{\dot{\psi}} &= 1 - \lambda_\beta. \end{aligned} \tag{5.23}$$

By the same reasoning $\lambda_\theta$ is related to $LTR$. $\lambda_\theta$ approaches to 0 when no rollover risk is detected ($LTR \leq \underline{LTR}$) and approaches to 1 when rollover risk is detected ($LTR \geq \overline{LTR}$). A "*sigmoid*" function (5.24) (Figure 5.6.b) governs the relation between $\lambda_\theta$ and $LTR$, to ensure a continuous and a relatively smooth variation of

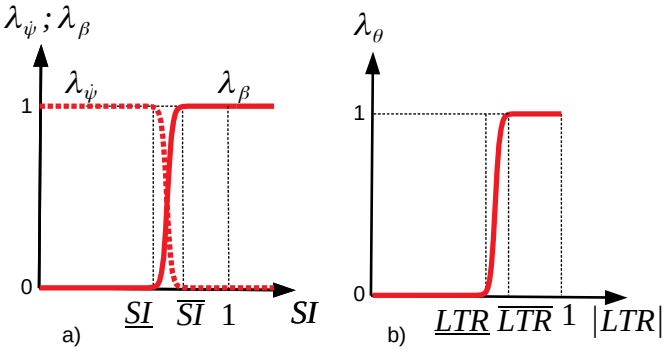


Figure 5.6 – Scheduling gains $\lambda_{\dot{\psi}}$ and $\lambda_\beta$

$\lambda_\theta$.

$$\lambda_\theta = \frac{1}{1 + e^{-\frac{8}{\overline{LTR}-\underline{LTR}}(LTR - \frac{\overline{LTR}+\underline{LTR}}{2})}}, \tag{5.24}$$

## 5.4 Controllers Validation

This section is dedicated to validate the proposed controllers. It is composed of two sub-sections. The first one is to show the effect of controlling the roll motion in a *GCC* architecture on the vehicle dynamics. To do so, the proposed $LPV/\mathcal{H}_\infty$ controller (centralized architecture of this chapter) is compared to the $LPV/\mathcal{H}_\infty$ controller of [Doumiati et al., 2014] (denoted by "[6]" in the simulations), where the roll angle is not introduced in the controller structure (as many powerful controllers developed in literature and cited in Section 0.2.1). The second sub-section is to validate and compare the proposed centralized and decentralized architectures. Parameters numerical values of the proposed controllers used in simulations are provided in Table 5.1.

Table 5.1 – Controllers' Parameters for Simulation

| Parameters | Values |
|---|---|
| $M_1 = M_2 = M_3; A_1 = A_2 = A_3; \kappa$ | $2; 0.1 = 10\%; 100$ |
| $f_1 = f_2 = f_3; f_4; f_5; f_6$ | $11.15\ Hz; 1\ Hz; 10\ Hz; 10\ Hz$ |
| $c_1; c_2; k_\theta$ | 1;1;1 |
| $\alpha_{\delta,1}; \tau_\delta; \alpha_{\delta,2}$ | 0.5;0.5;0.01 |
| $\alpha_{M_z,1}; \tau_{M_z}; \alpha_{M_z,2}$ | 500;0.5;0.1 |
| $\underline{\rho_1}; \overline{\rho_1}; \underline{\rho_2}; \overline{\rho_2}$ | $70; 85; 75; 85$ |
| $q_1; q_2; r_1; r_2$ | $9.55; 2.49; 12; 1$ |
| $\underline{SI}; \overline{SI}; \underline{LTR}; \overline{LTR}$ | $0.6; 0.7; 0.6; 0.7$ |
| $\delta^a_{c,max}; T^a_{b,max}$ | $5°; 1200\ N.m$ |

### 5.4.1 Roll Control Effect on Global Chassis Control

As mentioned above, this section is dedicated to compare the proposed *MIMO* $LPV/\mathcal{H}_\infty$ controller where the vehicle yaw motion, side-slip dynamics , and roll motion are controlled, with another *MIMO* $LPV/\mathcal{H}_\infty$ controller developed in

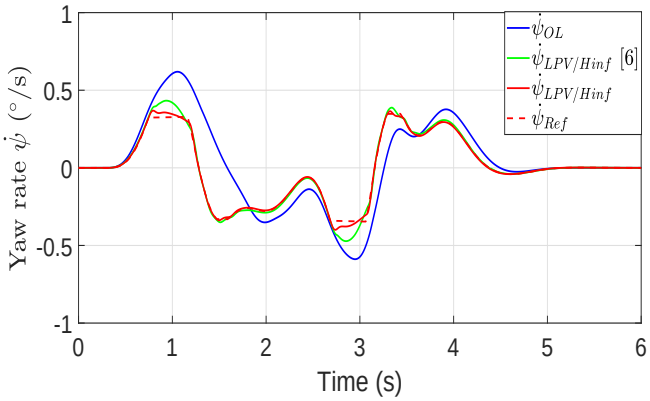


Figure 5.7 – Yaw rate comparison

literature [Doumiati et al., 2014] (denoted by "[6]" in the simulations), where the roll angle is not introduced in the controller structure. The objective is to highlight the effect of the roll motion control, in a $GCC$ architecture, using only the $AFS$ and $DYC$, on the vehicle dynamics, especially, the lateral stability and rollover avoidance. Comparison and validation are done on "SCANeR studio" simulator, by analyzing several vehicle variables on a $DLC$ test, with the steering angle represented by the variable $\delta_d$ on Figure 5.14, at an initial speed 110 $km/h$. In the $DLC$ test, the driver is intended to change the lane then go back to the same lane in a short duration. At high speed the vehicle is subjected to lateral stability and rollover risks. Comparison also includes an uncontrolled vehicle (denoted by "OL" as Open Loop), where any $GCC$ controller is implemented.
The yaw rate reference shown in Figure 5.7 is generated by the bicycle model. The figure also shows that the proposed $LPV/\mathcal{H}_\infty$ controller has a closest yaw rate to the desired one, compared to the uncontrolled vehicle and the vehicle controlled by the $LPV/\mathcal{H}_\infty$ controller of [6]. However, both controllers have satisfied the maneuverability objective. The small differences at the peak and trough is due to the fact that the $LPV/\mathcal{H}_\infty$ of [6] promotes the lateral stability in this zone, and attenuates the maneuverability objective, because a lateral stability risk appears in this zone as shown in Figure 5.8 (green curve). From the other side, the proposed controller, has a global vision on the system, especially on the roll angle, thus, by detecting a rollover risk, it activates a controller dedicated to rollover and maneuverability (vertex $\omega_3$) as shown by the curve $\alpha_3$ of Figure 5.12. Figure 5.10 validates the results by diminishing more the roll angle which reflects enhancements on the $LTR$ of Figure 5.11.

Moreover, the proposed controller enhances the lateral stability more than the one of [6] as can be seen from Figures 5.8 and 5.9, due to the fourth controller of vertex $\omega_4$ (Figure 5.12), which enhances the rollover and lateral stability at once. To summarize, both controllers are able to handle maneuverability and lateral stability objectives. The rollover problem is handled by the $LPV/\mathcal{H}_\infty$ controller of [6] as a consequence of the vehicle lateral control (close to a stable bicycle model as a reference). The advantage of the proposed controller is the integration of the rollover prevention objective into the controller structure. This feature has added to the

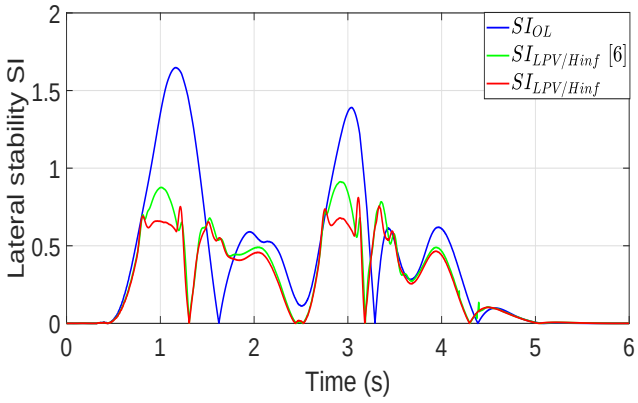


Figure 5.8 – Lateral stability comparison

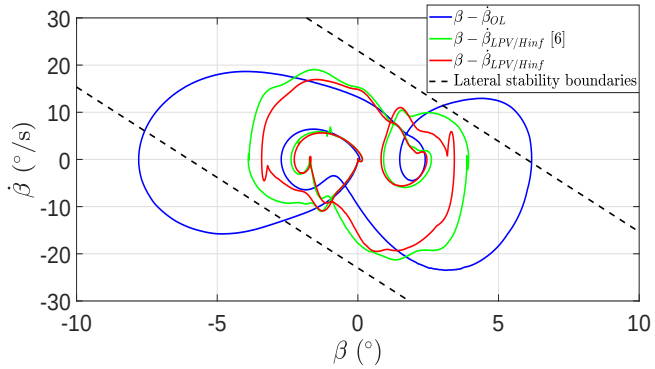


Figure 5.9 – $\beta - \dot{\beta}$ phase plane

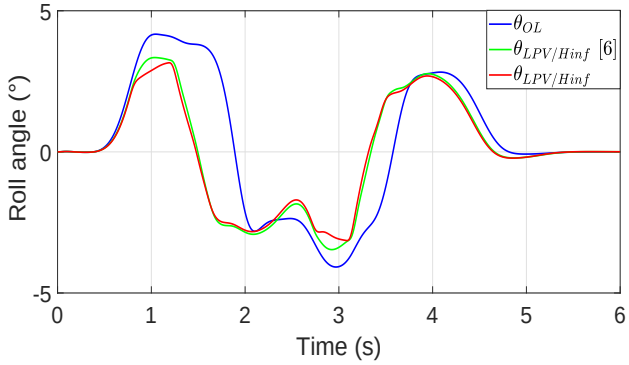


Figure 5.10 – Roll angle comparison

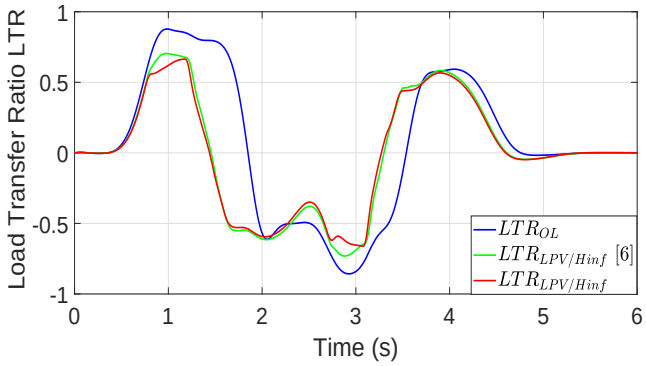


Figure 5.11 – $LTR$ comparison

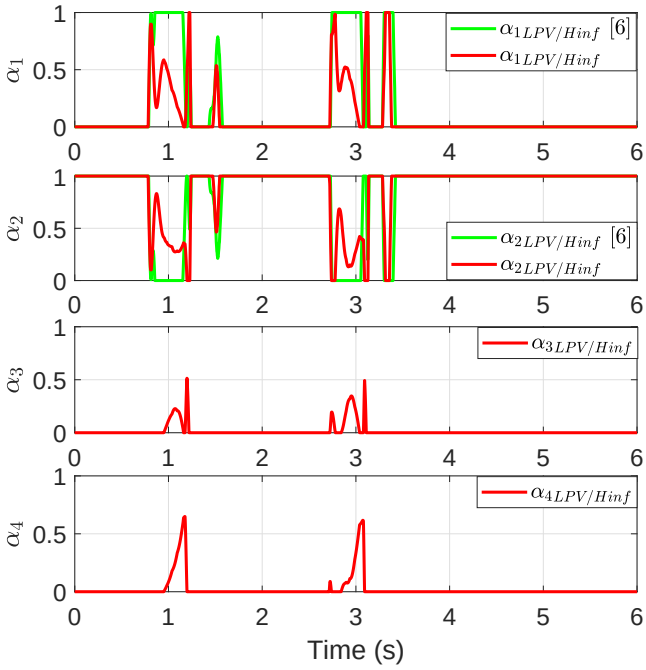


Figure 5.12 – Weights $\alpha_i$ - vertices controllers

proposed controller the ability to handle more combinations of complex situations like maneuverability and rollover at the same time by using only $AFS$, and lateral stability and maneuverability at the same time, by using $AFS$+$DYC$. This summary is illustrated by the weights $\alpha_i$ of Figure 5.12, which correspond to the controllers vertices of Figure 5.4. The controller of [6] has only two vertices, which oblige to switch between maneuverability and lateral stability objectives, while, the proposed controller is able to cover more complex combinations of situations thanks to four vertices controllers.

Figure 5.13 shows the fluctuations of the scheduling parameters $\rho_1$ and $\rho_2$, based on $SI$ and $LTR$ criteria. To be noted, $\rho_2$ remains at $\underline{\rho_2}$ the most of the time, this means the rollover risk is rarely detected, and thus, the proposed controller is not totally stimulated, to prove its effectiveness. This issue is due to the fact that lateral stability handling risk appears in passengers cars before rollover risk. Thus, enhancing the

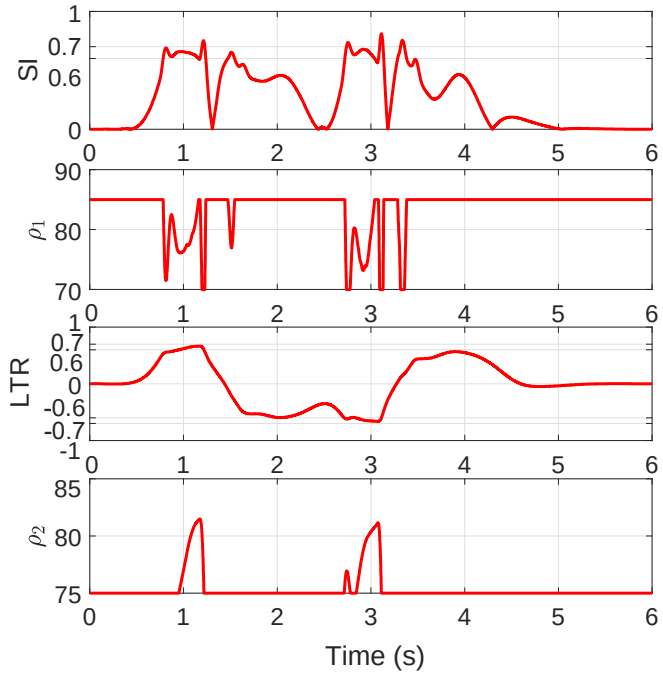


Figure 5.13 – Decision layer - Inputs vs Outputs

lateral stability, will enhance the rollover prevention. The proposed controller could provide more efficient results than the one in [6] for vehicles with higher center of gravity, where rollover risk can be detected at lower values than the lateral stability risk. Figure 5.14 shows the driver steering angle $\delta_d$, the $AFS$ steering angle of both controllers $\delta_c$, and the total steering $\delta_t$. One can notice, that both controllers provide similar steering control angles, except at peaks and troughs, where the proposed controller, actuates more the $AFS$ in order to handle all objectives (the combined complex objectives discussed before). Figure 5.15 shows the braking of the $EMB$ at the left and right rear wheels. The proposed controller less activates the braking with an overall enhancement of the root mean square by 59% at the left braking, and 22% at the right braking. The peak amount of the braking is also reduced by 72% at the left wheel, and 16% at the right wheel. The vehicle speed, which drops due to frictions, is slightly improved as shown in Figure 5.16.

### 5.4.2 Centralized and Decentralized Architectures Validation and Comparison

This section is dedicated to validate and compare the proposed centralized and decentralized control architectures of this chapter. Validation is done on "SCANeR studio" simulator, by analyzing several vehicle variables in two scenarios: the $DLC$ test performed before, and a fishhook test; both at an initial speed 110 $km/h$. Both scenarios are considered as hard tests which solicit the vehicle lateral stability, yet the fishhook test influences more the rollover risk phenomenon since a long duration constant high steering amplitude is applied on the vehicle.
In both scenarios, the comparison is done between an uncontrolled vehicle, where

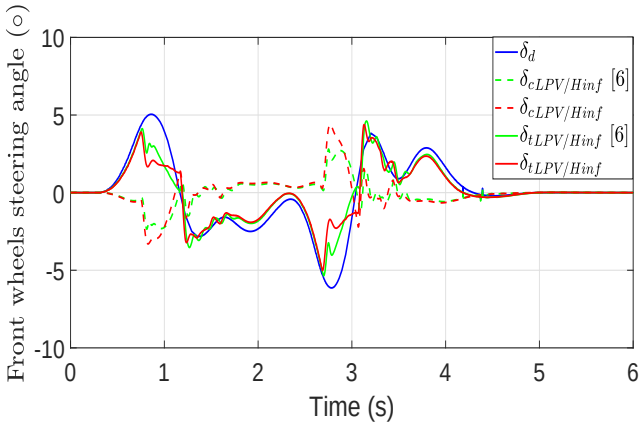


Figure 5.14 – Steering angle comparison

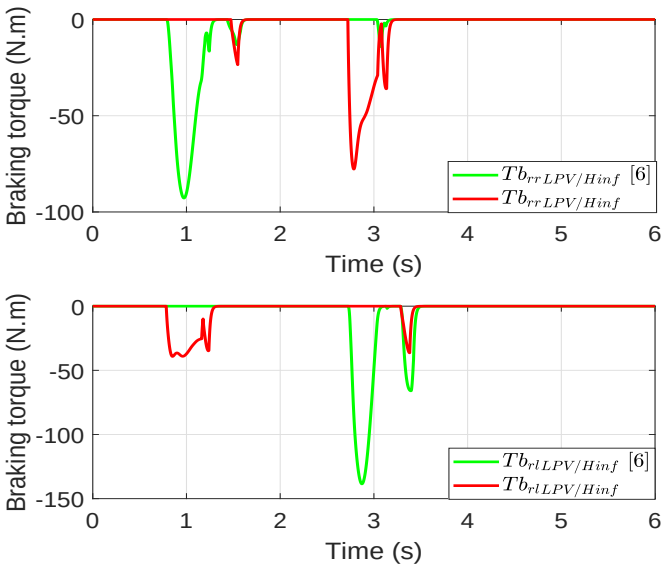


Figure 5.15 – Braking comparison

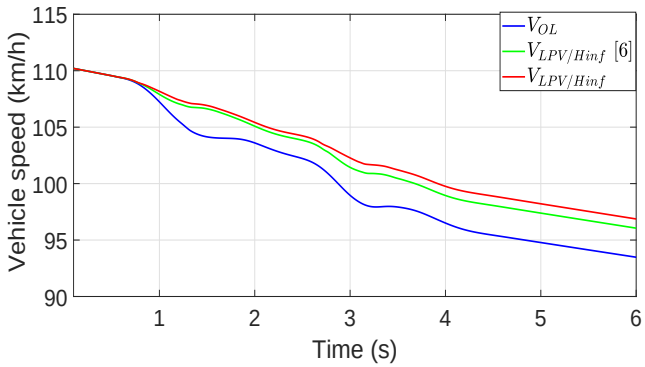


Figure 5.16 – Vehicle speed comparison

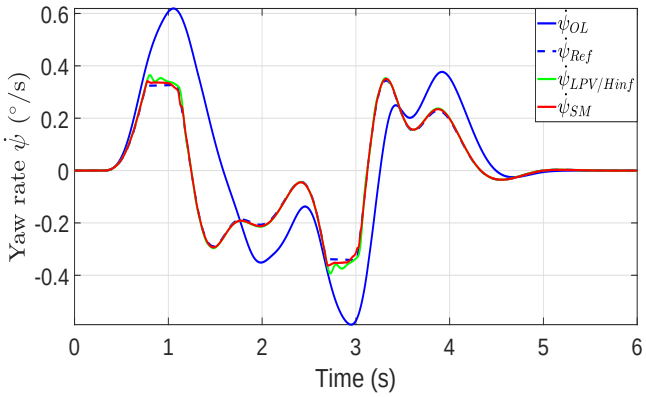


Figure 5.17 – Yaw rate comparison (DLC test)

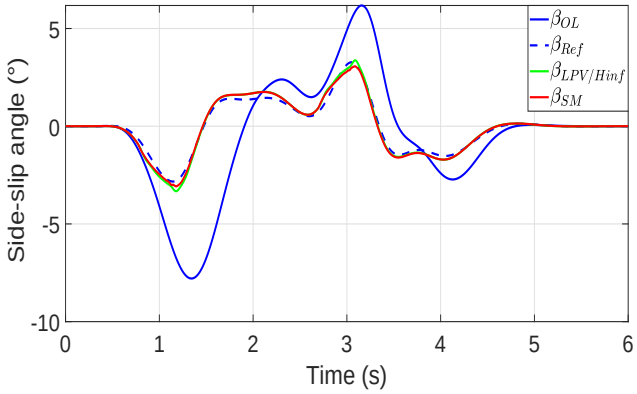


Figure 5.18 – Side-slip angle comparison (DLC test)

the controller is not implemented ("OL" as Open Loop), and by integrating the proposed controllers i.e. the centralized controller ("$LPV/\mathcal{H}_\infty$") and the decentralized controller ("SM" as Sliding Mode) into the vehicle. Several simulation tests for different scenarios have been done to select the best controller gains for both architectures.

#### 5.4.2.1 Double Lane Change Scenario

The same *DLC* test done before is performed here. This simulation test shows the advantage of having such *ADAS* systems implemented into the vehicle. The proposed control architectures monitor the vehicle situation and control its dynamics to follow, when necessary, the reference trajectories of the extended bicycle model in order to enhance the vehicle maneuverability, lateral stability and rollover avoidance. Figures 5.17, 5.18, and 5.19 respectively show the yaw rate, the side-slip angle and the roll angle which are the controlled variables. Both control architectures (centralized and decentralized) have achieved a high accuracy of tracking the yaw rate and the side-slip angle references, compared to the uncontrolled vehicle. Meanwhile, the roll angle has tracked its reference only in some regions (especially around 1 $s$ and 3 $s$). These tracking results can be further explained by observing

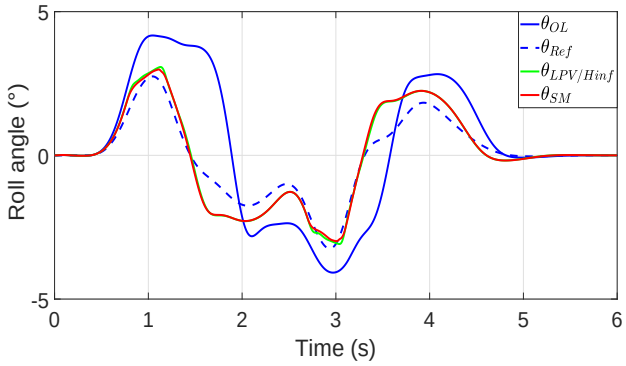


Figure 5.19 – Roll angle comparison (DLC test)

the monitoring criteria ($SI$ and $LTR$) and the scheduling gains of each architecture. Therefrom, Figure 5.20 and Figure 5.21 respectively show the lateral $SI$ and the $LTR$ with their corresponding scheduling gains of both control architectures. The lateral $SI$ of the uncontrolled vehicles (Figure 5.20) exceeds $SI = 1$, which means that the vehicle has lost its stability, while both control architectures have covered back the $SI$ under $SI = \underline{SI}$, and thus, they have succeeded to remain the vehicle stable on almost all the time. When $SI \leq \underline{SI}$ (almost all the time except around 1 $s$ and 3 $s$), the scheduling gain $\rho_1$ (resp. $\lambda_{\dot{\psi}}$) of the centralized (resp. decentralized) architecture is set to $\rho_1 = \overline{\rho_1}$ (resp. $\lambda_{\dot{\psi}} = 1$) which accounts for the maneuverability objective. When $SI \leq \overline{SI}$ (specifically around 1 $s$ and 3 $s$), the scheduling gain $\rho_1$ (resp. $\lambda_{\dot{\psi}}$) of the centralized (resp. decentralized) architecture deviates toward $\rho_1 = \underline{\rho_1}$ (resp. $\lambda_{\dot{\psi}} = 0$ or $\lambda_\beta = 1$) which accounts for the lateral stability objective. Based on this discussion, one can conclude on the yaw rate tracking of Figure 5.17 almost all the time except around 1 $s$ and 3 $s$, and on the side-slip angle tracking of Figure 5.18 only around 1 $s$ and 3 $s$. However, the side-slip angle tracks its reference all the time as a consequence of the yaw rate tracking, since both dynamics are correlated, and so their references. The $LTR$ of the uncontrolled vehicle (Figure 5.21) exceeds $LTR = \overline{LTR}$, which means that the vehicle is risky to roll-over, while both control architectures have covered back the $LTR$ under $LTR = \underline{LTR}$ almost all the time except around 1 $s$ and 3 $s$, and thus, they have succeeded to remove the rollover risk. The scheduling gain $\rho_2$ (resp. $\lambda_\theta$) of the centralized (resp. decentralized) architecture was $\rho_2 = \underline{\rho_2}$ (resp. $\lambda_\theta = 0$) almost all the time except around 1 $s$ and 3 $s$ where it deviates to a higher value. This means, only around 1 $s$ and 3 $s$ the proposed control architectures have switched the control objective to rollover avoidance, while at the remaining time of the simulation the $LTR$ is enhanced because the roll angle of Figure 5.19 is diminished compared to the uncontrolled one as a consequence of the yaw rate enhancement since both dynamics are correlated. Figure 5.22 shows the driver steering angle $\delta_d$, the $AFS$ steering angle of both controllers $\delta_c$, and the total steering $\delta_t$. One can notice, that both controllers provide similar steering control angles. Figure 5.23 shows the braking of the $EMB$ at the left and right rear wheels. The centralized controller activates a little bit more the braking since it is somehow useful to control the roll motion and the yaw rate, on contrary to the decentralized controller which activates the braking only to control the side-slip

angle when necessary. The vehicle speed, which drops due to frictions, is improved by both controllers compared to the uncontrolled vehicle since less lost in the lateral motion is achieved as shown in Figure 5.24.

#### 5.4.2.2 Fishhook Scenario

The fishhook test at high speed is a hard test used to perform extremely critical behaviors. It solicits both the lateral stability and the rollover more than in the $DLC$. The test consists of turning the steering angle to one direction, keeping a high steer constant angle, then doing the same in the opposite direction. The driver steering angle is shown in Figure 5.30. The uncontrolled vehicle yaw rate of Figure 5.25 shows that the vehicle turns in one side, and thus, it could not well perform the scenario as the ideal motion should be (reference vehicle). Only the vehicle implemented with the centralized controller could achieve an accurate yaw rate, while the decentralized controller was able to improve the motion without high accuracy. Similar results can be observed on the side-slip angle and the roll angle respectively in Figure 5.26 and Figure 5.27. Figure 5.28 and Figure 5.29 respectively show the $SI$ and the $LTR$ with their corresponding scheduling gains. These figures show that the extreme behavior of the uncontrolled vehicle could be reduced but remain unstable using the decentralized controller, while the centralized controller enhances more these behavior providing a marginal stability (the lateral stability and rollover avoidance are achieved but still risky). The fluctuations of the scheduling gains show that this time the controllers are more solicited to ensure the rollover avoidance objective in the presence of the lateral stability risk. The optimality of the centralized solution was more aware about these coupled dynamics which is reflected by the $AFS$ steering angle as can be seen from Figure 5.30, where the centralized steering angle was more stable than the decentralized one.

Figure 5.31 shows the braking of the $EMB$ at the left and right rear wheels. The centralized controller less activates the braking with an overall enhancement of the root mean square by 48% at the left braking, and 38% at the right braking. The peak amount of the braking is also reduced by 33% at the left wheel, and 14% at the right wheel. The vehicle speed is less dropped in the centralized approach since less braking is applied as can be seen from Figure 5.32.

## 5.5 Conclusion

In this chapter, decision-based centralized and decentralized $GCC$ architectures have been developed to improve the vehicle maneuverability, the lateral stability and the rollover prevention, by acting on the $AFS$ and the $ADB$. The effectiveness of the proposed architectures have been validated on SCANeR Studio simulator compared to an uncontrolled vehicle. Both the centralized and the decentralized architectures are relevant to control this complex system. It has been shown that the decentralized architecture is more simple to synthesize, while the centralized architecture handles more complex situations.

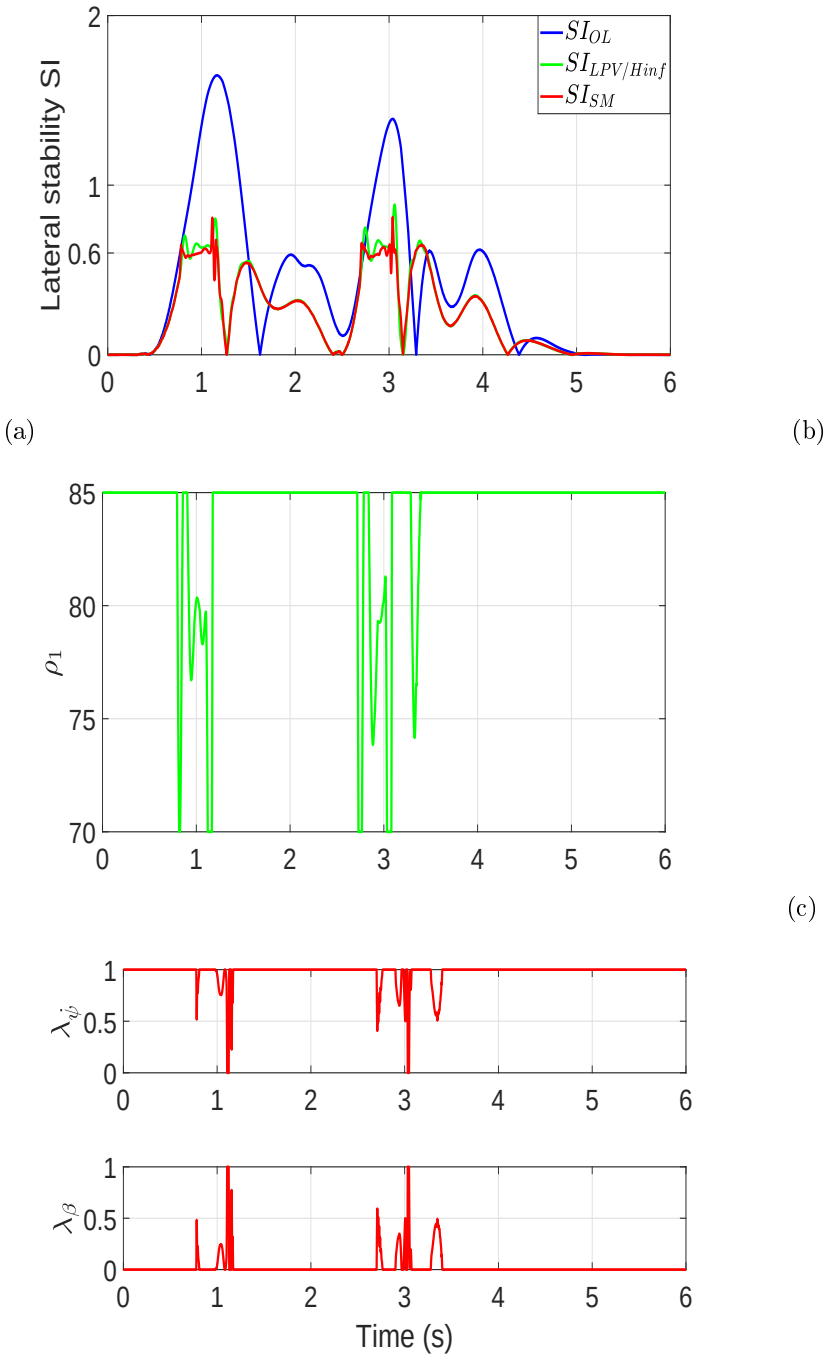


Figure 5.20 – Lateral stability and scheduling gains (DLC test)

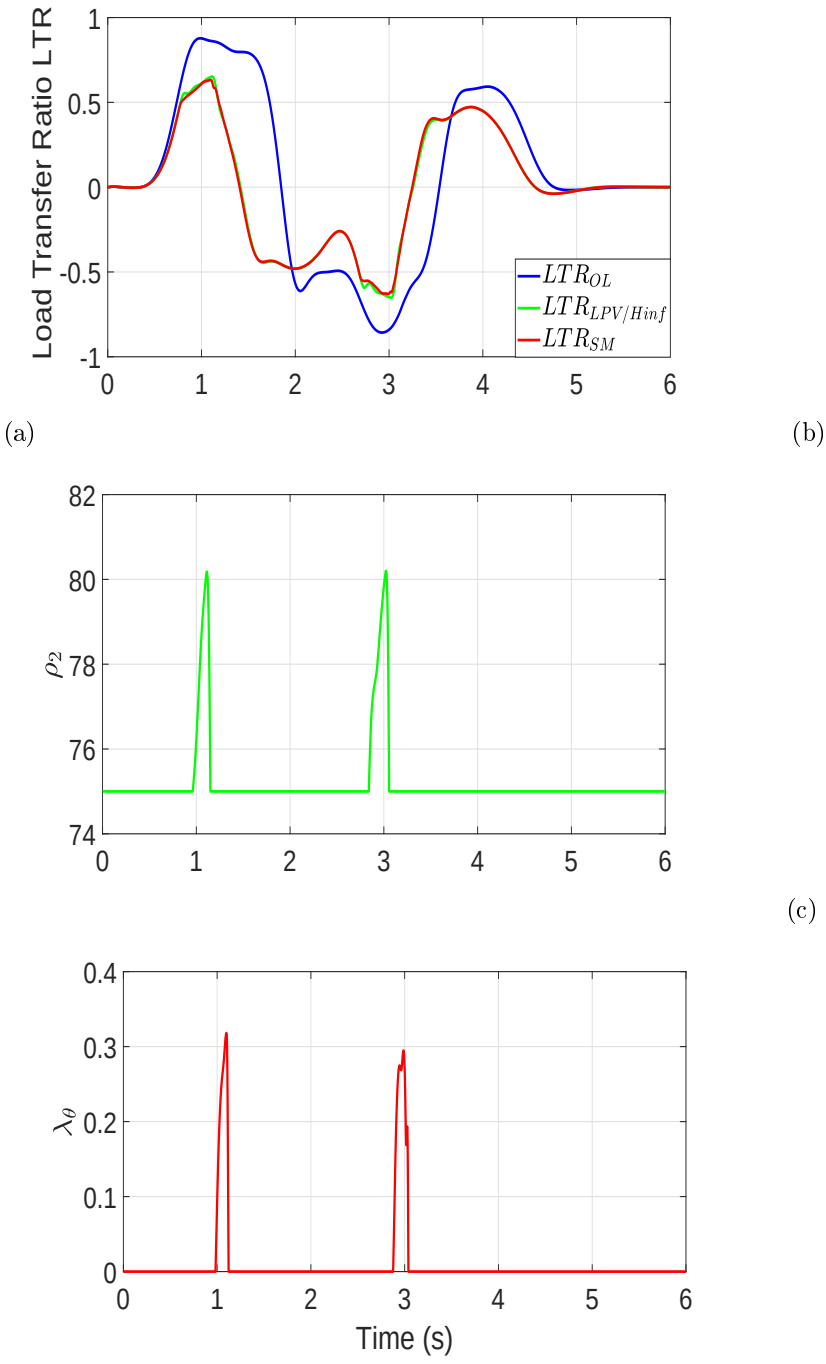


Figure 5.21 – Load transfer ratio $LTR$ and scheduling gains (DLC test)

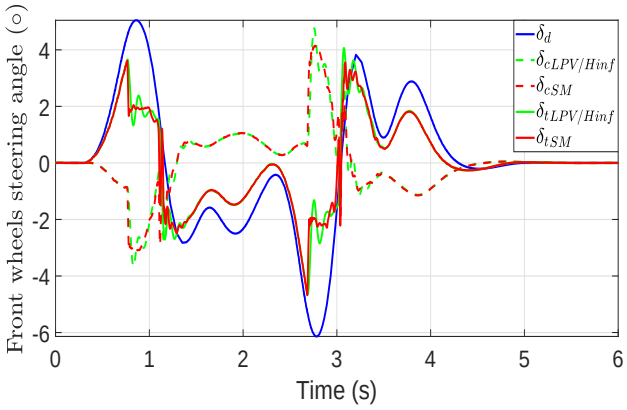


Figure 5.22 – Steering angle comparison (DLC test)

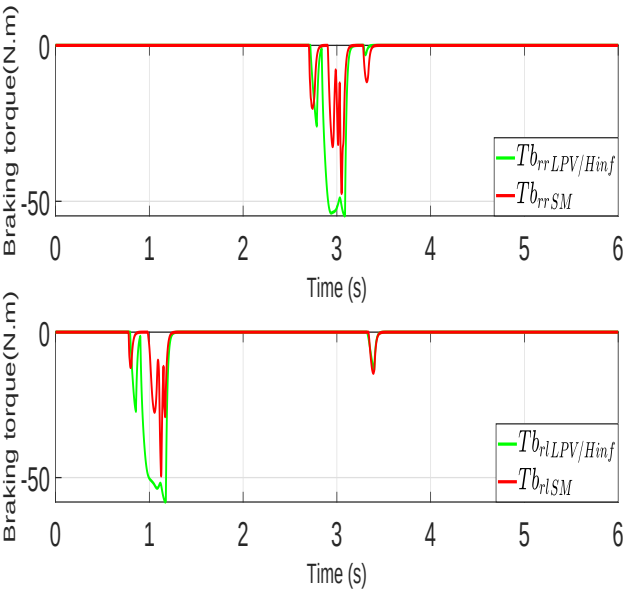


Figure 5.23 – Braking comparison (DLC test)

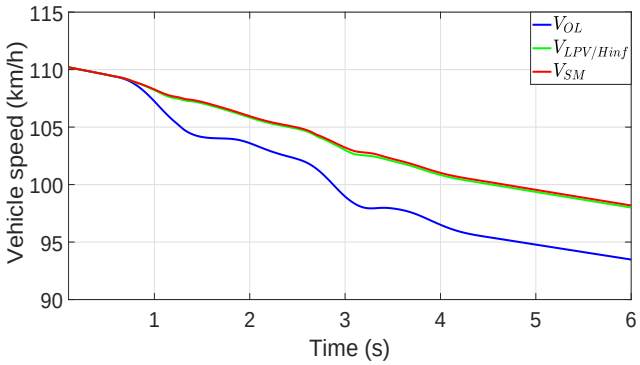


Figure 5.24 – Vehicle speed comparison (DLC test)

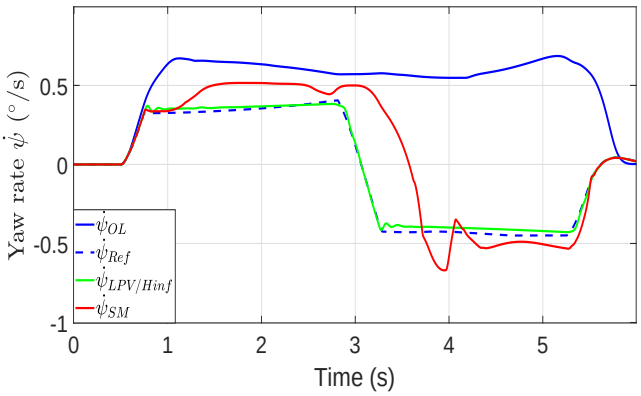


Figure 5.25 – Yaw rate comparison (Fishhook test)

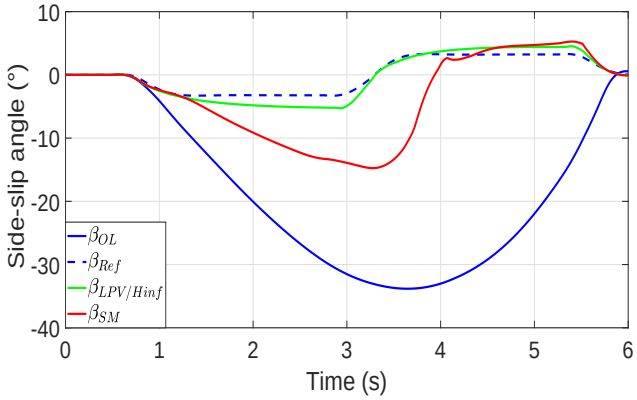


Figure 5.26 – Side-slip angle comparison (Fishhook test)

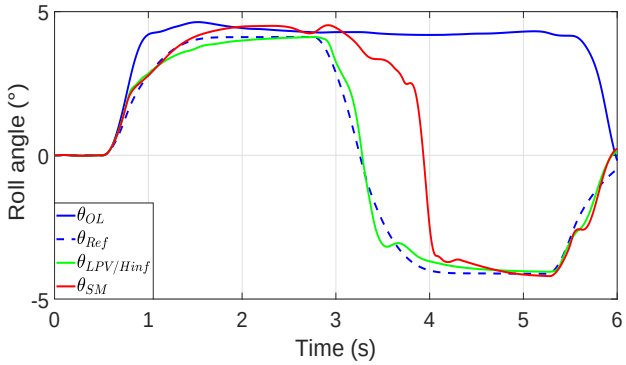


Figure 5.27 – Roll angle comparison (Fishhook test)

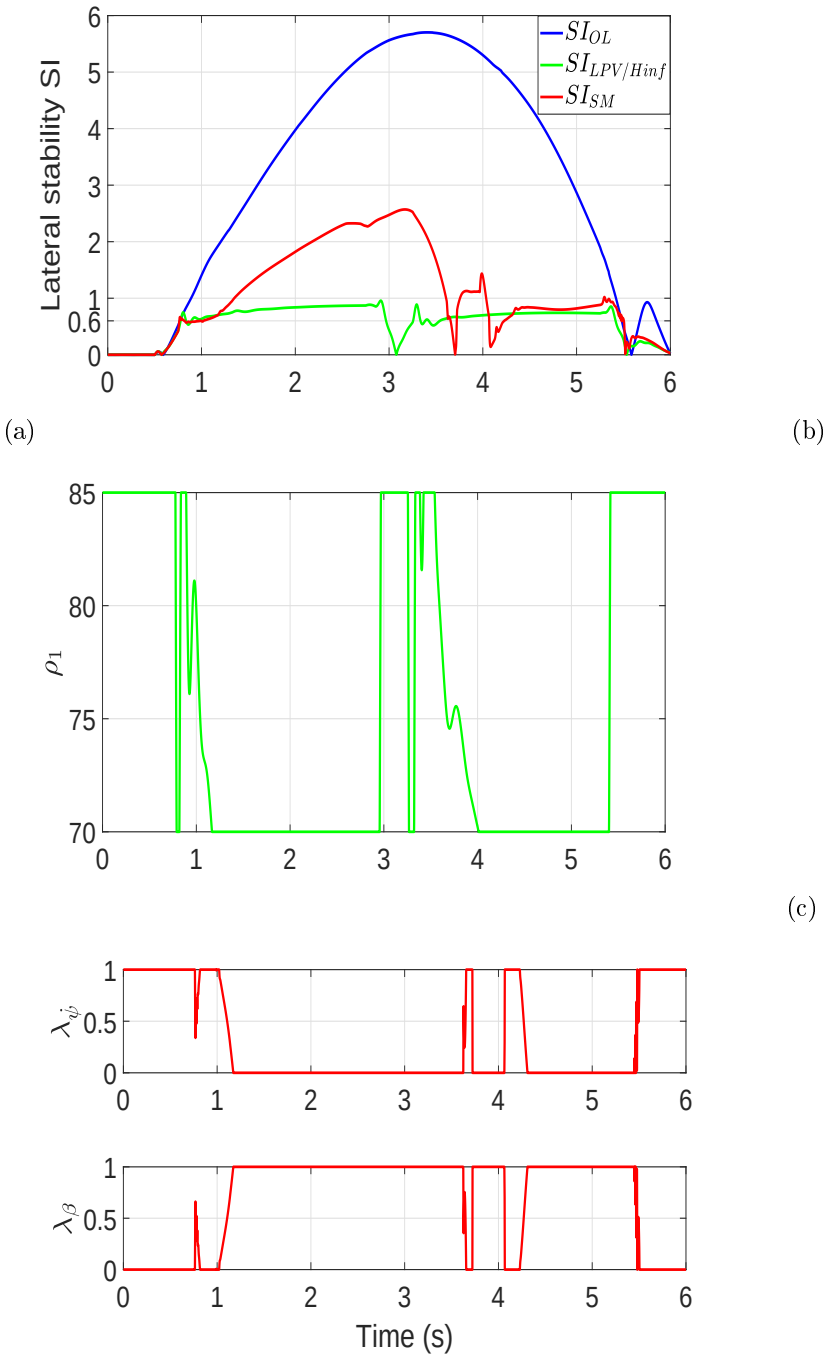


Figure 5.28 – Lateral stability and scheduled gains (Fishhook test)

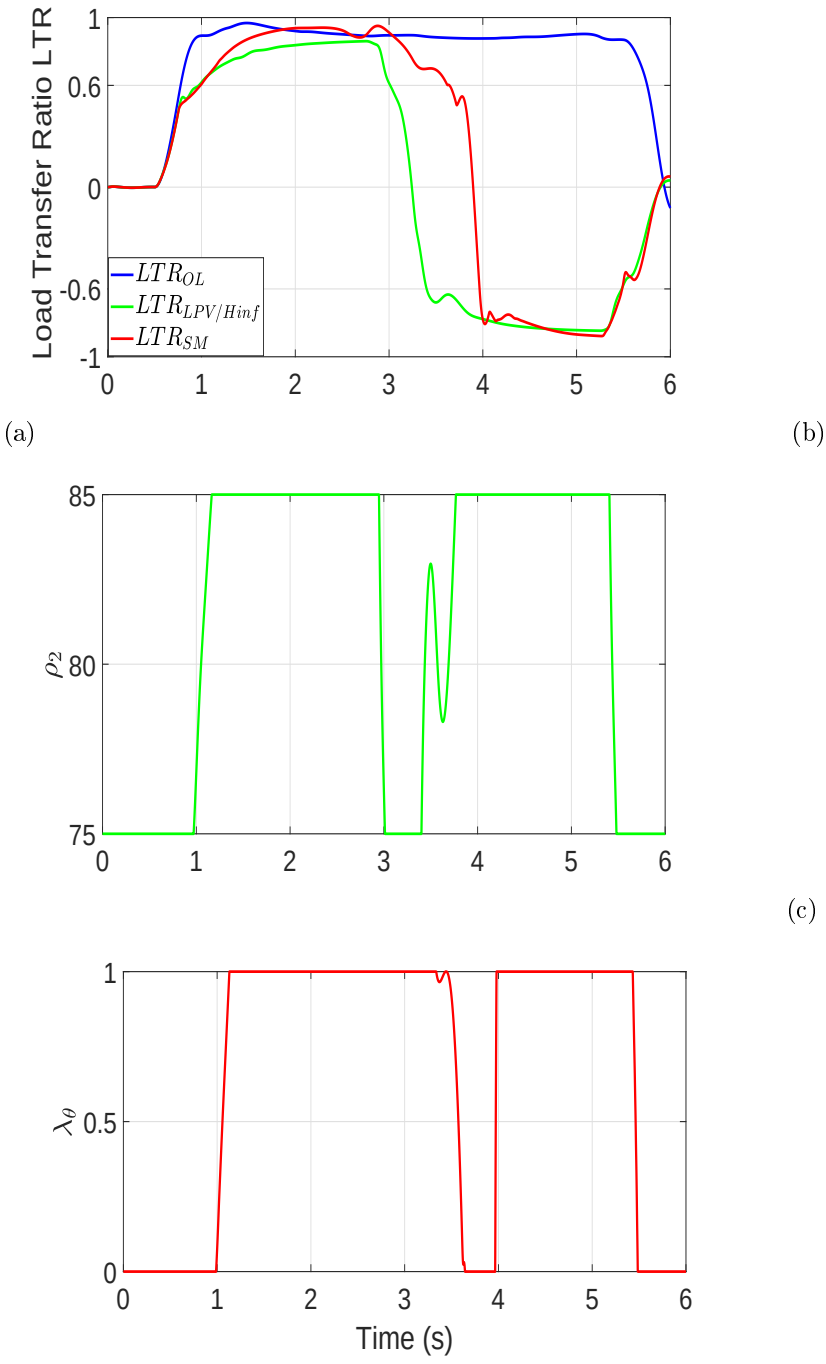


Figure 5.29 – Load transfer ratio $LTR$ and scheduling gains (Fishhook test)

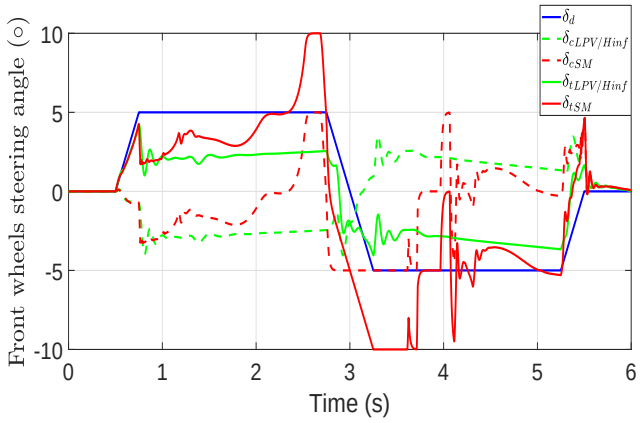


Figure 5.30 – Steering angle comparison (Fishhook test)

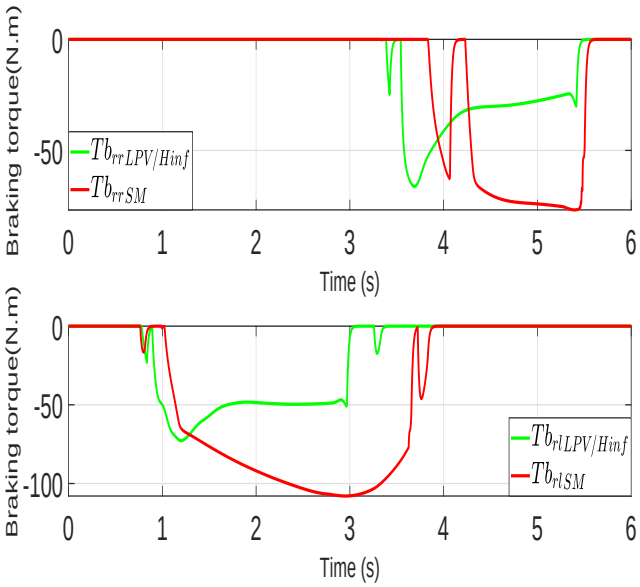


Figure 5.31 – Braking comparison (Fishhook test)

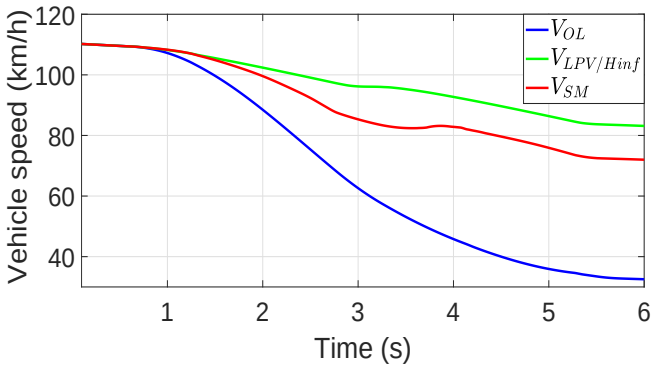


Figure 5.32 – Vehicle speed comparison (Fishhook test)

# *Conclusion and Perspectives*

In this final section, we first summarize the contributions concerning the developments of $GCC$ architectures. We then suggest possible improvements upon our work and topics for future studies.

## Conclusion

After reviewing the vehicle dynamics and control developed in literature, we have contributed, in this thesis, some achievements in $GCC$ that have led to several publications. We have proposed several original $GCC$ architectures, in complementary with the existing works in literature, through immersing in the analysis of every interconnection between the dynamics and thanks to the robust control techniques dealing with $MIMO$ complex and uncertain systems.
More precisely, in this thesis, we have contributed in the:

- exposition of the effect of the roll motion control through the $ASus$ on the ride comfort, rollover avoidance, and the lateral stability based on time and frequency domains analysis. To do so, several control laws and roll reference trajectories are developed and compared.

- development of a decentralized multilayer $GCC$ controller involving $AFS$, $DYC$, and $ASus$. Several control objectives are achieved, i.e, the maneuverability, lateral stability, rollover avoidance, and ride comfort. The $STSM$ technique is applied to develop the control layer, while some logic and fuzzy-logic rules are developed in the decision layer to coordinate the different controllers.

- development and comparison of a centralized and a decentralized multilayer architectures for $GCC$, involving only $AFS$ and $DYC$. The novelty w.r.t literature is the introduction of the roll control into the $GCC$ strategy without the need to include the suspensions. We have achieved several control objectives, i.e, the maneuverability, lateral stability, rollover avoidance, and ride comfort (only roll motion). The $MIMO\ LPV/\mathcal{H}_\infty$ (respectively $STSM$) robust control technique is applied to develop the control layer of the centralized (respectively decentralized) architecture, while endogenous weighting parameters are developed in the decision layer for both architectures to coordinate the different controllers and objectives.

To conclude, these are new features that can be embedded into on-road vehicles which enhance road safety and comfort. Of course, we have limited the studies to the scientific *GCC* aspect, without studying the feasibility of these developments which depends on several other factors, like actuator costs (especially for *ASus*), vehicle size and mechanical assembly, sensors precision, computational complexity for calculators... All these factors have to be studied to find the best architecture among others.

# Perspectives

In the following, we present some potential research improvements in *GCC*, and future works beyond *GCC*:

- Test and validate the proposed architectures in real-time experiments.
- Deepen the study in the vehicle dynamics modeling to include more interconnections in the full vehicle model. This can help to better understand the real vehicle behavior.
- Extend the cooperation between the active safety actuators to include more coordination in the *GCC* architecture.
- Consider the driver in the loop, to develop more intelligent and interactive *GCC* controllers. This task enhances the human-machine cooperation for assisted driving.
- Develop learning-based decision makers. This is a very interesting task to cover more vehicle situations and to take more delicate and precise decisions. The learning process can be done by simulations and experiments which is more precise than researcher tuned parameters.
- Proceed to fault-tolerant control via actuators tasks reconfiguration and controllers' adaptation. This task has been started at Heudiasyc Laboratory in SYSCOVI project within two masters internships.
- Adapt the proposed *GCC* architectures to autonomous vehicle. This task can provide safe autonomous driving.

# *Appendices*

## .1 Extended Bicycle Model

$$
\begin{aligned}
a_{11} &= (c_1 + I_{xz} * d_1 * (1 + b_1))/(d_4 * I_z),\\
a_{12} &= (c_2 + I_{xz} * d_1 * b_2)/(d_4 * I_z),\\
a_{13} &= I_{xz} * d_2/(d_4 * I_z),\\
a_{14} &= I_{xz} * d_3/(d_4 * I_z),\\
a_{21} &= b_1 + M_s * h_\theta * a_{41}/(M * V),\\
a_{22} &= b_2 + M_s * h_\theta * a_{42}/(M * V),\\
a_{23} &= M_s * h_\theta * a_{43}/(M * V),\\
a_{24} &= M_s * h_\theta * a_{44}/(M * V),\\
a_{41} &= d_1 * (1 + b_1)/d_4,\\
a_{42} &= d_1 * b_2/d_4,\\
a_{43} &= d_2/d_4 + d_5 * a_{13},\\
a_{44} &= d_3/d_4 + d_5 * a_{14},
\end{aligned}
\tag{25}
$$

$$
\begin{aligned}
b_{u,11} &= (c_\delta + I_{xz} * a_\delta/I_z)/c_4,\\
b_{u,21} &= b_\delta + M_s * h_\theta * b_{u,41}/(M * V),\\
b_{u,41} &= d_1 * b_\delta/d_4 + d_5 * b_{u,11},\\
b_{u,12} &= 1/(I_z * c_4),\\
b_{u,22} &= M_s * h_\theta * b_{u,42}/(M * V),\\
b_{u,42} &= d_5 * b_{u,12},\\
b_{u,13} &= d_5/I_z,\\
b_{u,23} &= M_s * h_\theta * d_5/(I_{xz} * M * V),\\
b_{u,43} &= d_5/I_{xz},
\end{aligned}
\tag{26}
$$

$$
\begin{aligned}
b_{d,11} &= 1/I_z,\\
b_{d,22} &= 1/M * V,\\
b_{d,22} &= 1/I_z.
\end{aligned}
\tag{27}
$$

where,

$$
\begin{aligned}
a_\delta &= d_1 * b_\delta / d_4, \\
b_\delta &= \mu * C_f / (M * V), \\
b_1 &= -1 + \mu * (C_r * l_r - C_f * l_f)/(M * V^2), \\
b_2 &= -\mu * (C_f + C_r)/(M * V), \\
c_\delta &= (1/I_z) * \mu * C_f * l_f, \\
c_1 &= -(1/I_z) * (\mu/V) * (C_f * (l_f^2) + C_r * l_r^2), \\
c_2 &= (1/I_z) * \mu * (C_r * l_r - C_f * l_f), \\
c_4 &= 1 - I_{xz} * d_5 / I_z, \\
d_1 &= M_s * h_\theta * V/(I_x + M_s * h_\theta^2), \\
d_2 &= (M_s * h_\theta * g - K_\theta)/(I_x + M_s * h_\theta^2), \\
d_3 &= -C_\theta/(I_x + M_s * h_\theta^2), \\
d_4 &= 1 - d_1 * M_s * h_\theta/(M * V), \\
d_5 &= I_{xz}/((I_x + M_s * (h_\theta^2)) * d_4).
\end{aligned}
\tag{28}
$$

# .2 Nonlinear Model

$$
\begin{aligned}
g_\theta(X) = \tfrac{1}{I_x + M_s h_\theta^2} [&(-F_{fr} + F_{fl})\, t_f + (-F_{rr} + F_{rl})\, t_r \\
&+ M_s\, (h_\theta\ cos\,(\theta) + z)\, a_y + M_s\, (h_\theta\ sin\,(\theta) + z)\, g],
\end{aligned}
\tag{29}
$$

$$
\begin{aligned}
g_\phi(X) = \tfrac{1}{I_y + M_s h_\phi^2} [&-(F_{fr} + F_{fl})\, l_f + (F_{rr} + F_{rl})\, l_r \\
&+ M_s\, (h_\phi\ cos\,(\phi) + z)\, a_x + M_s\, (h_\phi\ sin\,(\phi) + z)\, g],
\end{aligned}
\tag{30}
$$

$$
g_z(X) = \frac{1}{M_s}(F_{fr} + F_{fl} + F_{rr} + F_{rl}), \tag{31}
$$

$$
f_\theta = \frac{1}{I_x + M_s h_\theta^2}; f_\phi = \frac{1}{I_y + M_s h_\phi^2}; f_z = \frac{1}{M_s}, \tag{32}
$$

$$
\begin{aligned}
g_{\dot\psi}(X) = \tfrac{1}{I_z} [&-t_f (F_{x,fl} - F_{x,fr}) + l_f (F_{y,fl} + F_{y,fr}) \\
&- l_r (F_{y,rl} + F_{y,rr}) - t_r (F_{x,rl} - F_{x,rr})],
\end{aligned}
\tag{33}
$$

$$
f_{\dot\psi,\delta}(X) = \frac{1}{I_z}[t_f (F_{y,fl} - F_{y,fr}) + l_f (F_{x,fl} + F_{x,fr})], \tag{34}
$$

$$
f_{\dot\psi,C_z} = \frac{1}{I_z}, \tag{35}
$$

$$
\begin{aligned}
g_\beta(X) = &(-1 + \tfrac{l_r c_r - l_f c_f}{M {V_x}^2})(-\tfrac{{l_f}^2 c_f + {l_r}^2 c_r}{I_z V_x})\dot\psi \\
&+ (-1 + \tfrac{l_r c_r - l_f c_f}{M {V_x}^2})(\tfrac{l_r c_r - l_f c_f}{I_z})\beta + (-\tfrac{c_f + c_r}{M V_x})\dot\beta,
\end{aligned}
\tag{36}
$$

$$
f_{\beta,\delta}(X) = (-1 + \frac{l_r c_r - l_f c_f}{M {V_x}^2})\frac{l_f c_f}{I_z}, \tag{37}
$$

$$
f_{\beta,C_z}(X) = \frac{1}{I_z}(-1 + \frac{l_r c_r - l_f c_f}{M {V_x}^2}). \tag{38}
$$

$F_{ij}$, $F_{x,ij}$, and $F_{y,ij}$ are nonlinear functions of $X$ detailed in Section 1.1.

# *Bibliography*

[Ackermann and Bünte, 1997] Ackermann, J. and Bünte, T. (1997). Yaw disturbance attenuation by robust decoupling of car steering. *Control Engineering Practice*, 5(8):1131–1136.

[Ackermann and Odenthal, 1998] Ackermann, J. and Odenthal, D. (1998). Robust steering control for active rollover avoidance of vehicles with elevated center of gravity. *Citeseer*.

[Akhmetov et al., 2010] Akhmetov, Y., Rémond, D., Maiffredy, L., Di Loreto, M., Marquis-Favre, W., and Harth, V. (2010). Global Chassis Control for active safety of heavy vehicles. In *World Automotive Congress FISITA*, pages F2010–D–057.

[Alberding et al., 2009] Alberding, M. B., Tjønnås, J., and Johansen, T. A. (2009). Nonlinear hierarchical control allocation for vehicle yaw stabilization and rollover prevention. In *IEEE European Control Conference (ECC)*, pages 4229–4234.

[Anderson and Bevly, 2005] Anderson, R. and Bevly, D. M. (2005). Estimation of tire cornering stiffness using gps to improve model based estimation of vehicle states. In *IEEE Proceedings. Intelligent Vehicles Symposium, 2005.*, pages 801–806. IEEE.

[Andreasson and Bünte, 2006] Andreasson, J. and Bünte, T. (2006). Global chassis control based on inverse vehicle dynamics models. *Vehicle System Dynamics*, 44(sup1):321–328.

[Apkarian and Gahinet, 1995] Apkarian, P. and Gahinet, P. (1995). A convex characterization of gain-scheduled $h\infty$ controllers. *IEEE Transactions on Automatic Control*, 40(5):853–864.

[Apkarian et al., 1995] Apkarian, P., Gahinet, P., and Becker, G. (1995). Self-scheduled $h\infty$ control of linear parameter-varying systems: a design example. *Automatica*, 31(9):1251–1261.

[Aripin et al., 2014] Aripin, M., Md Sam, Y., Danapalasingam, K. A., Peng, K., Hamzah, N., and Ismail, M. (2014). A review of active yaw control system for

vehicle handling and stability enhancement. *International journal of vehicular technology*, 2014.

[Astolfi et al., 2007] Astolfi, A., Karagiannis, D., and Ortega, R. (2007). *Nonlinear and adaptive control with applications*. Springer Science & Business Media.

[Baffet et al., 2009] Baffet, G., Charara, A., and Lechner, D. (2009). Estimation of vehicle sideslip, tire force and wheel cornering stiffness. *Control Engineering Practice*, 17(11):1255–1264.

[Baffet et al., 2008] Baffet, G., Charara, A., Lechner, D., and Thomas, D. (2008). Experimental evaluation of observers for tire–road forces, sideslip angle and wheel cornering stiffness. *Vehicle System Dynamics*, 46(6):501–520.

[Bardawil et al., 2014] Bardawil, C., Talj, R., Francis, C., Charara, A., and Doumiati, M. (2014). Integrated vehicle lateral stability control with different coordination strategies between active steering and differential braking. In *IEEE 17th International Conference on Intelligent Transportation Systems (ITSC)*, pages 314–319.

[Canale and Fagiano, 2008] Canale, M. and Fagiano, L. (2008). Vehicle yaw control using a fast nmpc approach. In *2008 47th IEEE Conference on Decision and Control*, pages 5360–5365. IEEE.

[Canudas-de Wit et al., 2003] Canudas-de Wit, C., Tsiotras, P., Velenis, E., Basset, M., and Gissinger, G. (2003). Dynamic friction models for road/tire longitudinal interaction. *Vehicle System Dynamics*, 39(3):189–226.

[Chamseddine et al., 2006] Chamseddine, A., Noura, H., and Raharijaona, T. (2006). Control of linear full vehicle active suspension system using sliding mode techniques. In *2006 IEEE International Conference on Control Applications*, pages 1306–1311.

[Chen and Peng, 1999] Chen, B. and Peng, H. (1999). Rollover warning of articulated vehicles based on a time-to-rollover metric. In *ASME International Mechanical Engineering Conference and Exhibition*.

[Chen et al., 2006] Chen, W., Xiao, H., Liu, L., and Zu, J. W. (2006). Integrated control of automotive electrical power steering and active suspension systems based on random sub-optimal control. *International journal of vehicle design*, 42(3-4):370–391.

[Chen et al., 2016] Chen, W., Xiao, H., Wang, Q., Zhao, L., and Zhu, M. (2016). *Integrated vehicle dynamics and control*. John Wiley & Sons.

[Chokor et al., 2017] Chokor, A., Talj, R., Charara, A., Doumiati, M., and Rabhi, A. (2017). Rollover prevention using active suspension system. In *20th IEEE International Conference on Intelligent Transportation Systems (ITSC)*, pages 1706–1711.

[Chokor et al., 2016] Chokor, A., Talj, R., Charara, A., Shraim, H., and Francis, C. (2016). Active suspension control to improve passengers comfort and vehicle's stability. In *19th IEEE International Conference on Intelligent Transportation Systems (ITSC)*, pages 296–301.

[Chou and D'Andréa-Novel, 2005] Chou, H. and D'Andréa-Novel, B. (2005). Global vehicle control using differential braking torques and active suspension forces. *Vehicle System Dynamics*, 43(4):261–284.

[Chung and Yi, 2006] Chung, T. and Yi, K. (2006). Design and evaluation of side slip angle-based vehicle stability control scheme on a virtual test track. *IEEE Transactions on control systems technology*, 14(2):224–234.

[Dahlberg, 1999] Dahlberg, E. (1999). Commercial vehicle rollover prediction using energy consideration. In *Proc. of the European Automotive Congress, STA N99C203*.

[Dahlberg, 2000] Dahlberg, E. (2000). A method determining the dynamic rollover threshold of commercial vehicles. *SAE transactions*, pages 789–801.

[Deutermann, 2002] Deutermann, W. (2002). Characteristics of fatal rollover crashes. national center for statistics and analysis, national highway traffic safety administration, nhtsa. Technical report.

[DOT, 2010] DOT, H. (2010). Traffic safety facts research note: summary of statistical findings. highlights of 2009 motor vehicle crashes, dot hs 811 363, washington, dc.

[Doumiati et al., 2012] Doumiati, M., Charara, A., Victorino, A., and Lechner, D. (2012). *Vehicle dynamics estimation using Kalman filtering: experimental validation*. John Wiley & Sons.

[Doumiati et al., 2017] Doumiati, M., Martinez, J., Sename, O., Dugard, L., and Lechner, D. (2017). Road profile estimation using an adaptive youla–kučera parametric observer: Comparison to real profilers. *Control Engineering Practice*, 61:270–278.

[Doumiati et al., 2013] Doumiati, M., Sename, O., Dugard, L., Martinez-Molina, J.-J., Gaspar, P., and Szabo, Z. (2013). Integrated vehicle dynamics control via coordination of active front steering and rear braking. *European Journal of Control*, 19(2):121–143.

[Doumiati et al., 2011] Doumiati, M., Victorino, A., Charara, A., and Lechner, D. (2011). Estimation of road profile for vehicle dynamics motion: experimental validation. In *Proceedings of the 2011 American Control Conference*, pages 5237–5242. IEEE.

[Doumiati et al., 2010a] Doumiati, M., Victorino, A., Lechner, D., Baffet, G., and Charara, A. (2010a). Observers for vehicle tyre/road forces estimation: experimental validation. *Vehicle System Dynamics*, 48(11):1345–1378.

[Doumiati et al., 2014] Doumiati, M., Victorino, A., Talj, R., and Charara, A. (2014). Robust lpv control for vehicle steerability and lateral stability. In *53rd IEEE Conference on Decision and Control, pp. 4113–4118.*

[Doumiati et al., 2010b] Doumiati, M., Victorino, A. C., Charara, A., and Lechner, D. (2010b). Onboard real-time estimation of vehicle lateral tire–road forces and sideslip angle. *IEEE/ASME Transactions on Mechatronics*, 16(4):601–614.

[Dugoff et al., 1970] Dugoff, H., Fancher, P., and Segel, L. (1970). An analysis of tire traction properties and their influence on vehicle dynamic performance. *SAE transactions*, pages 1219–1243.

[Falcone et al., 2007a] Falcone, P., Borrelli, F., Asgari, J., Tseng, H. E., and Hrovat, D. (2007a). A model predictive control approach for combined braking and steering in autonomous vehicles. In *2007 Mediterranean Conference on Control & Automation*, pages 1–6. IEEE.

[Falcone et al., 2007b] Falcone, P., Borrelli, F., Asgari, J., Tseng, H. E., and Hrovat, D. (2007b). Predictive active steering control for autonomous vehicle systems. *IEEE Transactions on control systems technology*, 15(3):566–580.

[Fergani et al., 2016a] Fergani, S., Menhour, L., Sename, O., Dugard, L., and D'Andréa-Novel, B. (2016a). LPV/H$\infty$ suspension robust control adaption of the dynamical lateral load transfers based on a differential algebraic estimation approach. In *8th IFAC International Symposium on Advances in Automotive Control (AAC 2016).*

[Fergani et al., 2017] Fergani, S., Menhour, L., Sename, O., Dugard, L., and D'Andréa-Novel, B. (2017). Integrated vehicle control through the coordination of longitudinal/lateral and vertical dynamics controllers: Flatness and lpv/-based design. *International Journal of Robust and Nonlinear Control*, 27(18):4992–5007.

[Fergani et al., 2013] Fergani, S., Sename, O., and Dugard, L. (2013). A new lpv/h$\infty$ global chassis control through load transfer distribution and vehicle stability monitoring. *IFAC Proceedings Volumes*, 46(2):809–814.

[Fergani et al., 2016b] Fergani, S., Sename, O., and Dugard, L. (2016b). An $lpv/\mathcal{H}_\infty$ integrated vehicle dynamic controller. *IEEE Transactions on Vehicular Technology*, 65(4):1880–1889.

[Gaspar et al., 2007] Gaspar, P., Szabo, Z., Bokor, J., Poussot-Vassal, C., Sename, O., and Dugard, L. (2007). Global chassis control using braking and suspension systems.

[Gáspár et al., 2005] Gáspár, P., Szaszi, I., and Bokor, J. (2005). Reconfigurable control structure to prevent the rollover of heavy vehicles. *Control Engineering Practice*, 13(6):699–711.

[Gillespie, 1992] Gillespie, T. D. (1992). *Fundamentals of Vehicle Dynamics. Warrendale, PA: Society of Automotive Engineers.* Inc.

[Gu et al., 2005] Gu, D.-W., Petkov, P., and Konstantinov, M. M. (2005). *Robust control design with MATLAB®*. Springer Science & Business Media.

[Guglielmino et al., 2008] Guglielmino, E., Sireteanu, T., Stammers, C. W., Ghita, G., and Giuclea, M. (2008). *Semi-active suspension control: improved vehicle ride and road friendliness.* Springer Science & Business Media.

[Guldner et al., 1996] Guldner, J., Tan, H.-S., and Patwardhan, S. (1996). Analysis of automatic steering control for highway vehicles with look-down lateral reference systems. *Vehicle System Dynamics*, 26(4):243–269.

[He et al., 2006] He, J., Crolla, D. A., Levesley, M., and Manning, W. (2006). Coordination of active steering, driveline, and braking for integrated vehicle dynamics control. *Proceedings of the Institution of Mechanical Engineers, Part D: Journal of Automobile Engineering*, 220(10):1401–1420.

[Heißing and Ersoy, 2010] Heißing, B. and Ersoy, M. (2010). *Chassis handbook: fundamentals, driving dynamics, components, mechatronics, perspectives.* Springer Science & Business Media.

[Hsu, 2009] Hsu, Y.-H. J. (2009). *Estimation and control of lateral tire forces using steering torque.* Stanford University.

[Imine et al., 2005] Imine, H., Delanne, Y., and M'sirdi, N. (2005). Road profile inputs for evaluation of the loads on the wheels. *Vehicle System Dynamics*, 43(sup1):359–369.

[Inagaki et al., 1994] Inagaki, S., Kshiro, I., and Yamamoto, M. (1994). Analysis on vehicle stability in critical cornering using phase-plane method. In *International Symposium on Advanced Vehicle Control 1994*.

[Jin et al., 2016] Jin, X., Yin, G., Zhang, N., and Chen, J. (2016). Improving vehicle handling stability performance via integrated control of active front steering and suspension systems. In *Transportation Electrification Asia-Pacific (ITEC Asia-Pacific), IEEE Conference and Expo*, pages 621–625.

[Karbalaei et al., 2007] Karbalaei, R., Ghaffari, A., Kazemi, R., and Tabatabaei, S. (2007). A new intelligent strategy to integrated control of afs/dyc based on fuzzy logic. *International Journal of Mathematical, Physical and Engineering Sciences*, 1(1):47–52.

[Kiencke, 1993] Kiencke, U. (1993). Realtime estimation of adhesion characteristic between tyres and road. *IFAC Proceedings Volumes*, 26(2):15–18.

[Kiencke and Nielsen, 2000] Kiencke, U. and Nielsen, L. (2000). Automotive control systems: for engine, driveline, and vehicle.

[Klier et al., 2004] Klier, W., Reimann, G., and Reinelt, W. (2004). Concept and functionality of the active front steering system. Technical report, SAE Technical Paper.

[Li et al., 2008] Li, D., Du, S., and Yu, F. (2008). Integrated vehicle chassis control based on direct yaw moment, active steering and active stabiliser. *Vehicle System Dynamics*, 46(S1):341–351.

[Li et al., 2013] Li, Y., Sun, W., Huang, J., Zheng, L., and Wang, Y. (2013). Effect of vertical and lateral coupling between tyre and road on vehicle rollover. *Vehicle System Dynamics*, 51(8):1216–1241.

[Milliken et al., 1995] Milliken, W. F., Milliken, D. L., et al. (1995). *Race car vehicle dynamics*, volume 400. Society of Automotive Engineers Warrendale.

[Mirzaei and Mirzaeinejad, 2017] Mirzaei, M. and Mirzaeinejad, H. (2017). Fuzzy scheduled optimal control of integrated vehicle braking and steering systems. *IEEE/ASME Transactions on Mechatronics*, 22(5):2369–2379.

[Moradi and Fekih, 2013] Moradi, M. and Fekih, A. (2013). Adaptive pid-sliding-mode fault-tolerant control approach for vehicle suspension systems subject to actuator faults. *IEEE Transactions on Vehicular Technology*, 63(3):1041–1054.

[Moreau et al., 2003] Moreau, X., Altet, O., and Oustaloup, A. (2003). The crone suspension: Modelling and stability analysis. In *ASME 2003 International Design Engineering Technical Conferences and Computers and Information in Engineering Conference*, pages 685–694. American Society of Mechanical Engineers.

[Moreau et al., 2009] Moreau, X., Rizzo, A., and Oustaloup, A. (2009). Application of the crone control-design method to a low-frequency active suspension system. *International Journal of Vehicle Autonomous Systems*, 7(3-4):172–200.

[Nassirharand and Karimi, 2002] Nassirharand, A. and Karimi, H. (2002). Input/output characterization of highly nonlinear multivariable systems. *Advances in Engineering Software*, 33(11-12):825–830.

[Nwagboso et al., 2002] Nwagboso, C., Ouyang, X., and Morgan, C. (2002). Development of neural-network control of steer-by-wire system for intelligent vehicles. *International Journal of Heavy Vehicle Systems*, 9(1):1–26.

[Odenthal et al., 1999] Odenthal, D., Bunte, T., and Ackermann, J. (1999). Nonlinear steering and braking control for vehicle rollover avoidance. In *IEEE European Control Conference (ECC), pp. 598–603.*

[Oh et al., 2003] Oh, S.-W., Yun, S.-C., Chae, H.-C., Jang, S.-H., Jang, J.-H., and Han, C.-S. (2003). The development of an advanced control method for the steer-by-wire system to improve the vehicle maneuverability and stability. Technical report, SAE Technical Paper.

[Oustaloup et al., 1997] Oustaloup, A., Moreau, X., and Nouillant, M. (1997). From fractal robustness to non-integer approach in vibration insulation: the crone suspension. In *Proceedings of the 36th IEEE Conference on Decision and Control*, volume 5, pages 4979–4984. IEEE.

[Pacejka and Besselink, 1997] Pacejka, H. and Besselink, I. (1997). Magic formula tyre model with transient properties. *Vehicle system dynamics*, 27(S1):234–249.

[Pedro et al., 2013] Pedro, J. O., Dangor, M., Dahunsi, O. A., and Ali, M. M. (2013). Differential evolution-based pid control of nonlinear full-car electrohydraulic suspensions. *Mathematical Problems in Engineering*, 2013.

[Peng and Eisele, 2000] Peng, H. and Eisele, D. (2000). Vehicle dynamics control with rollover prevention for articulated heavy trucks. In *Proceedings of 5th International Symposium on Advanced Vehicle Control, University of Michigan, Ann Arbor. Michigan USA*. Citeseer.

[Poussot-Vassal, 2008] Poussot-Vassal, C. (2008). *Commande robuste LPV multivariable de chassis automobile*. PhD thesis, Grenoble INPG.

[Poussot-Vassal et al., 2009] Poussot-Vassal, C., Sename, O., and Dugard, L. (2009). Robust vehicle dynamic stability controller involving steering and braking systems. In *IEEE European Control Conference (ECC), pp. 3646–3651.*

[Rajamani, 2012] Rajamani, R. (2012). *Vehicle Dynamics and Control*. Springer.

[Ray, 1997] Ray, L. R. (1997). Nonlinear tire force estimation and road friction identification: simulation and experiments. *Automatica*, 33(10):1819–1833.

[Reznik, 1997] Reznik, L. (1997). *Fuzzy controllers handbook: how to design them, how they work*. Elsevier.

[Savaresi et al., 2010] Savaresi, S. M., Poussot-Vassal, C., Spelta, C., Sename, O., and Dugard, L. (2010). *Semi-active suspension control design for vehicles*. Elsevier.

[Scherer et al., 1997] Scherer, C., Gahinet, P., and Chilali, M. (1997). Multiobjective output-feedback control via lmi optimization. *IEEE Transactions on automatic control*, 42(7):896–911.

[Sename et al., 2013] Sename, O., Gaspar, P., and Bokor, J. (2013). *Robust control and linear parameter varying approaches: application to vehicle dynamics*. Springer, vol. 437.

[Shtessel et al., 2014] Shtessel, Y., Edwards, C., Fridman, L., and Levant, A. (2014). *Sliding mode control and observation*. Springer.

[Sierra et al., 2006] Sierra, C., Tseng, E., Jain, A., and Peng, H. (2006). Cornering stiffness estimation based on vehicle lateral dynamics. *Vehicle System Dynamics*, 44(sup1):24–38.

[Smith and Starkey, 1995] Smith, D. E. and Starkey, J. M. (1995). Effects of model complexity on the performance of automated vehicle steering controllers: Model development, validation and comparison. *Vehicle System Dynamics*, 24(2):163–181.

[Solmaz et al., 2007] Solmaz, S., Corless, M., and Shorten, R. (2007). A methodology for the design of robust rollover prevention controllers for automotive vehicles with active steering. *International Journal of Control*, 80(11):1763–1779.

[Tagne et al., 2015] Tagne, G., Talj, R., and Charara, A. (2015). Design and validation of a robust immersion and invariance controller for the lateral dynamics of intelligent vehicles. *Control Engineering Practice*, 40:81–92.

[Utkin, 2013] Utkin, V. (2013). On convergence time and disturbance rejection of super-twisting control. *IEEE Transactions on Automatic Control*, 58(8):2013–2017.

[Villagra et al., 2007] Villagra, J., d'Andréa Novel, B., Pengov, M., Bösiger, M., and Devouge, Q. (2007). A realistic vehicle model for esp-like control laws synthesis. In *2007 European Control Conference (ECC)*, pages 644–651. IEEE.

[Vivas-Lopez et al., 2015] Vivas-Lopez, C. A., Tudon-Martinez, J. C., Hernandez-Alcantara, D., and Morales-Menendez, R. (2015). Global chassis control system using suspension, steering, and braking subsystems. *Mathematical Problems in Engineering*, 2015.

[Vu et al., 2017] Vu, V. T., Sename, O., Dugard, L., and Gáspár, P. (2017). Enhancing roll stability of heavy vehicle by lqr active anti-roll bar control using electronic servo-valve hydraulic actuators. *Vehicle System Dynamics*, 55(9):1405–1429.

[Wang and Wang, 2013] Wang, R. and Wang, J. (2013). Tire–road friction coefficient and tire cornering stiffness estimation based on longitudinal tire force difference generation. *Control Engineering Practice*, 21(1):65–75.

[Wei et al., 2006] Wei, J., Zhuoping, Y., and Lijun, Z. (2006). Integrated chassis control system for improving vehicle stability. In *2006 IEEE International Conference on Vehicular Electronics and Safety*, pages 295–298. IEEE.

[Xiao et al., 2009] Xiao, H., Chen, W., Zhou, H., and Zu, J. W. (2009). Integrated vehicle dynamics control through coordinating electronic stability program and active suspension system. In *2009 IEEE International Conference on Mechatronics and Automation*, pages 1150–1155.

[Yao et al., 2017] Yao, J., Lv, G., Qv, M., Li, Z., Ren, S., and Taheri, S. (2017). Lateral stability control based on the roll moment distribution using a semiactive suspension. *Proceedings of the Institution of Mechanical Engineers, Part D: Journal of Automobile Engineering*, 231(12):1627–1639.

[Yoon et al., 2007] Yoon, J., Kim, D., and Yi, K. (2007). Design of a rollover index-based vehicle stability control scheme. *Vehicle system dynamics*, 45(5):459–475.

[Yoon et al., 2010] Yoon, J., Yim, S., Cho, W., Koo, B., and Yi, K. (2010). Design of an unified chassis controller for rollover prevention, manoeuvrability and lateral stability. *Vehicle system dynamics*, 48(11):1247–1268.

[Yu and Huang, 2008] Yu, H. and Huang, M. (2008). Potential energy analysis and limit cycle control for dynamics stability of in-wheel driving electric vehicle. In *2008 IEEE Vehicle Power and Propulsion Conference*, pages 1–5.

[Zhao et al., 2014] Zhao, S.-e., Li, Y., and Qu, X. (2014). Vehicle chassis integrated control based on multimodel and multilevel hierarchical control. *Mathematical Problems in Engineering*, 2014.

[Zhou et al., 1996] Zhou, K., Doyle, J. C., Glover, K., et al. (1996). *Robust and optimal control*, volume 40. Prentice hall New Jersey.

[Zulkarnain et al., 2012] Zulkarnain, N., Imaduddin, F., Zamzuri, H., and Mazlan, S. A. (2012). Application of an active anti-roll bar system for enhancing vehicle ride and handling. In *IEEE Colloquium on Humanities, Science and Engineering (CHUSER)*, pages 260–265.